Order Number 9207058

Raman and dielectric studies of structurally modulated crystals: Thiourea and TMATC-Zn

Chen, Xiaoke, Ph.D.

City University of New York, 1991

U·M·I
300 N. Zeeb Rd.
Ann Arbor, MI 48106

RAMAN AND DIELECTRIC STUDIES OF STRUCTURALLY MODULATED CRYSTALS: THIOUREA AND TMATC-Zn

by

XIAOKE CHEN

A dissertation submitted to the Graduate Faculty in Physics in partial fulfillment of the requirements for the degree of Doctor of Philosophy, The City University of New York.

1991

This manuscript has been read and accepted for the Graduate Faculty in Physics in satisfaction of the dissertation requirement for the degree of Doctor of Philosophy.

July 25, 1991
Date

Herman Z. Cummins
Chair of Examining Committee

Aug 5, 1991
Date

Joseph B. Krieger
Executive Officer

Janos Bergou

Joseph L. Birman

Frederick W. Smith

Michael J. Stephen

Supervisory Committee

The City University of New York

Abstract

RAMAN AND DIELECTRIC STUDIES OF STRUCTURALLY MODULATED CRYSTALS: THIOUREA AND TMATC-Zn

by

Xiaoke Chen

Adviser: Professor Herman Z. Cummins

The complex dielectric constant of thiourea has been measured in the temperature range from 80 K to 300 K with different measuring-field levels and frequencies, with and without d.c. biasing fields. The temperature interval between the two peaks in the $\varepsilon^*(T)$ curve near 177 K was found to extrapolate to 0.7 K at zero measuring field, which indicates that the $\frac{1}{8}$ ferroelectric lock-in phase is intrinsic in a non-zero temperature range. Slowing-down of dielectric relaxation processes was observed at both the upper and lower transition points of this phase. The E-T phase diagram near the $\frac{1}{8}$ lock-in region was surveyed by investigating the effects of biasing fields. D-E hysteresis loops were investigated in the vicinity of the $\frac{1}{8}$ ferroelectric phase with measuring frequencies from 0.5Hz to 5mHz. The different D-E loops observed clearly demonstrate the difference between the intrinsic and "field-induced" lock-in mechanisms. The spontaneous polarization and the coercive field in the $\frac{1}{8}$ phase were measured. The experimental results can be well explained by the phenomenological Landau theory of phase transitions.

Low-frequency Raman-scattering experiments on tetramethylammonium tetrachlorozincate crystals have been performed in the temperature range from $310\,K$ to $80\,K$, which includes the five successive phase transitions. As the temperature decreased, an $11\,cm^{-1}$ mode appeared in the (aa) scattering geometry in the incommensurate phase II and lock-in phases III and IV, which have modulation wavevectors $q_0 = (\frac{2}{5}+\delta)a^*$, $\frac{2}{5}a^*$, and $\frac{1}{3}a^*$ respectively, disappeared in phase V ($q_0 = 0$), and reappeared in phase VI ($q_0 = \frac{1}{3}a^*$). The temperature dependence of the observed frequency shift demonstrates that this mode is the folded Σ_3 acoustic mode scattering via a second-order process. A weak $15\,cm^{-1}$ mode observed in phase VI can be interpreted as the folded Σ_4 acoustic mode scattering via a third-order process.

Acknowledgements

I express my deep gratitude to Professor Herman Z. Cummins for his patient guidance and continued support during the course of this research.

I am grateful to Prof. F. Ullman and Dr. D. Billesbach, Prof. L. Isaacs and Ms. R. Ledesma, Prof. A. Lopez-Echarri and Mr. B. Zhou for their efforts in searching for zero-field experimental evidence of the existence of the intrinsic 1/8 ferroelectric phase in thiourea.

I thank Prof. R. Pick, Prof. J. Birman, Dr. A. Moudden, Prof. T. Yagi and Prof. A. Levanyuk for their helpful discussions and suggestions in the theoretical and experimental aspects of this research.

I thank all the members of the Light Scattering Group, Dr. Wing-kee Lee, Dr. Gen Li, Dr. Nongjian Tao, Prof. J.S. Hwang, Dr. Xiaowen Qian, Dr. Henry Chou, Mr. Weimin Du, Mr. Martin Muschol, Mr. Lloyd Williams Mr. Dongning Liu and Ms. Tracy Turner for their collaboration and for the pleasant working atmosphere.

I thank all the members of my thesis committee, Prof. J. Bergou, Prof. J. Birman, Prof. F. Smith and Prof. M. Stephen for their guidance and help.

I also thank my family, my relatives and friends for their encouragement and concern for my Ph.D. study.

Foreword

The concept of symmetry of crystals has played a central role in the development of traditional solid state physics. The translational periodicity of the arrangement of the atoms is considered as a universal property of classical ideal crystals. This is in sharp contrast to disordered amorphous materials in which there is no long-range order in the positions of the atoms.

Since the middle of 1970s, extensive research has been focused on incommensurate materials which exhibit perfect three dimensional long-range order represented by the lattice vectors and a structural modulation wavevector, but no translational periodicity in the modulated direction. A number of interesting phenomena have been found in incommensurate systems, such as multi-soliton ground states, devil's staircase, amplitudon and phason excitations, temperature-dependent zone-folding Raman modes, etc. The studies of incommensurate systems have revealed a new aspect of the physics in solids.

Thiourea and TMATC-Zn are both incommensurate materials with rich phases. We have carried out an experimental dielectric study and theoretical analysis of the phase transitions in thiourea (focusing on the mechanism of the $\frac{1}{8}$ ferroelectric phase transition), which will be presented in Part I. We also performed low-frequency Raman scattering experiments and studied the zone-folding acoustic modes in TMATC-Zn, which will be discussed in Part II.

Table of Contents

Abstract iii

Acknowledgements v

Foreword vi

Table of Contents vii

List of Tables xi

List of Figures xii

Part I. STRUCTURAL PHASE TRANSITIONS IN THIOUREA 1-125

I.1 Introduction (thiourea) 2

I.1.1 Crystal Structure of Thiourea 2

I.1.2 Historical Review 8

a) Experimental studies 8

b) Theories 22

I.1.3 Current Research 25

I.2 Landau Theory of Phase Transitions in Thiourea 27

I.2.1 Base Form of the Free Energy 27

I.2.2 Incommensurate Plane Wave Approximation 30

a) The structural distortion 30

b) N-Inc-F transitions 31

I.2.3 Umklapp Terms and the Phase diagram 35

a) Commensurate lock-in Transitions and Umklapp terms 35

b) Possible wavevectors on the basis of symmetry considerations 36

c) The commensurate lock-in phases 39

d) (E-T) phase diagram near the 1/8 lock-in region 45

I.2.4 Dielectric Behavior and corrections to the IPW approximation 54

a) Harmonics of the primary order parameter 54

b) Dielectric properties near the 1/9 lock-in transition 57

c) Dielectric properties near the 1/8 phase boundary 63

d) Dielectric properties without the lock-in terms 69

I.2.5 Dielectric Relaxation Mechanism Near the 1/8 Phase 72

a) The equation of motion of the phase mode 72

b) The dynamic susceptibility 73

I.3 Dielectric Constant Measurements 79

I.3.1 Sample Preparation and Experimental Apparatus 79

a) Crystal growth and sample preparation 79

b) Dielectric constant measurement apparatus 79

I.3.2 The Observed Anomalies 85

I.3.3 Dielectric Behavior Pertaining to the 1/8 lock-in transition 91

a) $\epsilon(T)$ at different measuring field levels 91

b) Thermal hysteresis 95

c) Frequency dependence of the complex dielectric constant 98

d) The effects of biasing fields 100

e) Summary 103

I.4 D-E Hysteresis Loops and Spontaneous Polarization Measurements 105

I.4.1 Predictions of the D-E Hysteresis Loops 105

I.4.2 The Computerized Sawyer-Tower Circuit 109

I.4.3 Results 112

a) D-E hysteresis loops 112

b) Spontaneous polarization and coercive field 114

I.5 Determination of the Coefficients in the Free Energy Expansion 117

I.5.1 The Constants a, T_0, α, β, and $\frac{B}{\gamma}$ 117

I.5.2 The Constants B, γ and b_9 121

a) B and γ 121

b) b_9 122

I.5.3 Discussions of the Stability of the Free energy expansion 123

I.6 Discussions 125

Part II. ZONE-FOLDING RAMAN MODES IN TMATC-Zn 126-150

II.1 Introduction (TMATC-Zn) 127

II.2 Theory of Zone-folding Modes in TMATC-Zn 130

II.2.1 Raman Activation of Zone-folding Modes 130

II.2.2 Selection Rules of FAM's in TMATC-Zn 134

II.2.3 Raman Shift of FAM's in TMATC-Zn 137

II.3 Experiment 140

II.3.1 Crystal Growth and Raman Scattering Apparatus 140

II.3.2 Data Analysis 143

a) Raman spectra 143

b) Fitting models 143

II.4 Conclusions 149

Appendix A. Data Acquisition Programs for Impedance Measurements 151

Appendix B. Basic Program for Dielectric Hysteresis Loop Measurements 157

References 166

List of Tables

table page

table 1.1 2

table 1.2 4

table 1.3 37

table 1.4 102

table 1.5 123

table 2.1 127

table 2.2 134

table 2.3 135

table 2.4 135

table 2.5 136

table 2.6 146

List of Figures

figure	page
fig.1.1	3
fig.1.2	5
fig.1.3	7
fig.1.4	9
fig.1.5	1
fig.1.6	14
fig.1.7	15
fig.1.8	17
fig.1.9	18
fig.1.10	21
fig.1.11	34
fig.1.12	42
fig.1.13	43
fig.1.14	46
fig.1.15	47
fig.1.16	50
fig.1.17	51
fig.1.18	55
fig.1.19	59
fig.1.20	61

fig.1.21 64

fig.1.22 66

fig.1.23 68

fig.1.24 71

fig.1.25 76

fig.1.26 78

fig.1.27 80

fig.1.28 82

fig.1.29 84

fig.1.30 86

fig.1.31 89

fig.1.32 90

fig.1.33 92

fig.1.34 93

fig.1.35 94

fig.1.36 96

fig.1.37 97

fig.1.38 99

fig.1.39 101

fig.1.40 106

fig.1.41 108

fig.1.42 110

fig.1.43 113

fig.1.44 115

fig.1.45 116

fig.1.46 119

fig.1.47 120

fig.2.1 129

fig.2.2 133

fig.2.3 138

fig.2.4 139

fig.2.5 141

fig.2.6 144

fig.2.7 150

Part I

Structural Phase Transitions in Thiourea

Chapter I.1

Introduction (Thiourea)

I.1.1. Crystal Structure of Thiourea

Thiourea was one of the earliest organic crystal structures to be investigated [W1]. The thiourea molecule was found to be planar with C_{2v} point symmetry and to possess a permanent dipole moment along its 2-fold axis (see fig.1.1)[K1]. At room temperature thiourea crystalizes in the orthorhombic centrosymmetric space group D_{2h}^{16} with four molecules per unit cell (a=7.655$\dot{A}$, b=8.537$\dot{A}$, c=5.520$\dot{A}$). The symmetry elements of the space group are listed in table 1.1. The crystal structure has been

table 1.1 Symmetry elements of the space group D_{2h}^{16}(Pnma)

Symmetry elements	Equivalent positions			Molecule labels
$\{E \mid 0\}$	x	y	z	(1)
$\{C_{2x} \mid \frac{1}{2}(a+b+c)\}$	$\frac{1}{2}+x$	$\frac{1}{2}-y$	$\frac{1}{2}-z$	(2)
$\{C_{2y} \mid \frac{1}{2}b\}$	$\bar{x}$	$\frac{1}{2}+y$	$\bar{z}$	(4)
$\{C_{2z} \mid \frac{1}{2}(a+c)\}$	$\frac{1}{2}-x$	$\bar{y}$	$\frac{1}{2}+z$	(3)
$\{I \mid 0\}$	$\bar{x}$	$\bar{y}$	$\bar{z}$	(4')
$\{\sigma_z \mid \frac{1}{2}(a+b+c)\}$	$\frac{1}{2}-x$	$\frac{1}{2}+y$	$\frac{1}{2}+z$	(3')
$\{\sigma_y \mid \frac{1}{2}b\}$	x	$\frac{1}{2}-y$	z	(1')
$\{\sigma_z \mid \frac{1}{2}(a+c)\}$	$\frac{1}{2}+x$	y	$\frac{1}{2}-z$	(2')

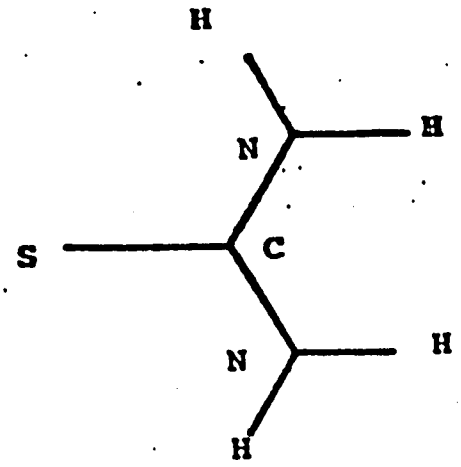

Fig. 1.1. Thiourea Molecule (Elcombe and Taylor 1968).

thoroughly studied by X-ray diffraction [K1][T1], electron diffraction [D1] and neutron diffraction [E1] experiments. The projection of the unit cell in the (a,c) plane is shown in fig.1.2. The molecular dipole moments are parallel to the (a,c) plane and the resulting dipole moment of a unit cell cancels due to the symmetry of the n- and a-glide planes (see fig.1.2 and table 1.1).

table 1.2 Phases of thiourea at atmospheric pressure

Phase	Transition Temp. T(K)	Modulation Wavevector $q_0(b^*)$	Z Formula Units per unit cell
I		normal phase (Pnma)	4
	$T_1 = 202$		
II		0.141 ~ 1/8 incommensurate	
	$T_8^+ = 178.3$		
(IIx) ?		1/8 ferroelectric (E-field induced)	32
	$T_8^- = 177.6$		
II		1/8 ~ 0.115 incommensurate	
	$T_9 = 171$		
III		1/9	36
	$T_c = 169$		
IV		0 ferroelectric	4

On cooling at atmospheric presure, thiourea undergoes a series of phase transitions as shown in table 1.2 [C1]. A second-order transition occurs at 202K and the crystal becomes incommensurate with a structural modulation wavevector $q_0 = \delta b^*$ where $\delta \sim 0.141$. The structural modulation can be described by a condensed normal mode Q_{q_0} of τ_4 symmetry along with harmonics [M1][S1][S2][S3][S4]. The modulation wavevector, which has been measured by several groups by means of neutron and X-ray diffraction experiments [F2][M2][D2][D3], decreases with decreasing temperature till 171K, where it locks-in at $q_c = \frac{1}{9}b^*$. The commensurate $\frac{1}{9}$ phase (III) persists to 169K where a first-order lock-in transition occurs to a proper ferroelectric phase (IV), which

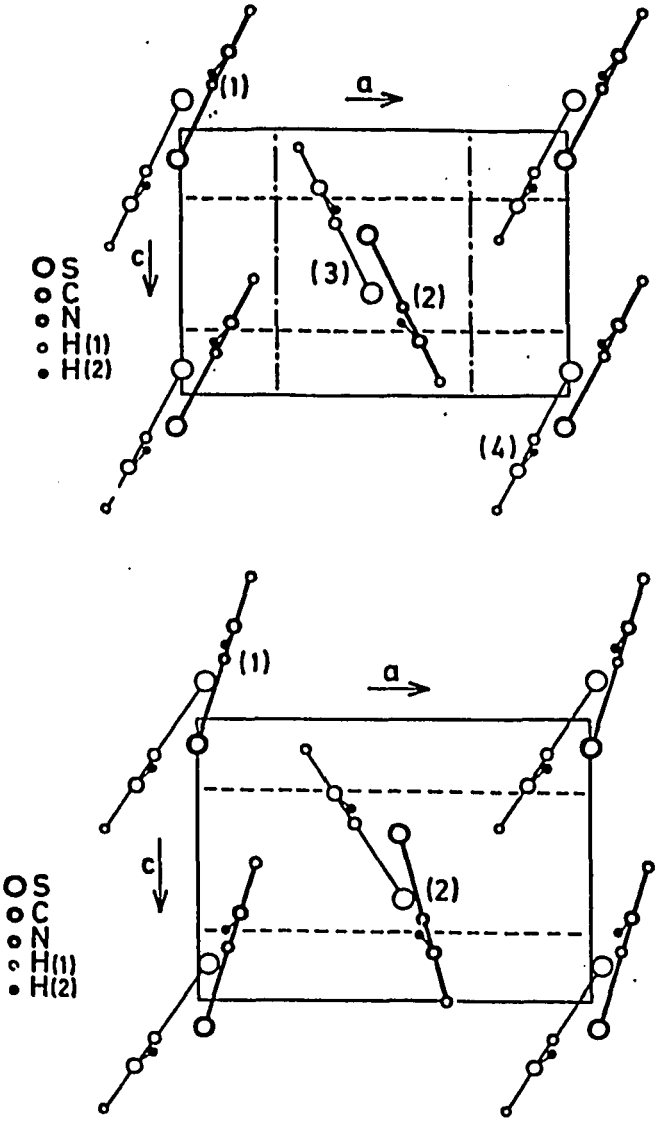

Fig. 1.2. The unit cell of thiourea projected onto the (a, c) plane in the normal phase I (above) and the ferroelectric phase IV (below). The light molecules are in the $y = 0$ plane, the dark ones in the $y = b/2$ plane (Simonson *et al* 1985).

restores the unit cell to its initial size with z=4.

The crystal structure in the final ferroelectric phase IV was analyzed by Goldsmith and White [G1], and Elcombe and Taylor [E1]. As shown in fig.1.2b, the space group becomes C_{2v}^2 ($P2_1ma$) which is still orthorhombic, but the two nonequivalent pairs of molecules tilt differently with respect to the crystal **a** axis, which breaks the n-glide symmetry and results in a net dipole moment along the **a** direction.

There has been a controversy about the existence of an $\frac{1}{8}$ ferroelectric lock-in phase near 177K (phase IIx in table 1.2). On the one hand, a dielectric anomaly and spontaneous polarization were observed at the temperature where the modulation wavevector is about $\frac{1}{8}$ [G1][G2]. On the other hand, other experiments have not confirmed the existence of this phase without an external electric field [D4]. An elastic neutron scattering experiment on deuterated thiourea by Moudden *et al* showed that in the absence of an E-field the temperature-dependent wavevector smoothly passes the $\frac{1}{8}$ point, whereas it does lock-in at $\frac{1}{8}$ when an E-field is applied (see fig.1.3)[M3]. Similar E-field effects were found by optical birefringence measurement on deuterated thiourea. Therefore, it has been widely accepted that this $\frac{1}{8}$ ferroelectric lock-in phase is induced by the external E-field. However, this "field induced" mechanism is not entirely certain because it can not explain some of the published experimental facts [G2][M4] or some of our results. We will focus on this problem and discuss it in detail.

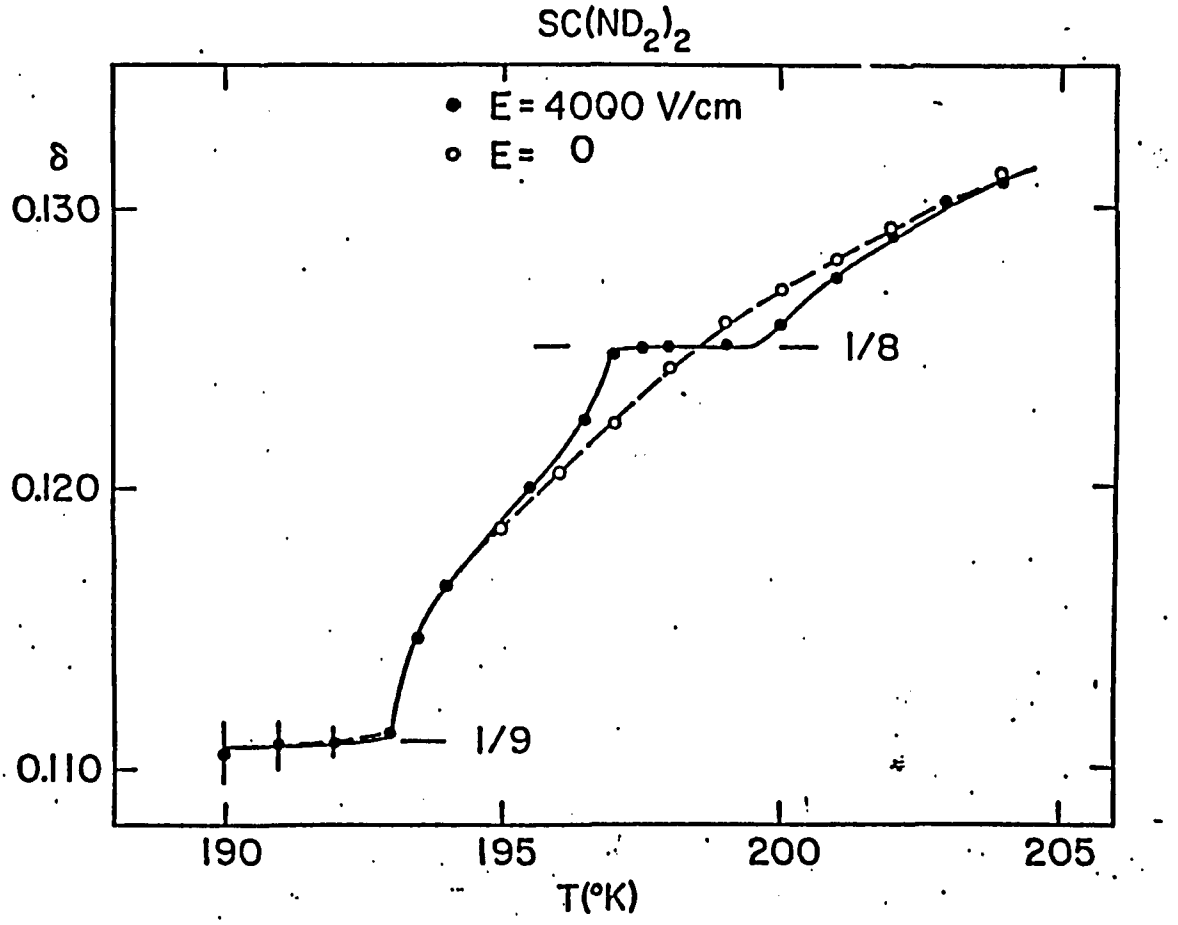

Fig.1.3. Modulation wavevector as a function of temperature with and without an external electric field (Moudden *et al* 1982).

I.1.2. Historical Review

a) Experimental studies

Ferroelectricity in thiourea was discovered by Solomon in 1956 [S5]. Since then, thiourea has been extensively studied by many groups all over the world. The experimental work is summarized here and then a brief review of the theories will be given.

(i) *Dielectric studies*

Goldsmith and White discovered a series of phase transitions in thiourea by dielectric constant measurements in 1959 [G1]. They found four dielectric anomalies in $\varepsilon_a(T)$ at 169K, 170.5K, 177K and 202K (see fig.1.4), and observed spontaneous polarizations along the a axis in two regions, one below 169K, the other between 176K and 180K. They analyzed the crystal structure at 120K by X-ray diffraction and explained the origin of the ferroelectric property in the lowest temperature phase. The anomaly at 202K was not understood until the discovery of the incommensurate structure by Futama *et al* in 1963 [F1][F2]. The small inflection at 170.5K is now understood to be caused by the $\frac{1}{9}$ lock-in transition. The anomaly near 177K is more complicated. It is believed to be related to the $\frac{1}{8}$ lock-in transition, but the transition mechanism is still not clear, and the existence of the transition in the absence of an applied electric field is a matter of ongoing controversy [M4][C1]. Goldsmith and White also measured the dielectric constant of deuterated thiourea and found that the anomalies are similar to those of the h-compound but the temperatures of the peak positions are shifted.

Gesi reexamined the dielectric anomaly near 177K with better temperature resolution in 1982 [G2]. He found that this anomaly consists of two peaks separated by a

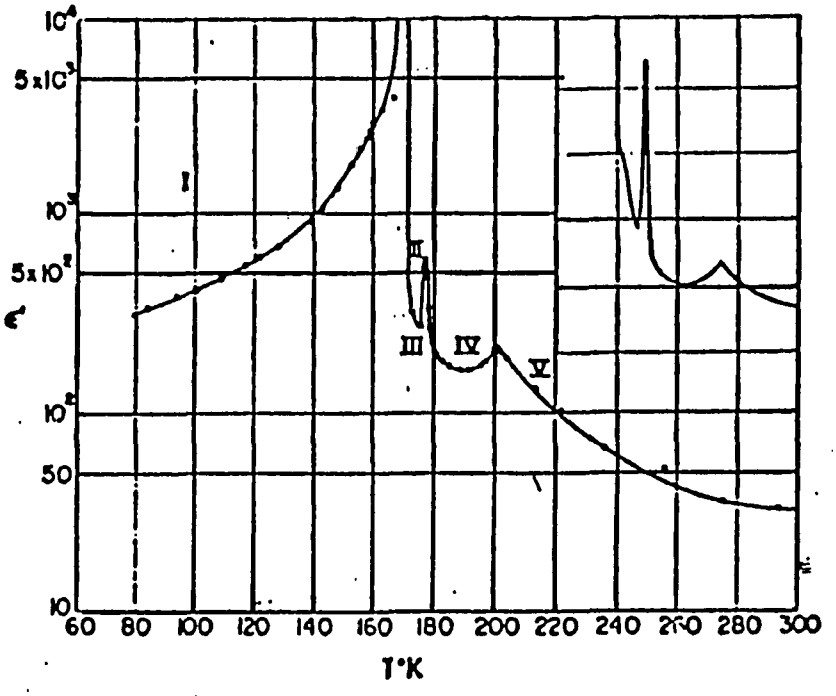

Fig.1.4. Dielectric constant of thiourea (Goldsmith and White 1959).

temperature interval $\Delta T \sim 0.5$K (for deuterated thiourea $\Delta T < 0.3$K). When a biasing E-field is applied, ΔT increases with E roughly obeying a square root law (see fig.1.5). Jamet *et al* performed similar experiments on deuterated thiourea [J1]. They proposed that the two peaks near 177K indicate the boundary of a $\frac{1}{8}$ ferroelectric lock-in phase, but this phase is induced by the external E-field. They interpretated the mechanism of this phase transition by a phenomenological model previously discussed by Denoyer *et al* [D6]. The free energy expansion contains a term $P_0 P^8(\mathbf{r})$ where P_0 is the homogeneous part of the electric polarization and $P(\mathbf{r})$ is the spatially varying part. This lock-in term leads to the $\frac{1}{8}$ ferroelectric phase transition. Assuming P_0 is proportional to the external E-field, the $\frac{1}{8}$ phase can be stable only in the presence of an E-field. However, one should be aware that, as shown by Gesi's experiment, $\Delta T \neq 0$ at zero bias E-field, especially for h-thiourea, which is in disagreement with the "field induced" interpretation.

Besides the anomalies at the phase transition points, the dielectric constant ε_a shows a sharp peak at 160K which does not correspond to any reported phase transition. Mckenzie and Dryden observed this peak in 1973 without suggesting any interpretation [M5]. Recently, Mashiyama *et al* reinvestigated this peak and studied the crystal structure in the related temperature region by X-ray scattering [M6]. They found that a number of discommensurations still remain after the final ferroelectric transition (i.e. $T < 169K$). They proposed that the interaction between discommensurations changes from oscillatory to exponential at $T_x = 160$K, which gives rise to the extra dielectric anomaly.

(ii) *X-ray diffraction and neutron scattering*

X-ray diffraction satellites characterizing the modulated structure of thiourea in the incommensurate phase were first observed by Futama *et al* in 1963 [F1][M7][F2].

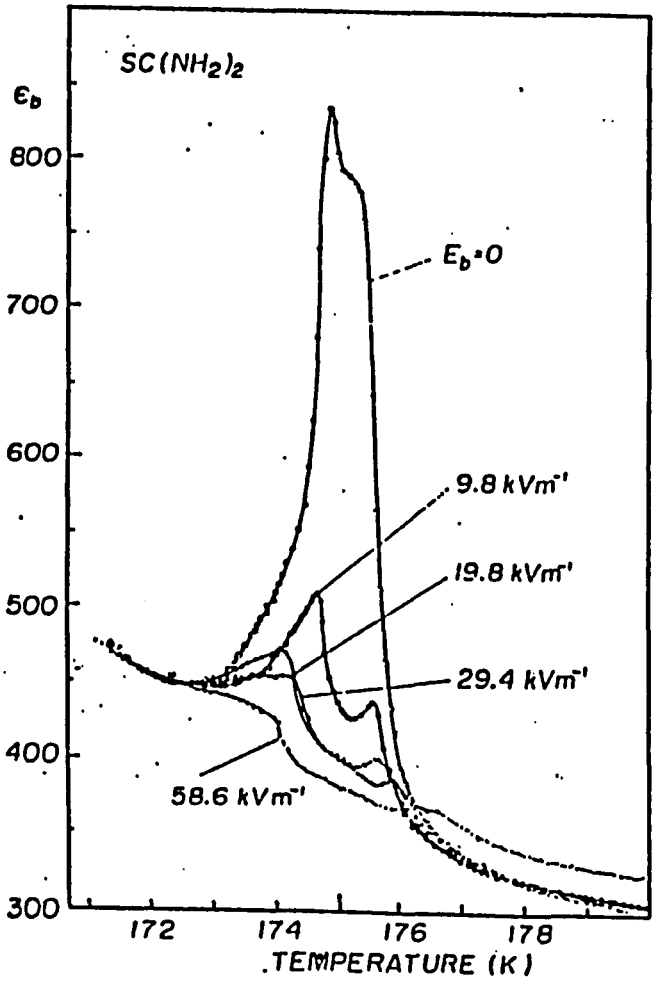

Fig.1.5. Dielectric constant of thiourea with different biasing E-fields (Gesi 1982).

They measured the temperature dependence of the satellite locations in the reciprocal space, described by Miller indices $(h, k+n\delta, l)$. It was found that δ decreases with decreasing temperature in the range from 202K to 169K [F2][T2]. It was shown that in first-order approximation the structural modulation could be described as condensed molecular displacements of τ_4 symmetry, varying sinusoidally in space with wavevector $\mathbf{q}_0$ [F3][S1][M1]. On the other hand, second and third order satellites with much weaker intensities were also observed. It was shown by Moudden *et al* that the higher order satellites arise not only from diffraction harmonics of a sinusoidally distorted lattice, but correspond to harmonics of the structural distortion itself [F2][M2]. After carefully analyzing the structure, Simonson *et al* found that the modulation should be more precisely described by a condensed τ_4 normal mode Q_{q_0} along with harmonics $Q_{2q_0}, Q_{3q_0}, \ldots$ [S2][S3][S4].

The $\frac{1}{9}$ commensurate lock-in structure has been observed by elastic neutron scattering [M2][D2][D3], and X-ray diffraction [T3]. However, no structural evidence was found for the existence of a $\frac{1}{8}$ lock-in phase from neutron scattering data. In 1982, Moudden *et al* measured the modulation wavevector in d-thiourea under E-fields [M3][G3] and observed the $\frac{1}{8}$ commensurate lock-in when the applied E-field along a was on the order of 1 $\frac{KV}{cm}$ (see fig.1.3). This result appears to support the "field induced" interpretation of the $\frac{1}{8}$ lock-in. On the other hand, Mashiyama *et al* recently measured the modulation wavevector of h-thiourea by X-ray diffraction and observed two weak inflections in the q_0 vs. T curve near 177K even without an E-field, which does not support the "field induced" idea [M8].

Thiourea has an unusual property that it is sensitive to X-ray damage. Moudden *et al* observed higher order commensurate lock-ins such as $\frac{2}{15}$, $\frac{4}{29}$ and $\frac{6}{43}$ in their

high field X-ray diffraction measurements [M9][M10]. Subsequent neutron scattering measurements proved that the extra commensurate lock-ins reported by Moudden *et al* were caused by the X-ray beam itself (radiation damage and defect-induced memory effects).

In the area of dynamic properties of thiourea, softening of the τ_4 branch has been observed by inelastic neutron scattering [M9][M10]. A distinct minimum was found near 0.15 b^* which decreases with decreasing temperature so that the normal to incommensurate phase transition in thiourea is considered as a soft-mode driven transition (displacive type). However, due to the fact that there are several interacting phonon branches below 1THz, and some of them are heavily damped, the study of low frequency lattice dynamics is fairly complicated (see fig.1.6).

(iii) *Raman and infrared spectroscopy*

The amplitudon in thiourea has been studied by Raman scattering by several groups [B1][C2][S6][W2]. The frequency of the amplitudon increases with decreasing temperature obeying a square root law, and can be adequately described by mean field theory [C2]. The intensity also increases with decreasing temperature, but it has not been quantitatively studied yet, presumably because it is difficult to analyze the Raman data near T_I where the low-frequency amplitudon is overlapped by the Rayleigh wing [W2]. The linewidth of the amplitudon increases with increasing temperature and tends to diverge at T_I, in common with many other incommensurate materials (see fig.1.7) [L2]. The origin of this linewidth behavior has not been fully explained yet [L1][L2][S7]. The amplitudon becomes a polar mode in the lowest ferroelectric phase (IV) and L-T splitting has been observed [C2].

In the normal phase, the softening of a polar optic B_{3u} mode (the $q = 0$ mode on the soft τ_4 branch) was observed from room temperature down to T_I by Siapkas by infrared reflection spectroscopy [S6]. This B_{3u} mode does not go completely soft at T_I

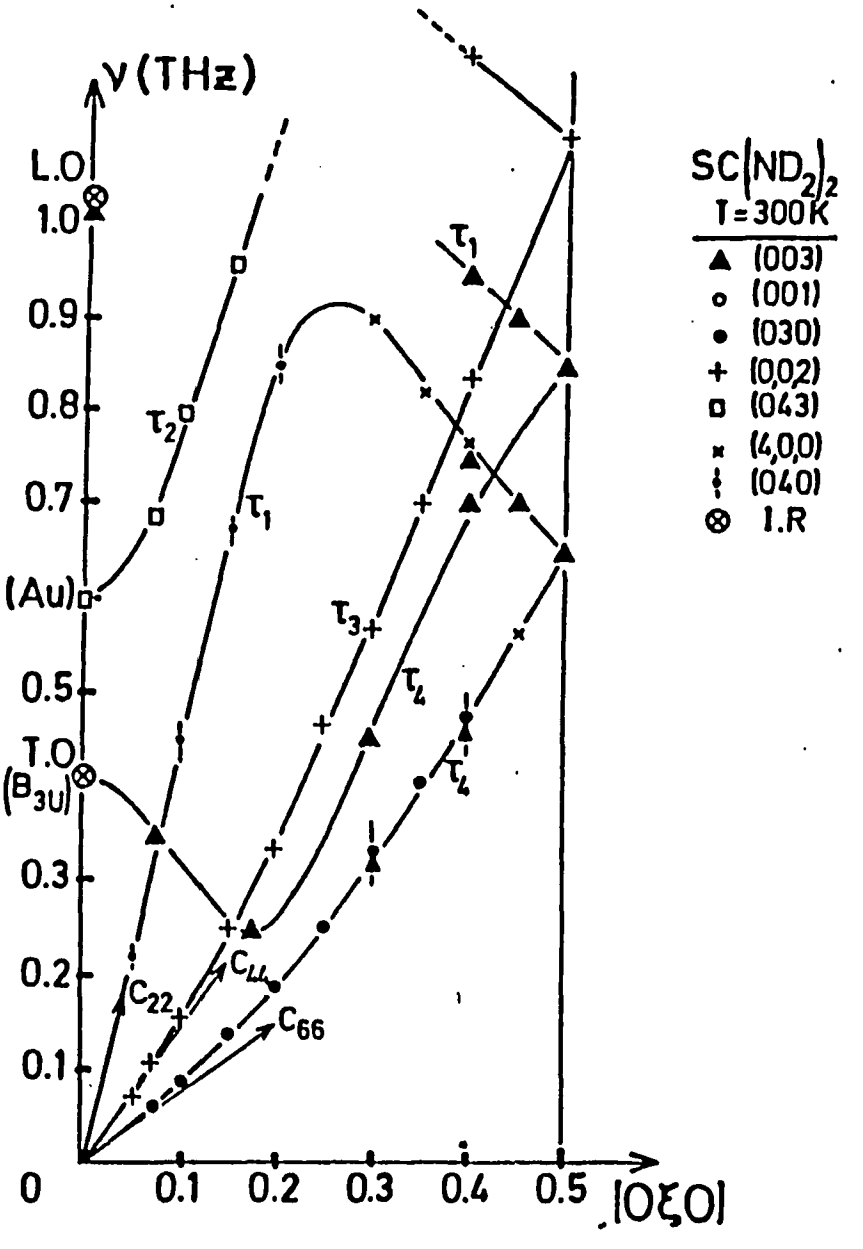

Fig. 1.6. Dispersion curves along the modulation direction at room temperature (Moudden 1980).

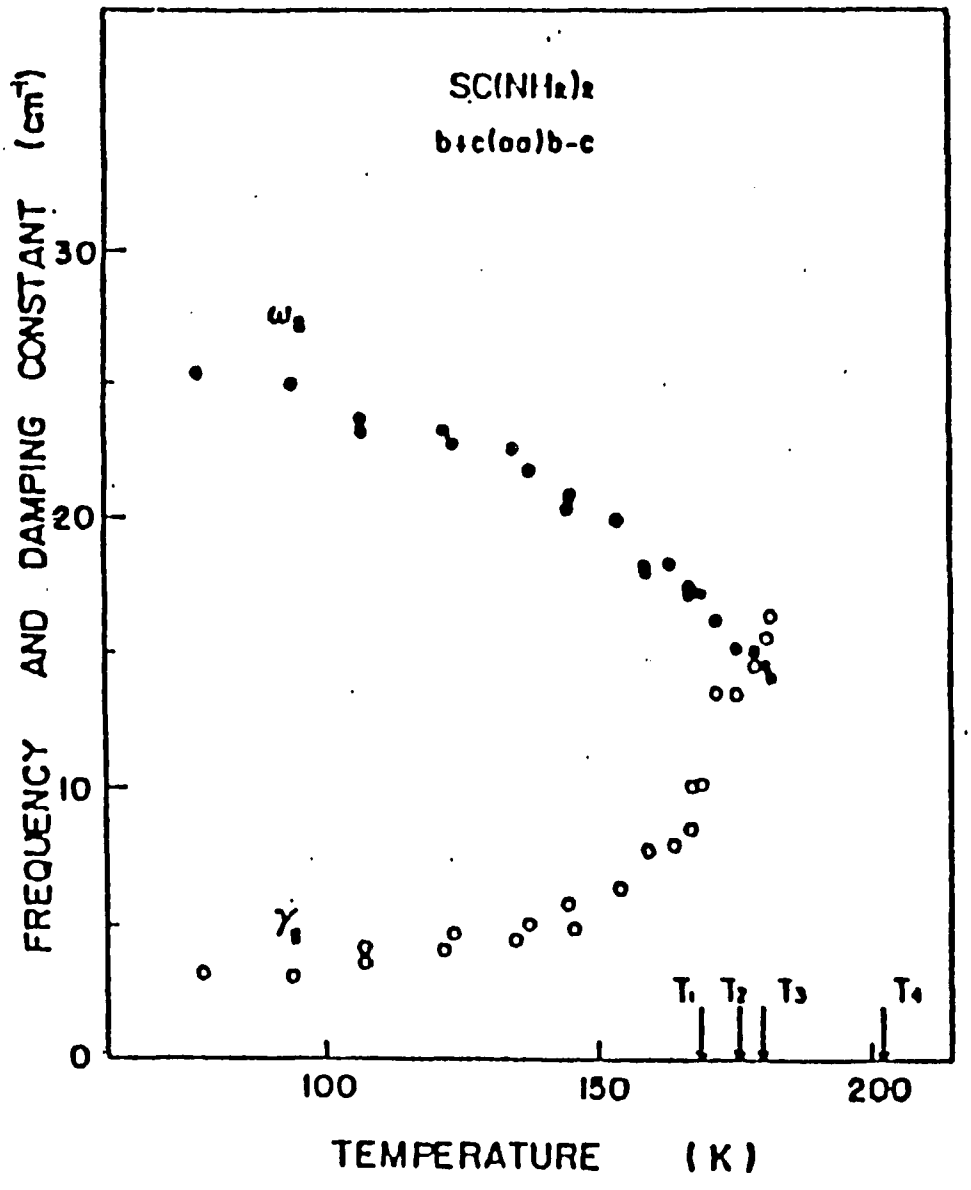

Fig.1.7. Frequency ω_S and damping constant γ_S of the amplitudon as a function of temperature. The solid circles represent ω_S and the open circles represent γ_S (Siapkas 1980).

because the minimum of the τ_4 soft branch is about $0.15b^*$ away from the Brillouin zone center.

(iv) *Optical birefringence measurements*

Optical birefringence measurements have been performed on both deuterated and normal thiourea [J2][B2][F3]. Jamet and his coworkers used optical birefringence to map out the (E-T) phase diagram of d-thiourea (see fig.1.8). They found that the temperature range of the modulated phases decreases with increasing E-field and eventually vanishes for E > 2300 $\frac{V}{mm}$. The overall shape of the (E-T) phase diagram can be explained by the phenomenological Landau theory in terms of a simple form of the free energy initially proposed by Ishibashi and Shiba in 1978 [I1]. The basic idea is that a field term $-EP_0$ in the free energy stablizes states with large homogeneous polarization P_0 while another term $+P_0^2P_\delta^2$ increases the energy of states in which both P_0 and P_δ are non-zero (P_δ is the modulation amplitude).

Following the "field induced" idea proposed by Denoyer and Jamet *et al* , Barreto *et al* gave a semiquantitative description of the birefringence anomaly near the $\frac{1}{8}$ phase in d-thiourea. However, they noticed that from their free energy analysis, the predicted temperature interval of the $\frac{1}{8}$ phase would not be zero even in the absence of an external E-field, although it may be small [B2][L3].

(v) *Specific heat measurement*

The specific heat of thiourea was measured by Chang and Westrum in 1963 [C3]. Three distinct anomalies were observed (see fig.1.9). The specific heat shows a clear jump of about 1.17 $\frac{cal}{K\ mole}$ at the incommensurate transition point (202K). This step-like anomaly indicates that the phase transition is continuous. A small peak appears at 171K corresponding to the $\frac{1}{9}$ lock-in phase transition. A strong peak

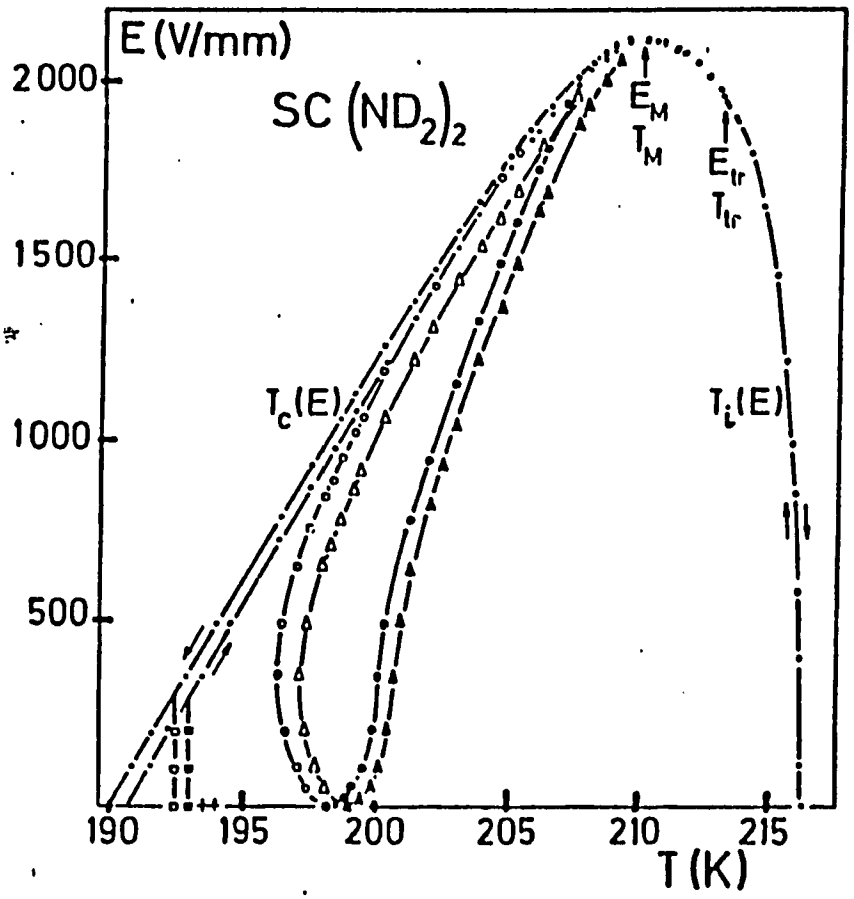

Fig. 1.8. (E-T) phase diagram measured from optical birefringence measurements (Barreto *et al.*1983).

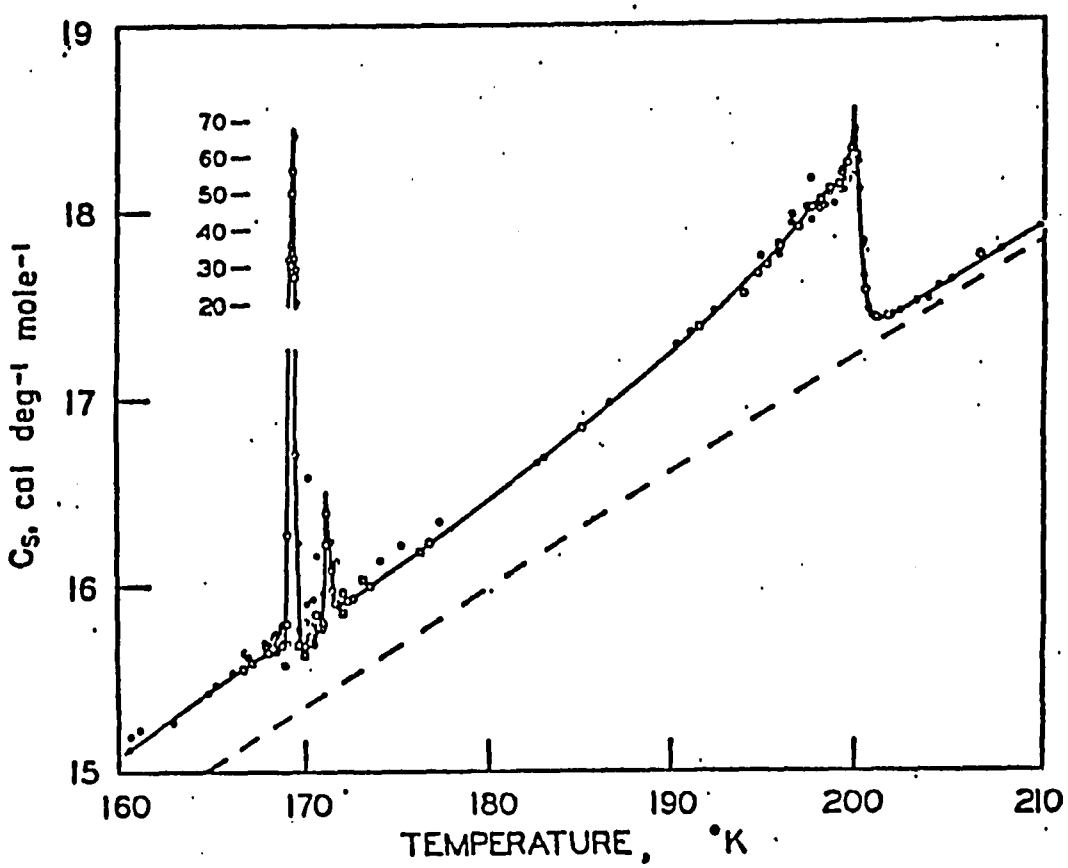

Fig.1.9. Specific heat of thiourea (Chang and Westrum 1963).

shows up at 169K indicating the first-order transition from the $\frac{1}{9}$ phase (III) to the final ferroelectric phase (IV). No anomaly was observed near 177K within their experimental accuracy. The specific heat with applied E-fields has not yet been measured.

(vi) *Elastic constant measurements by Ultrasonic and Brillouin scattering* [C1]

Benoit and Chapelle first measured the complete set of elastic constants of thiourea by Brillouin scattering [B3]. They observed discontinuities in C_{11} and C_{33} at T_I and T_c with a particularly strong anomaly in both the velocity and damping of the C_{33} mode near T_I, in agreement with previous ultrasonic measurements [T4]. This experiment was extended by Cao *et al* who investigated the dependence of C_{33} on scattering angle [C4]. They concluded that the anomaly comes from the coupling of the sound wave to a relaxing order parameter. Rehwald and Vonlanthen performed extensive ultrasonic measurements on thiourea which revealed anomalies in the shear elastic constants in addition to the major anomalies in C_{11} and C_{33} [R1]. They considered various coupling mechanisms involving amplitudons, phasons, and energy density fluctuations. Estimation of the relaxation times deduced from their data was in reasonable agreement with the Brillouin results.

(vii) *Effects of hydrostatic pressure*

Hydrostatic pressure produces dramatic effects on the modulated structure of thiourea. Early pressure investigations revealed the presence of a new phase above 2 *Kbar* [B4][G4][F4], which was later shown to be a $\frac{1}{3}b^*$ commensurate phase [K3][M11]. The dielectric constant ε_a as a function of temperature and pressure was measured by Gesi in 1969, and by Klimowski *et al* in 1976 [G4][K4]. It was found that T_I and T_c both decrease with increasing pressure and the $\frac{1}{9}$ and $\frac{1}{8}$ commensurate lock-ins disappear above 1 *Kbar*.

The modulated structure under pressure below 2*Kbar* was not clear until neutron diffraction measurements were performed by Denoyer *et al* in 1981 and 1982 [D6][D7]. The modulation wavevector q_0, which is always less than $\frac{1}{7}b^*$ at atmospheric pressure, increases with pressure and becomes greater than $\frac{1}{7}b^*$ in some region of the (P-T) phase diagram. A pressure-induced $\frac{1}{7}$ lock-in phase has been observed in the temperature range between 205K and 156K. The (P-T) phase diagram is shown in fig.1.10 [D7].

(viii) *Defect density wave and memory effect*

The memory effect in thiourea was discovered by Jamet and Lederer in 1983 [J3]. If thiourea is cooled with an interruption at a temperature T_m within the modulated phases for some time (ranging from a few minutes to a few hours), when the crystal is subsequently reheated through the "write up" temperature T_m, an anomaly is observed in the dielectric constant or birefringence. This memory effect can be understood as the result of the interaction between the modulated dipolar potential of the lattice and the mobile impurities or defects [L3][J5]. During the period of temperature stablization at T_m, the extrinsic defects or impurities with high mobility can relax in the modulated dipolar field. If a sufficient number of impurities exist with relaxation times shorter than the temperature stablization time, the incommensurate modulation wavevector $q_0(T_m)$ will be "written" on the impurity concentration, which forms a defect density wave. On heating, when the structural modulation wavevector passes through the wavevector of the defect density wave ("locked" at the earlier time), the anomaly shows up. Jamet and Lederer also found that the strength of the memory effect can be enhanced by using a longer stablization time, which indicates the importance of the low-mobility defects [J4].

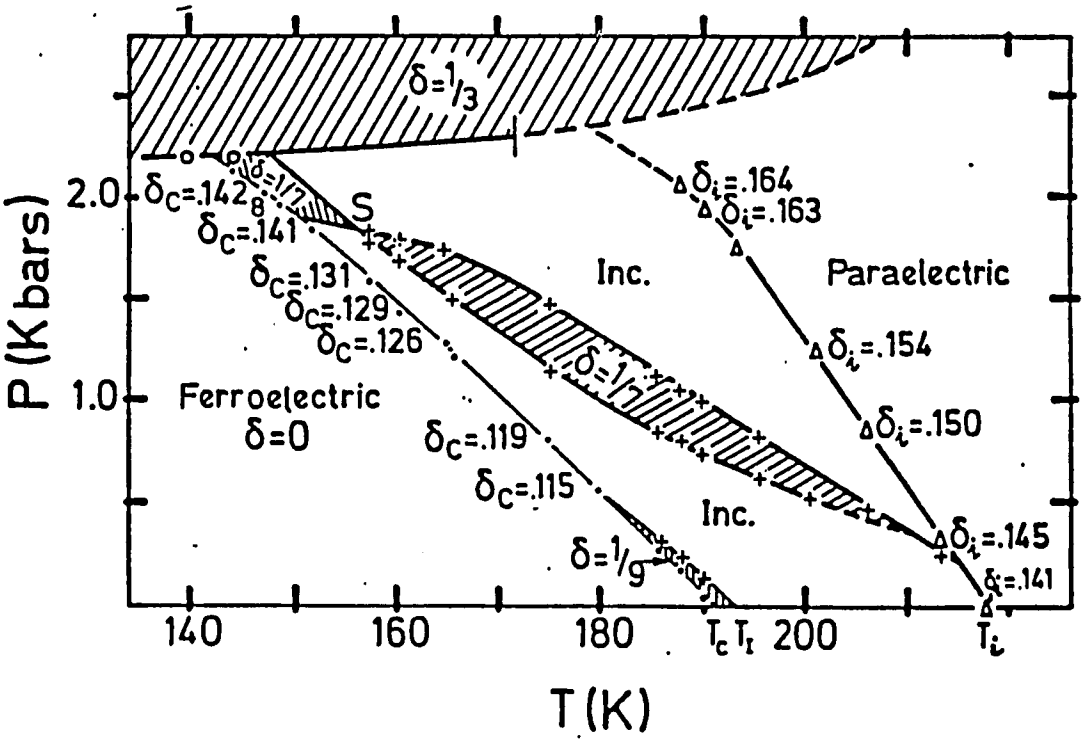

Fig.1.10. (P-T) phase diagram of thiourea. The hatched areas correspond to commensurate phases (Denoyer *et al* 1982).

b) Theories

There have been several theoretical models developed to study the successive phase transitions in thiourea. The one most commonly used is a phenomenological Landau theory initially proposed by Ishibashi and Shiba for $NaNO_2$ and thiourea in 1978 [I1]. They started with a free energy expansion as a functional of the order parameter P_x and its spatial derivatives (see section I.2.1),

$$F_B = \frac{1}{V}\int dV\left[\frac{1}{2}AP_x^2+\frac{1}{4}BP_x^4+\frac{1}{2}\alpha\left[\frac{dP_x}{dy}\right]^2+\frac{1}{4}\beta\left[\frac{d^2P_x}{dy^2}\right]^2+\gamma\left[P_x\frac{dP_x}{dy}\right]^2\right], \qquad (1.1)$$

The sign of the coefficient α is chosen negative so that the free energy will have a minimum at a finite modulation wavevector. The last term couples the modulation wavevector to the modulation amplitude and results in the temperature dependence of the wavevector q_0 of the structural distortion. This term also plays an important role when the structural modulation is deformed from the single plane wave, which explains the increase of the dielectric constant near T_c in thiourea and $NaNO_2$. The free energy (1.1) is directly applicable to $NaNO_2$ which does not have commensurate lock-in phases. Although it also explains many physical properties related to the phase transitions in tiourea [I2][C5], it must be supplemented with additional lock-in terms to explain the commensurate lock-in transitions.

To discuss the mechanism of the commensurate lock-in transitions in thiourea, Denoyer *et al* considered the possible lock-in terms in the free energy expansion [D7] (Their approach was similar to the discussion of the Umklapp terms in the case of K_2SeO_4 by Iizumi *et al* [I3]). Based on the space group symmetry consideration, they discussed the possible commensurate lock-in phases and explained the $\frac{1}{3}$, $\frac{1}{7}$ and $\frac{1}{9}$ lock-in transitions observed in their neutron scattering experiments (under pressure).

They also proposed that the existence of an external E-field can cause an 8th-order lock-in term to be allowed by the symmetry and to lead to a $\frac{1}{8}$ lock-in transition. A detailed discussion of the free energy of thiourea with Umklapp lock-in terms has been given by Lederer *et al* and Denoyer *et al* [L3][D4].

Before Ishibashi and Shiba's approach, a different type of free energy expansion was proposed by Levanyuk and Sanikov in 1976 [L4][S8]. They constructed a Lifshitz gradient invariant term of the form $(\xi\frac{\partial P}{\partial y}-P\frac{\partial \xi}{\partial y})$ to explain the incommensurate structure formation , where P is the order parameter and ξ corresponds to another normal mode such as acoustic shear wave with the same transformation properties as $\frac{\partial P}{\partial y}$. However, as pointed out by Levanyuk [L5], this model is not very fruitful because it provides no additional information beyond the simpler model proposed by Ishibashi and Shiba.

A microscopic model describing the successive phase transitions in deuterated thiourea has been developed by Parlinski and Michel [P1] and Parlinski [P2]. They modeled the crystal structure by a discrete one-dimensional chain of molecules and constructed the corresponding free energy in terms of orientational displacements of the molecules in the successive planes perpendicular to the chain. Taking into account the intermolecular interaction up to nine neighbors and the coupling between different harmonics, they worked out a numerical solution of the model and an analytical solution under the plane wave approximation. By properly selecting the model parameters, they could explain the successive phase transitions. As a result of their theory, the $\frac{1}{7}$, $\frac{1}{8}$ and $\frac{1}{9}$ commensurate lock-in phases are all mainly produced by third-order Umklapp terms, and the $\frac{1}{8}$ lock-in phase is a narrow one with ferroelectricity. Furthermore, they discussed the effect of an external E-field and

sketched out the (E-T) phase diagram. In their model, the Umklapp term leading to the $\frac{1}{8}$ lock-in phase transitions does not require the presence of an E-field; the $\frac{1}{8}$ ferroelectric lock-in phase can exist even in the absence of an external electric field.

I.1.3. Current Research

Although thiourea has been the subject of extensive studies for over thirty years, there are still some unresolved problems which need additional research. We are mainly interested in the mechanism of the $\frac{1}{8}$ ferroelectric lock-in transition. We have carried out an experimental dielectric and spontaneous polarization study and a theoretical analysis based on the Landau phenomenological theory.

We started with the free energy expansion proposed by Ishibashi and Shiba [11] plus the lock-in terms allowed by symmetry, and used our experimental data along with published data by other groups to determine the coefficients in the free energy expansion, and obtained the phase diagram by minimizing the free energy. In particular, we calculated the temperature width of the $\frac{1}{8}$ ferroelectric phase with and without an external E-field and determined the field-induced region and the intrinsic region respectively. The conclusion of our theoretical study is that the temperature interval of the intrinsic $\frac{1}{8}$ phase is non-zero, about $0.5\,K$. Furthermore, to explain the dielectric anomalies near the $\frac{1}{8}$ and the final ferroelectric phase transitions, we went beyond the single plane wave approximation in describing the structural modulation and obtained predictions for the dielectric anomalies consistent with our experimental observations. We also carried out a theoretical analysis for the phase-mode dynamics in the constant-amplitude continuum approximation and qualitatively explained the observed slowing-down of dielectric relaxation processes near the upper and lower transition points of the $\frac{1}{8}$ phase.

We have measured the real and imaginary part of the dielectric constant along the a axis between room temperature and liquid nitrogen temperature. To clarify the

origin of the $\frac{1}{8}$ lock-in phase, we examined the effects of both the measuring and biasing fields (down to very low levels $\sim 20\frac{mV}{cm}$ so that the (E-T) phase diagram near the $\frac{1}{8}$ region could be mapped out. In order to have a clearer picture of the nature of this transition, we also analyzed the frequency dependence of the dielectric constant near the transition points.

It is well known that D-E dielectric hysteresis loops are different in an intrinsic ferroelectric material than in a field-induced one [D8][G1]; the former are single loops while the latter are double loops. Therefore, we set up a computerized Sawyer-Tower circuit [S9] to observe the D-E hysteresis loops and to measure the spontaneous polarization.

Although both our theoretical and experimental studies lead to the conclusion that the $\frac{1}{8}$ ferroelectric lock-in phase is intrinsic in a finite temperature range, we are still unable to confirm it by other experimental evidence that does not involve an external E-field, which would definitely resolve the controversy about the origin of the $\frac{1}{8}$ phase.

Chapter I.2

Landau Theory of the Phase Transitions of Thiourea

I.2.1. Base Form of the Free Energy

The Landau theory of phase transitions consists of constructing a free energy expansion as a functional of the order parameter $P_x(y)$ and its spatial derivatives. As far as the basic phase transition features are concerned, thiourea is considered as similar to $NaNO_2$ although $NaNO_2$ does not have commensurate lock-in phases in the modulated state. Actually, the commensurate lock-in transitions in thiourea have much weaker effects on physical quantities than the final ferroelectric lock-in [D4][L3]. Therefore, it is reasonable to construct the free energy in two parts: the first part describes the basic features of the overall Normal-Incommensurate-Ferroelectric transitions; The second part contains the higher-order lock-in terms and gives rise to the commensurate lock-in transitions within the modulated state. For convenience, we will designate the free energy without lock-in terms as the **base form** of the free energy.

Following Ishibashi and Shiba [I1] and Denoyer and Currat [D4], the base form free energy functional can be written as

$$F_B = \frac{1}{V}\int dV\left[\frac{1}{2}AP_x^2+\frac{1}{4}BP_x^4+\frac{1}{2}\alpha\left[\frac{dP_x}{dy}\right]^2+\frac{1}{4}\beta\left[\frac{d^2P_x}{dy^2}\right]^2+\gamma\left[P_x\frac{dP_x}{dy}\right]^2\right], \qquad (1.1)$$

where

$$A = a(T-T_0). \qquad (1.2)$$

a, B, β, γ are positive constants and α is a negative constant. T_0 is the virtual para-ferroelectric transition temperature.

(1.1) is considered to be the simplest possible expression of the base form of the free energy. In order to explain the overall N-Inc-F transitions, every term in (1.1) must be included. The first two terms, representing the basic idea of Landau theory of second-order phase transitions, lead to a homogeneous structural distortion. The other terms containing spatial derivatives of the order parameter are required to explain the temperature-dependent incommensurate structural modulation. The third term $\left[\frac{dP_x}{dy}\right]^2$ represents the interaction between nearest neighbor planes and the fourth term $\left[\frac{d^2P_x}{dy^2}\right]^2$ includes the interaction between second nearest neighbor planes. This picture can be easily seen by changing the differential forms to difference forms. As we can see in the following discussion, the signs of α and β force the free energy to have a minimum at finite (generally incommensurate) wavevector q_0, which explains the incommensurate structure formation [M12]. The last term $\left[P_x\frac{dP_x}{dy}\right]^2$ couples the modulation wavevector to the modulation amplitude so that the increase of the order parameter in the modulated phases makes q_0 vary continuously with temperature.

As suggested by Birman, a term $P_x\frac{\partial^2 P_x}{\partial y^2}$ is allowed by the symmetry and is not of higher order [B11]. Under a first-order approximation (IPW), which will be discussed in the next section, this term can be renormalized into the third term in (1.1) and has no extra contribution. Beyond the IPW approximation, it is not clear that the effects of this term can be absorbed into the terms presenting in (1.1). However, since our aim is to construct a simplest possible free energy expression to explain the phase transitions, we will only consider the terms that are necessary to produce the structural changes. Term $P_x\frac{\partial^2 P_x}{\partial y^2}$, as well as the sixth- and eighth-order terms will be

neglected.

In thiourea, the order parameter characterizing the structural phase transitions is the x-component of the electric polarization:

$$P_x(y) = P_0 + P(y). \tag{1.3}$$

The uniform part P_0 represents the spontaneous polarization in the ferroelectric phases and the spatially varying part $P(y)$ represents the structural distortion in the modulated phases. Several different models have been proposed to describe the form of the structural modulation. We will start with a simple one, the incommensurate plane wave (IPW) approximation.

I.2.2. Incommensurate Plane Wave Approximation

a) The Structural Distortion

An arbitrary structural distortion in a crystal can be described in terms of a normal mode expansion. i.e,

$$P_x(y) = \sum_{\sigma,q} Q_{\sigma q} e^{iq\cdot r}, \tag{1.4}$$

where σ is the branch index of the normal mode $Q_{\sigma q}$ and q is the wavevector. A careful structural analysis has been carried out by Simonson *et al* [S2,S3,S4] by neutron scattering experiments. They found that the structural distortion in the modulated phases can be described by a condensed τ_4 mode with a temperature-dependent wavevector $q_0(T) = \delta(T)b^*$ along with higher-order harmonics. As a first order approximation, we only keep the primary mode and write down the order parameter as:

$$P_x(y) = Q_0 + Q_{q_0} e^{iq_0 y} + Q_{-q_0} e^{-iq_0 y}, \tag{1.5}$$

The condition that $P_x(y)$ is real requires that

$$Q_{-q_0} = Q^*_{q_0}. \tag{1.6}$$

Writing

$$Q_{q_0} = |Q_{q_0}| \, e^{i\phi_0} \tag{1.7}$$

and

$$\eta = \langle |Q_{q_0}| \rangle \tag{1.8}$$

$$\eta_0 = \langle |Q_0| \rangle \tag{1.9}$$

where the bracket <> stands for expectation value, we have

$$\begin{aligned} P_x(y) &= Q_0 + Q_{q_0} e^{iq_0 y} + Q^*_{q_0} e^{-iq_0 y} \\ &= \eta_0 + 2\eta \cos(q_0 y + \phi_0). \end{aligned} \tag{1.10}$$

Therefore, the structural distortion in the modulated phases is approximately described by a pure sinusoidal form, which is known as the IPW (incommensurate plane wave) approximation.

b) The Normal-Incommensurate-Ferroelectric transitions

Substituting eq.(1.10) into eq.(1.1) yields:

$$F_B = \frac{1}{2}A\eta_0^2+\frac{1}{4}\beta\eta_0^4+(A+\alpha q_0^2+\frac{1}{2}\beta q_0^4)\eta^2+(\frac{3}{2}B+2\gamma q_0^2)\eta^4+(3B+2\gamma q_0^2)\eta_0^2\eta^2. \tag{1.11}$$

Minimizing F_B with respect to η_0, η and q_0,

$$\frac{\partial F_B}{\partial \eta_0} = 0 \tag{1.12}$$

$$\frac{\partial E_B}{\partial \eta} = 0 \tag{1.13}$$

$$\frac{\partial F_B}{\partial q_0} = 0 \tag{1.14}$$

leads to

$$\eta\left[A+\alpha q_0^2+\frac{1}{2}\beta q_0^4+(3B+4\gamma q_0^2)\eta^2+(3B+2\gamma q_0^2)\eta_0^2\right] = 0 \tag{1.15}$$

$$\eta_0\left[A+B\eta_0^2+2(3B+2\gamma q_0^2)\eta^2\right] = 0 \tag{1.16}$$

$$q_0\eta^2\left[\alpha+\beta q_0^2+2\gamma(\eta^2+\eta_0^2)\right] = 0. \tag{1.17}$$

The three possible solutions of eqs(1.15)-(1.17) are:

(i). *Normal Phase.*

$$\eta_0 = 0 \tag{1.18}$$

$$\eta = 0. \tag{1.19}$$

The minimized free energy is

$$F_B^N = 0. \tag{1.20}$$

When the temperature is lowered the normal phase becomes unstable at

$$T_I = T_0+\frac{\alpha^2}{2a\beta}, \tag{1.21}$$

where the crystal undergoes a second-order phase transition to the incommensurate state. The corresponding solution is:

(ii). *Incommensurate Phase*

$$q_0^2(T) = \frac{1}{3}\left[(q_i^2 - \frac{3B}{2\gamma}) + \sqrt{(\frac{3B}{2\gamma}+2q_i^2)^2 + \frac{6a}{\beta}(T-T_1)}\right] \tag{1.22}$$

$$\eta^2(T) = \frac{\beta}{2\gamma}[q_i^2 - q_0^2(T)] \tag{1.23}$$

$$\eta_0 = 0, \tag{1.24}$$

where q_i is the incommensurate modulation wavevector at $T = T_1$:

$$q_i = \sqrt{\frac{-\alpha}{\beta}} \tag{1.25}$$

From (1.19) and (1.20) it is easily seen that the modulation wavevector decreases with decreasing temperature while the modulation amplitude increases with decreasing temperature, which agrees with experimental results [D4].

The minimized free energy in the incommensurate phase F_B^{Inc} is

$$F_B^{Inc} = -\frac{(A+\alpha q_0^2+\frac{1}{2}\beta q_0^4)^2}{6B+8\gamma q_0^2}. \tag{1.26}$$

where the modulation wavevector $q_0(T)$ is given by eq.(1.22). Forcing the modulation wavevector to deviate from q_0 to q_c would cost elastic energy (because of the gradient terms):

$$F_B(q_c) - F_B(q_0) = \frac{1}{2}\beta\eta^2(q_0^2 - q_c^2)^2. \tag{1.27}$$

The third solution to eqs.(1.15)-(1.17) is:

(iii). *Final ferroelectric phase*

$$\eta_0 = \sqrt{-\frac{A}{B}} \tag{1.28}$$

$$\eta = 0, \tag{1.29}$$

with minimized free energy

$$F_B^F = -\frac{A^2}{4B}. \tag{1.30}$$

When the temperature is lowered to $T = T_c < T_0$, $F_B^F(T)$ will cross $F_B^{Inc}(T)$. Since the curves cross with different slopes, the crystal undergoes a first-order transition to a

proper ferroelectric phase with spontaneous polarization η_0.

The minimized free energy as a function of temperature in the temperature range covering the N-Inc-F transition points obtained from numerical calculation is plotted in fig(1.11). The coefficients in the free energy expansion were determined from experimental results (see ch. I.5). The values of the coefficients used in all the numerical calculations in this chapter (ch.I.2) are listed in table 1.5.

It is clear that the base form of free energy expansion (1.1) explains the normal to incommensurate and incommensurate to final ferroelectric phase transitions. This model is sufficient to describe sodium nitrite which does not have $q_0 \neq 0$ commensurate lock-in phases. However, it cannot explain the $\frac{1}{9}$ and $\frac{1}{8}$ commensurate lock-in transitions in thiourea. For a quantitative discussion of the phase diagram of thiourea, we need to take the lattice periodicity into account and consider the lock-in terms in the free energy expression.

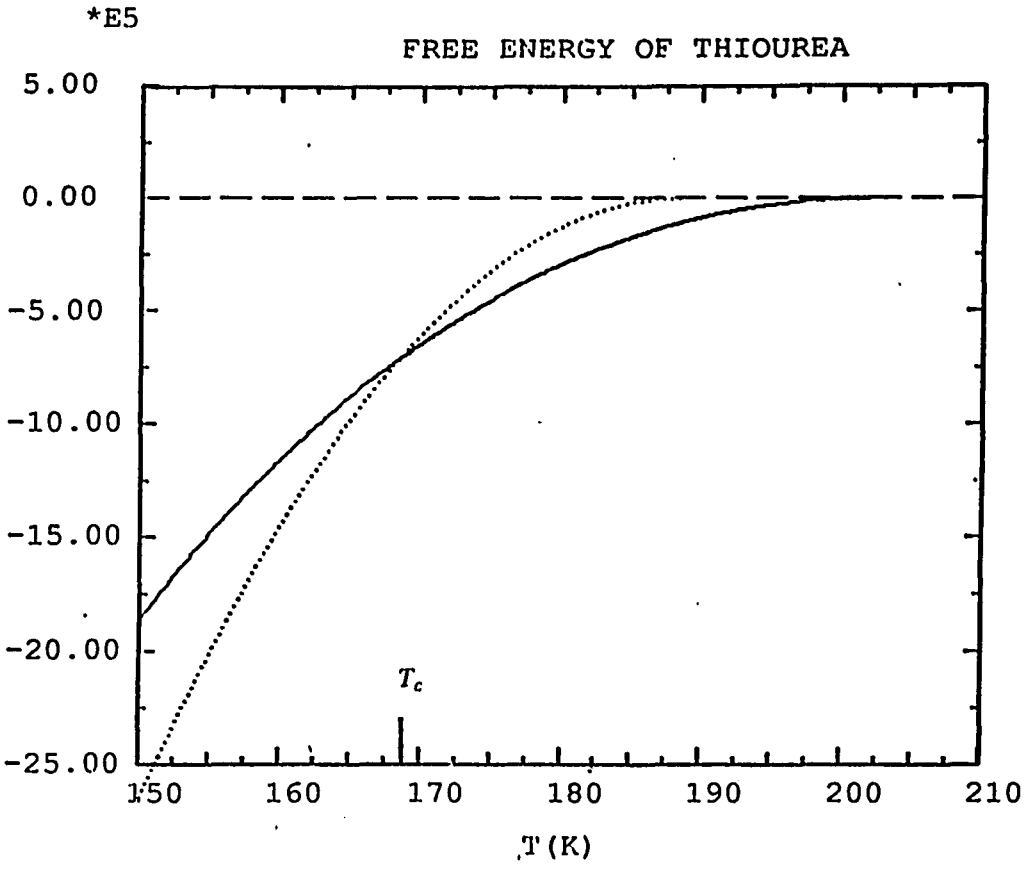

Fig.1.11. Minimized free energy vs. temperature (base form). Solid line: incommensurate solution. Dotted line: ferroelectric solution. The crossing point at T_c indicates the first-order final lock-in transition.

I.2.3. Umklapp Terms and the Phase Diagram

a) Commensurate lock-in transitions and Umklapp terms

A commensurate lock-in transition occurs as a consequence of the lattice translational periodicity [A2][C6]. In the framework of the Landau theory, the lock-in or Umklapp terms representing the periodic lattice potential lower the free energy when the modulation periodicity is commensurate with the lattice periodicity.

An Umklapp term that can be added to the free energy expansion (1.1) has the general form [L3]:

$$\Delta F_n = \frac{1}{V}\int dV\left[b_n P_x^n(y)\right]. \tag{1.31}$$

The complete form of the free energy is:

$$F = F_B + \sum_n \Delta F_n. \tag{1.32}$$

In terms of a normal mode expansion, ΔF_n can be expressed as

$$\Delta F_n = b_n \sum_{q_1 \cdots q_n} Q_{q_1} \cdots Q_{q_n} \Delta(q_1 + \cdots + q_n), \tag{1.33}$$

where the branch index has been suppressed since all the Q_{q_i} are on the same (τ_4) branch. The periodic delta function

$$\Delta(q_1 + \cdots + q_n) = \sum_G \delta(q_1 + \ldots + q_n + G) \tag{1.34}$$

(where G is a reciprocal lattice vector) insures translational symmetry.

Under the IPW approximation (1.10), the structural modulation is described by a sinusoidal wave with a single q_0. Thus,

$$\begin{aligned}\Delta F_n &= b_n (Q^n_{q_0} + Q^{*n}_{q_0}) \Delta(n q_0) \\ &= 2 b_n \eta^n \cos(n\phi_0) \Delta(n q_0).\end{aligned} \tag{1.35}$$

To minimize the free energy (1.32), the initial phase ϕ_0 can be properly chosen so that

$$b_n \cos(n\phi_0) = -|\, b_n \,| \,.$$
$$\Delta F_n = -2|\, b_n \,|\, \eta^n. \qquad (1.36)$$

From (1.36), it is clear that the Umklapp term lowers the free energy of the commensurate solution by an amount on the order of η^n. On the other hand, forcing the modulation wave to be commensurate costs elastic energy because of the gradient term in the free energy [A2] (see eq.1.27). A first-order incommensurate-commensurate transition occurs when the elastic energy cost is offset by the "lock-in" energy of the Umklapp term [B4]. i.e.

$$F_B(q_c)+\Delta F_n(q_c) < F_B(q_0). \qquad (1.37)$$

In principle, the detailed phase diagram within the plane wave approximation can be worked out by taking into account all the lock-in terms allowed by symmetry.

b) Possible commensurate wavevectors on the basis of symmetry considerations

One of the basic rules of Landau theory is that the free energy must be invariant under all the transformations of the space group of the crystal in the parent phase [L6]. Most potential Umklapp terms do not satisfy this invariance condition so that they are not allowed in the free energy expansion and play no role in the commensurate lock-in transitions. Therefore, it is very important to determine which Umklapp terms are allowed by symmetry and which are not. Such a symmetry invariant analysis of Umklapp terms for thiourea has been given by Denoyer and Currat [D4]. We will follow their approach.

In thiourea, the space group is D_{2h}^{16} (Pnma) and the order parameter in the modulated phases Q_{q_0} is of τ_4 symmetry with wavevector along the $\mathbf{b}^*$ direction. The transformation properties of the normal mode Q_{q_0} under the space group operations $\{S \mid V(S)\}$, which leave q_0 invariant, are expressed by

$$\{S \mid \mathbf{V}(S)\}Q_{\mathbf{q}_0} = \chi_S(\tau_4)e^{i\mathbf{q}_0\cdot\mathbf{V}(S)}Q_{\mathbf{q}_0} \tag{1.38}$$

$$S\ \mathbf{q}_0 = \mathbf{q}_0, \tag{1.39}$$

where the point group (group of $\mathbf{q}_0$) characters $\chi_S(\tau_4)$ are given in table 1.3.

table 1.3 Characters of irreducible representations of the group of $\mathbf{q}_0 = \delta\mathbf{b}^*$ in Pnma symmetry.

G_δ	$\{E \mid 0\}$	$\{C_{2y} \mid \frac{1}{2}\mathbf{b}\}$	$\{\sigma_z \mid \frac{1}{2}(\mathbf{a}+\mathbf{b}+\mathbf{c})\}$	$\{\sigma_z \mid \frac{1}{2}(\mathbf{a}+\mathbf{c})\}$
τ_1	1	1	1	1
τ_2	1	1	-1	-1
τ_3	1	-1	1	-1
τ_4	1	-1	-1	1

A necessary condition for an Umklapp term (1.33) to be invariant is

$$\{S \mid \mathbf{V}(S)\}Q^n_{q_c} = Q^n_{q_c}. \tag{1.40}$$

According to (1.38) with $nq_c = G$,

$$\{S \mid \mathbf{V}(S)\}Q^n_{q_c} = [\chi_S(\tau_4)]^n e^{i\mathbf{G}\cdot\mathbf{V}(S)}Q^n_{q_c}. \tag{1.41}$$

Let

$$\mathbf{G} = m\mathbf{b}^*, \tag{1.42}$$

then,

$$\mathbf{q}_c = \frac{m}{n}\mathbf{b}^*. \tag{1.43}$$

Thus, from (1.40) and (1.42),

$$[\chi_S(\tau_4)]^n e^{im\mathbf{b}^*\cdot\mathbf{V}(S)} = 1. \tag{1.44}$$

This condition is obviously satisfied for elements $\{E \mid 0\}$ and $\{\sigma_z \mid \frac{1}{2}(\mathbf{a}+\mathbf{c})\}$ (see table 1.3). However, for $\{\sigma_z \mid \frac{1}{2}(\mathbf{a}+\mathbf{b}+\mathbf{c})\}$ and $\{C_{2y} \mid \frac{1}{2}\mathbf{b}\}$ condition (1.44) reduces to

$$(-1)^{n+m} = 1. \tag{1.45}$$

Namely, n and m must have the same parity. All lock-in terms not satisfying (1.45)

are thus excluded by symmetry.

At atmospheric pressure, the variation range of the modulation wavevector in thiourea is from zero to q_i, where $q_i < \frac{1}{7}$. Therefore, we need only consider possible commensurate lock-in phases with wavevector $q_c < \frac{1}{7}b^*$.

According to condition (1.45), the 8th-order lock-in term ($n = 8$) is not allowed. Thus the lowest order lock-in term is ($n = 9$):

$$b_9(Q_{q_c}^9 + Q^{*9}_{q_c}) \qquad (q_c = \frac{1}{9}b^*). \tag{1.46}$$

This term leads to the $\frac{1}{9}$ lock-in transition which has been observed by experiments.

A 16th-order term

$$b_{16}(Q_{q_c}^{16} + Q^{*16}_{q_c}) \qquad (q_c = \frac{2}{16}b^*) \tag{1.47}$$

is allowed and can possibly cause an $\frac{1}{8}$ lock-in transition by lowering the free energy by an amount on the order of η^{16}, which is presumably much smaller than the 9th-order term (1.47). However, in addition to (1.46), ΔF_9 also contains a term

$$9b_9Q_0(Q_{q_c}^8 + Q^{*8}_{q_c}) \qquad (q_c = \frac{1}{8}b^*) \tag{1.48}$$

which is allowed by the symmetry requirements and can also lead to an $\frac{1}{8}$ lock-in. After eliminating Q_0 by minimizing the free energy with respect to Q_0, the term (1.48) turns out to be effectively a 16th-order term (see the following derivation). However, it is reasonable to assume that it has a much stronger effect than (1.47) because $9b_9$ is presumably much greater than b_{16}. Furthermore, the $Q_0Q_{q_c}^8$ coupling makes the $\frac{1}{8}$ lock-in phase ferroelectric, which agrees with experimental observation [G1]. Naturally, the term (1.48) will become more important when an external electric field is applied. An E-field will increase Q_0 (electric polarization) and make (1.48)

act as an effective 8th-order term.

As mentioned in the introduction, there has been a long-standing controversy about the origin of the $\frac{1}{8}$ ferroelectric lock-in phase. Based on the above discussion, it is possible that the term (1.48) is not negligibly small so that the $\frac{1}{8}$ ferroelectric lock-in phase exists in a finite temperature range even without the presence of an external E-field. Let us work out the phase diagram and then examine the effect of external E-fields.

c) The commensurate lock-in phases

(i) *The condition for commensurate lock-in transitions*

Taking into account the Umklapp terms (1.46), (1.47) and (1.48), the free energy can be written as:

$$F = F_B + 2b_9\eta^9\cos(9\phi_0)\Delta(9q_0) + 18b_9\eta_0\eta^8\cos(8\phi_0)\Delta(8q_0) + 2b_{16}\eta^{16}\cos(16\phi_0)\Delta(16q_0) \quad (1.49)$$

where the base form of free energy F_B has been given in eq.(1.1) and (1.11), and Umklapp terms beyond the $\frac{1}{8}$ and $\frac{1}{9}$ have been neglected.

In the modulated phases, the structural distortion is predominantly due to the spatially varying Q_{q_0} mode. The presence of a small η_0 in the $\frac{1}{8}$ phase is due to the $Q_0Q_{q_0}^8$ coupling. Our experimental results indicate that without an applied electric field the maximum value of η_0 in the modulated phases is $\leq 0.3\%$ of η. Therefore, it is reasonable to treat η_0 as a secondary parameter and eliminate it first. Minimizing the free energy (1.49) with respect to η_0 yields

$$\eta_0 = -\frac{18b_9\eta^8\cos(8\phi_0)}{A + B\eta_0^2 + (6B + 4\gamma q_0^2)\eta^2}\Delta(8q_0)$$

$$= -18b_9 R\eta^8\cos(8\phi_0)\Delta(8q_0), \tag{1.50}$$

where R is defined as

$$R = \frac{1}{A+B\eta_0^2+(6B+4\gamma q_0^2)\eta^2} \approx \frac{1}{A+(6B+4\gamma q_0^2)\eta^2}. \tag{1.51}$$

Then,

$$F = (A+\alpha q_0^2+\frac{1}{2}\beta q_0^4)\eta^2+(\frac{3}{2}B+2\gamma q_0^2)\eta^4+2b_9\eta^9\cos(9\phi_0)\Delta(9q_0)- -2R(9b_9)^2\eta^{16}\cos^2(8\phi_0)\Delta(8q_0)+2b_{16}\eta^{16}\cos(16\phi_0)\Delta(16q_0) \tag{1.52}$$

where $\frac{1}{4}B\eta_0^4$ is neglected.

Eq.(1.50) explains the fact that the $\frac{1}{8}$ commensurate lock-in phase is ferroelectric. When the modulation wavevector is exactly $\frac{1}{8}b^*$, the $Q_0Q_{q_0}^8$ coupling gives rise to a non-zero spontaneous polarization η_0, which has been observed in experiments.

To force the modulation wavevector from an incommensurate value q_0 to a commensurate value q_c costs elastic energy

$$F_B(q_c)-F_B(q_0) = (\alpha q_c^2+\frac{1}{2}\beta q_c^4)\eta^2+2\gamma q_c^2\eta^4-(\alpha q_0^2+\frac{1}{2}\beta q_0^4)\eta^2-2\gamma q_0^2\eta^4. \tag{1.53}$$

Generally, it costs less energy to deform the static modulation (e.g. changing the wavevector) than to change the amplitude of the distortion [A2][M13]. Thus it is reasonable to assume that a high-order Umklapp term could stablize a commensurate lock-in phase but will not change the temperature dependence of the modulation amplitude. Actually, it has been observed in many incommensurate materials that the modulation amplitude continues to vary with temperature in commensurate lock-in phases where the modulation wavevector is constant. That is why the same η was used for both $F_B(q_0)$ and $F_B(q_c)$ in eq.(1.53). Substituting (1.23) and (1.25) into (1.53) gives

$$F_B(q_c)-F_B(q_0) = \frac{1}{2}\beta\eta^2(q_0^2-q_c^2)^2 \tag{1.54}$$

This energy loss must be compensated by the "lock-in" energy of the Umklapp terms. i.e.,

$$-\Delta F_n(q_c) > \frac{1}{2}\beta\eta^2(q_0^2-q_c^2)^2 \tag{1.54}$$

This is the condition of stablizing a commensurate lock-in phase with modulation wavevector q_c.

(ii) *The* $\frac{1}{9}$ *commensurate lock-in*

For the $q_c = \frac{1}{9}b^*$ lock-in phase, condition (1.54) is:

$$2|b_9|\eta^9 > \frac{1}{2}\beta\eta^2(q_0^2-q_c^2)^2. \tag{1.55}$$

where we assume that $\phi_0 = 0$ and $b_9 < 0$ so that (1.36) holds. The temperature range satisfying (1.55) can be obtained by numerical analysis (see sec.I.5). The temperature-dependence $2|b_9|\eta^9$ and $\frac{1}{2}\beta\eta^2(q_0^2-q_c^2)^2$ are plotted in fig.1.12. The crossing points indicate the upper and lower boundary of the range of stability of the $\frac{1}{9}$ lock-in phase relative to the incommensurate phase:

$$T_9^+ = 170.6.K$$
$$T_9^- = 161.0K$$

In the temperature range $T_9^+ > T > T_9^-$, the free energy with $q_c = \frac{1}{9}b^*$ (including the $\frac{1}{9}$ lock-in term) is lower than the free energy with an incommensurate q_0 (see fig.1.12). That means the $\frac{1}{9}$ commensurate structure is preferred to the incommensurate one. However, since T_9^- is lower than the final ferroelectric phase transition point T_c, which is 168.7 K. T_9^- is not a real phase transition point. As shown in fig.1.13, the minimized free energy corresponding to the final ferroelectric phase crosses the free energy corresponding to the $\frac{1}{9}$ phase at 168.6K, where a first-order transition from the $\frac{1}{9}$ phase to the final ferroelectric phase occurs. Namely, the $\frac{1}{9}$ phase region is

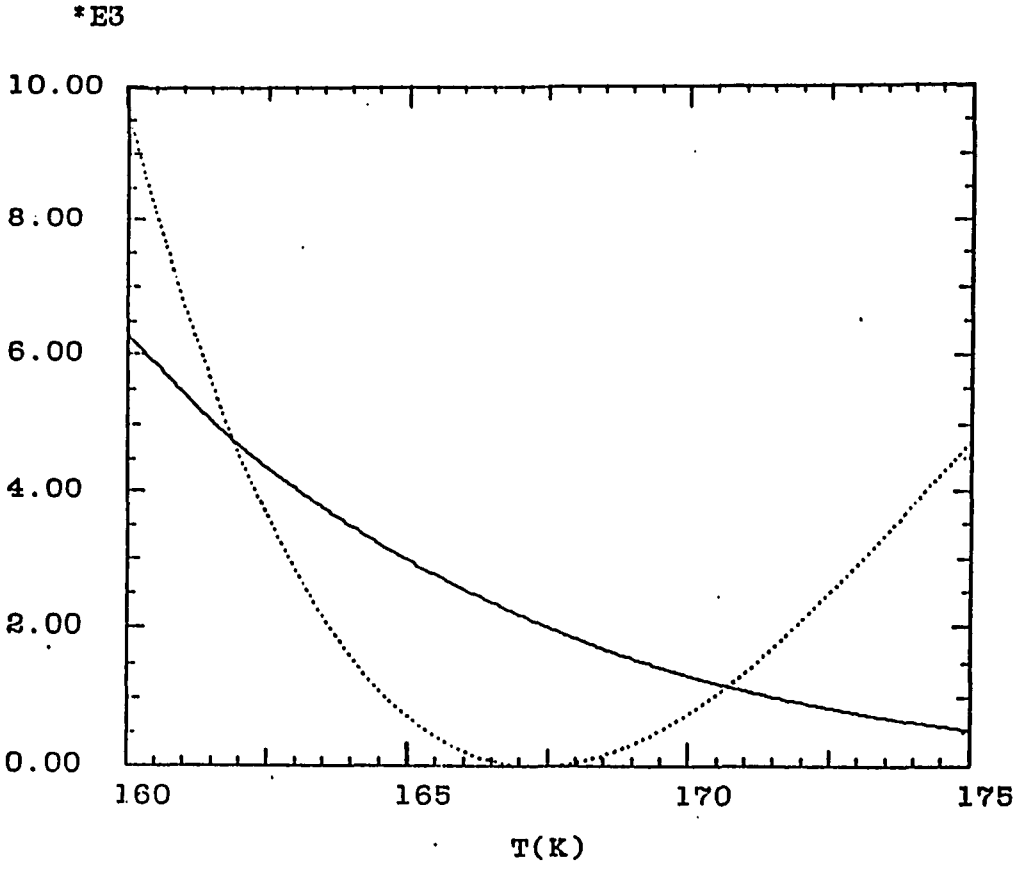

Fig.1.12. Solid line: the lock-in energy of the 1/9 Umklapp term. Dotted line: the elastic energy cost for the 1/9 commensurate lock-in.

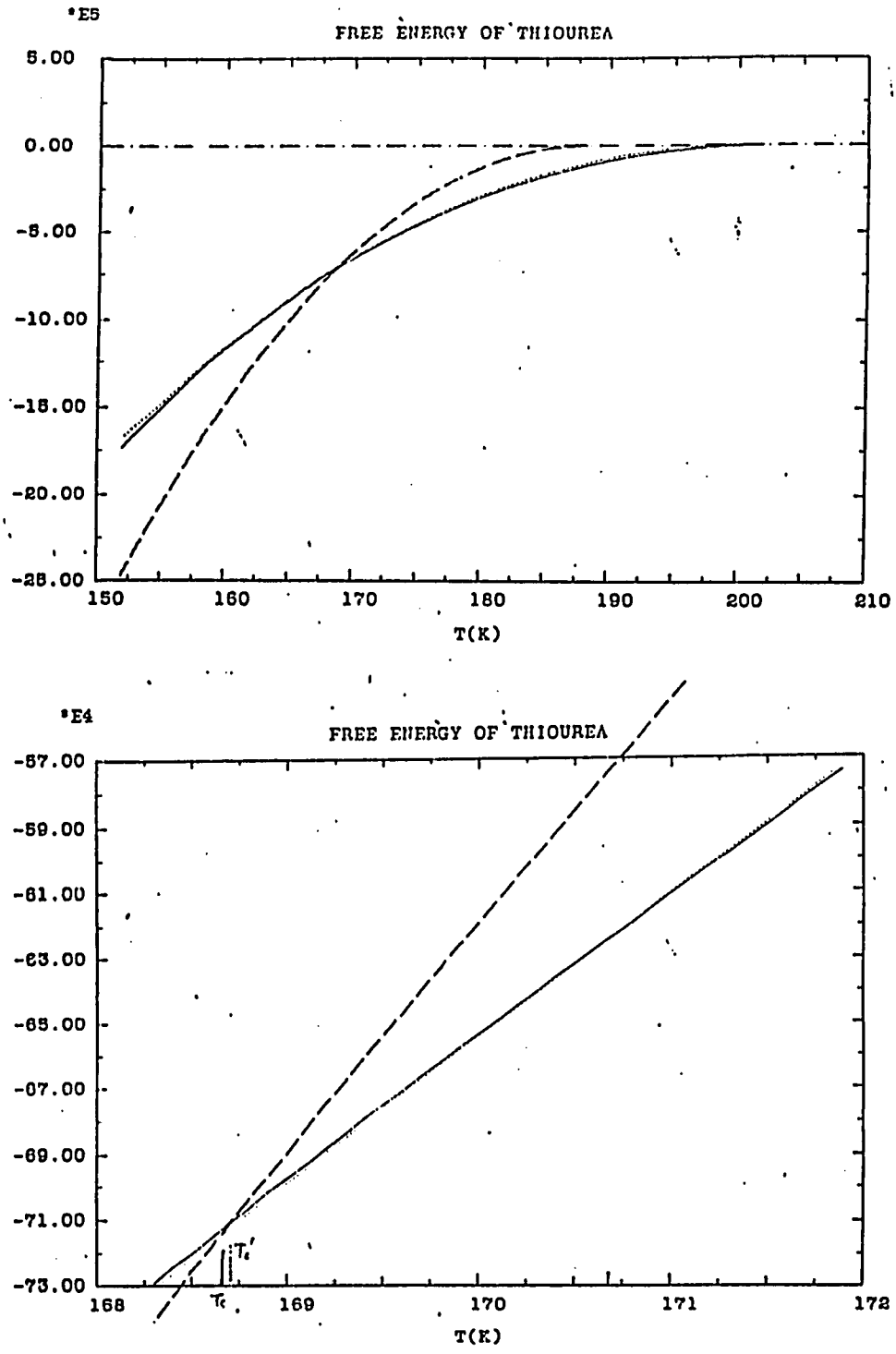

Fig.1.13. Free energy of thiourea. Solid line: incommensurate solution. Dotted line: 1/9 commensurate solution. Broken line: final ferroelectric lock-in phase.

between 168.6K and 170.6K, which is very close to experimental observations.

(iii) *The* $\frac{1}{8}$ *commensurate lock-in*

The last two terms in (1.52) can stablize a $\frac{1}{8}$ commensurate lock-in phase. ϕ_0 should be chosen as either 0 or $\frac{\pi}{8}$, corresponding to the two possible signs of the spontaneous polarization in (1.50), and b_{16} should be negative. Then, the condition for stablizing a $\frac{1}{8}$ lock-in phase is:

$$2R(9b_9)^2\eta^{16}+2|b_{16}|\eta^{16} > \frac{1}{2}\beta\eta^2(q_0^2-q_c^2)^2, \tag{1.56}$$

where $q_c = \frac{1}{8}b^*$.

Basically, the two terms on the left hand side of (1.56) are both responsible for the $\frac{1}{8}$ lock-in and could be renormalized as one 16th-order term. On the other hand, as shown in our numerical analysis, the coefficients of the free energy expansion decrease rapidly with increasing orders ($a^2 \gg B$, $B^2 \gg |b_9|$), which suggests that

$$2R(9b_9)^2 \gg 2|b_{16}|. \tag{1.57}$$

Assuming that the term $2R(9b_9)^2\eta^{16}$ plays the major role in stablizing the $\frac{1}{8}$ commensurate phase while the term $2|b_{16}|\eta^{16}$ makes a supplemental correction which will slightly increase the temperature interval of the $\frac{1}{8}$ phase, condition (1.56) can be approximated by:

$$2Rv^2\eta^{16} > \frac{1}{2}\beta\eta^2(q_0^2-q_c^2)^2, \tag{1.58}$$

where

$$v = \sqrt{(9b_9)^2+\frac{|b_{16}|}{R}} \approx -9b_9. \tag{1.59}$$

The value of v (> 0) can be determined from the spontaneous polarization meas-

ured in the $\frac{1}{8}$ phase along with the coefficients in the base form of the free energy (see eq.(1.50)). The temperature range of the $\frac{1}{8}$ phase can be obtained by numerically solving (1.58). The upper and lower transition temperatures are found to be (see fig.1.14):

$$T_{\frac{1}{8}}^{+} = 179.5K$$
$$T_{\frac{1}{8}}^{-} = 179.0K$$

Therefore, the predicted temperature interval of this $\frac{1}{8}$ ferroelectric phase is about $0.5K$, which certainly is experimentally measurable. However, the difference between the incommensurate wavevector and the commensurate wavevecotr $|q_0-q_c|$ at the transition temperatures is only about $3\times10^{-4}b^*$ (0.24% of q_c), which presumably is difficult to distinguish by neutron scattering experiments.

The free energy for the $\frac{1}{8}$ phase and the free energy for the incommensurate phase near the $\frac{1}{8}$ lock-in region are shown in fig.1.15. They cross at the transition points $T_{\frac{1}{8}}^{+}$ and $T_{\frac{1}{8}}^{-}$ with slightly different slopes, which indicates that the incommensurate to $\frac{1}{8}$ transition at $T_{\frac{1}{8}}^{+}$, and the $\frac{1}{8}$ to incommensurate phase transitions at $T_{\frac{1}{8}}^{-}$ are both weakly first order.

d) (E-T) phase diagram near the $\frac{1}{8}$ lock-in region

In the above analysis, we have shown that the $\frac{1}{8}$ ferroelectric phase should be intrinsic in a non-zero temperature interval. Namely, its existence does not require an external electric field. To make this point clearer, it is worthwhile to examine the effects of an applied electric field. Considering that the applied E-field is an experi-

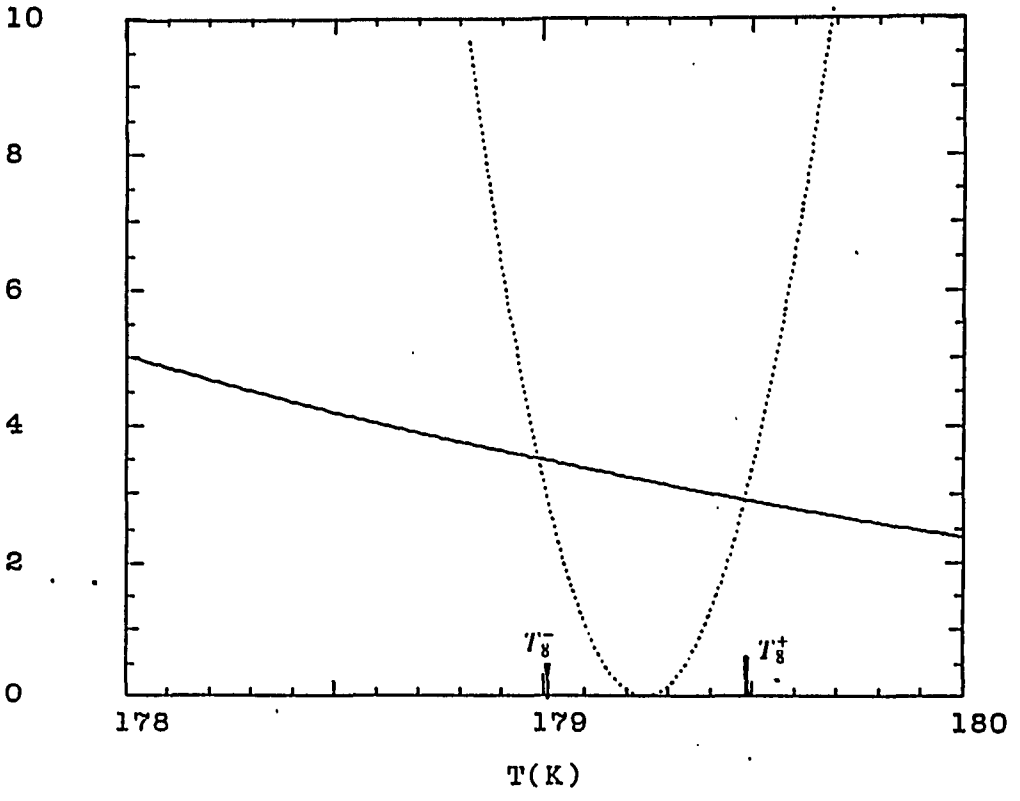

Fig.1.14. Competition between the "elastic energy" and the "lock-in energy" for the 1/8 commensurate phase. Solid line: lock-in energy of the 1/8 Umklapp term. Dotted line: elastic energy cost for the 1/8 lock-in phase. The crossing points of the two curves indicate the upper and lower transition points of the 1/8 commensurate phase.

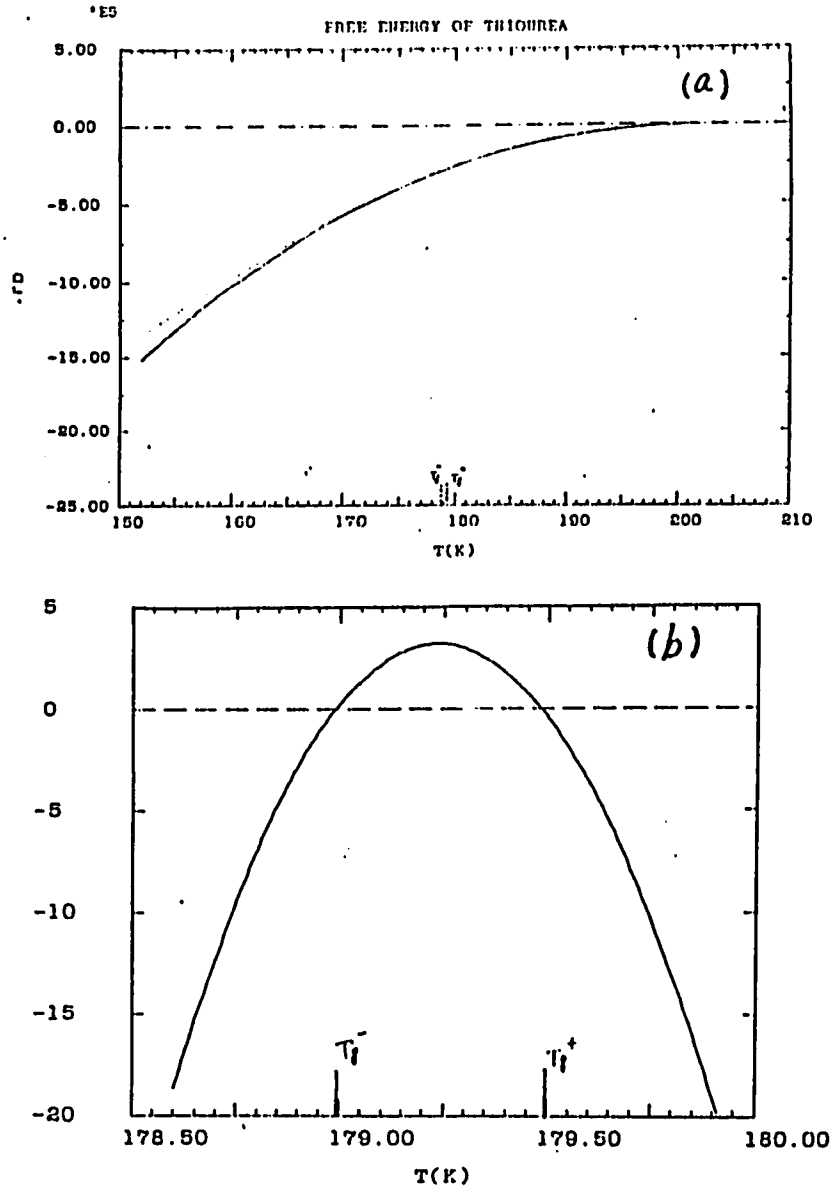

Fig.1.15. Free energy of thiourea in the vicinity of the 1/8 phase.

(a). Solid line: incommensurate solution. Dotted line: 1/8 commensurate solution. The two curves cross at T_8^+ and T_8^- with slightly different slopes and values.

(b). Solid line: $F(q_0=\delta b^*) - F(q_c=b^*/8)$ (difference between the minimized free energy of the incommensurate phase and the 1/8 commensurate phase). Broken line: zero.

mentally accessible parameter, it is interesting to work out the (E-T) phase diagram in the Landau theory and compare with experimental results. Since we are mainly interested in distinguishing the field-induced effects and the intrinsic effects near the $\frac{1}{8}$ phase region, we will only consider the low field case where $\eta_0 \ll \eta$ still holds.

When an electric field E is applied along the x-axis, a field term $-E\langle P_x\rangle$ must be added to the free energy expansion:

$$F_E = F - \frac{1}{V}\int EP_x(y)dV, \tag{1.60}$$

where F is the free energy including the base form and the lock-in terms. Under the IPW approximation,

$$F_E = \frac{1}{2}A\eta_0^2+\frac{1}{4}F\eta_0^4+(A+\alpha q_0^2+\frac{1}{2}\beta q_0^4)\eta^2+(\frac{3}{2}B+2\gamma q_0^2)\eta^4+(3B+2\gamma q_0^2)\eta_0^2\eta^2+$$
$$+2b_9\eta^9\cos(9\phi_0)\Delta(9q_0)+18b_9\eta_0\eta^8 cos(8\phi_0)\Delta(8q_0)+2b_{16}\eta^{16}\cos(16\phi_0)\Delta(16q_0)-E\eta_0. \tag{1.61}$$

Minimizing the free energy (1.61) with respect to η_0 yields:

$$F_E = (A+\alpha q_0^2+\frac{1}{2}\beta q_0^4)\eta^2+(\frac{3}{2}B+2\gamma q_0^2)\eta^4+2b_9\eta^9\cos(9\phi_0)\Delta(9q_0)+2b_{16}\eta^{16}\cos(16\phi_0)\Delta(16q_0)+$$
$$+18b_9RE\eta^8\cos(8\phi_0)\Delta(8q_0)-2R(9b_9)^2\eta^{16}\cos^2(8\phi_0)\Delta(8q_0)-\frac{1}{2}RE^2 \tag{1.62}$$

$$\eta_0 = \frac{E-18b_9\eta^8\cos(8\phi_0)}{A+(6B+4\gamma q_0^2)\eta^2+B\eta_0^2}\Delta(8q_0)$$

$$= R[E-18b_9\eta^8 cos(8\phi_0)\Delta(8q_0)] \tag{1.63}$$

where R is defined by eq.(1.51), $b_9 < 0$, $cos(8\phi_0) = \pm 1$. To minimize F_E, the sign of $\cos(8\phi_0)$ must be the same as that of the external electric field E.

The condition for the commensurate lock-in transitions can be derived in the same way as we did for the case without an E-field. To force the modulation wavevector from an incommensurate value q_0 to a commensurate value q_c costs elastic energy

$$F_B(q_c)-F_B(q_0) = \frac{1}{2}\beta\eta^2(q_0^2-q_c^2)^2 \tag{1.64}$$

which is exactly the same as the zero-field case (1.54). When the Umklapp term lowers the free energy by an amount greater than this value, the corresponding commensurate lock-in phase become stable.

It can be seen from (1.62) that the electric field does not affect the lock-in energy corresponding to the $\frac{1}{9}$ commensurate phase. Therefore, the features of the $\frac{1}{9}$ commensurate phase are essentially the same as the zero-field case. However, the situation would become complicated when the applied E-field is high enough to have substantial effects on the overall N-Inc-F transitions [12].

On the other hand, the E-field effects on the $\frac{1}{8}$ commensurate phase are more significant. The lock-in energy of the related Umklapp terms is ($q_c = \frac{b^*}{8}$) :

$$-18b_9RE\eta^8\cos(8\phi_0)+2R(9b_9)^2\eta^{16}\cos^2(8\phi_0)-2b_{16}\eta^{16} = 2\nu R\eta^8(|E|+\nu\eta^8). \qquad (1.65)$$

where the positive constant ν is given by (1.59). Consequently, the $\frac{1}{8}$ lock-in condition is

$$2\nu R\eta^8(|E|+\nu\eta^8) > \frac{1}{2}\beta\eta^2(q_0^2-q_c^2)^2 \qquad (1.66)$$

The temperature dependence of the lock-in energy (left hand side of (1.66)) and the elastic energy cost due to the gradient terms in free energy (right hand side of (1.66)) are plotted in fig.1.16. The upper and lower transition points of the $\frac{1}{8}$ phase determined form numerical calculation (the crossing points in fig.1.16) are shown in the (E-T) phase diagram (see fig.1.17).

Compared to the field-induced effects caused by E, the intrinsic lock-in effects are characterized by the quantity $\nu\eta^8$. If $\nu\eta^8$ were small in comparison with a realistic E-field level, it would not have any measurable effects and the $\frac{1}{8}$ lock-in transitions observed in dielectric constant measurements would be basically caused by the

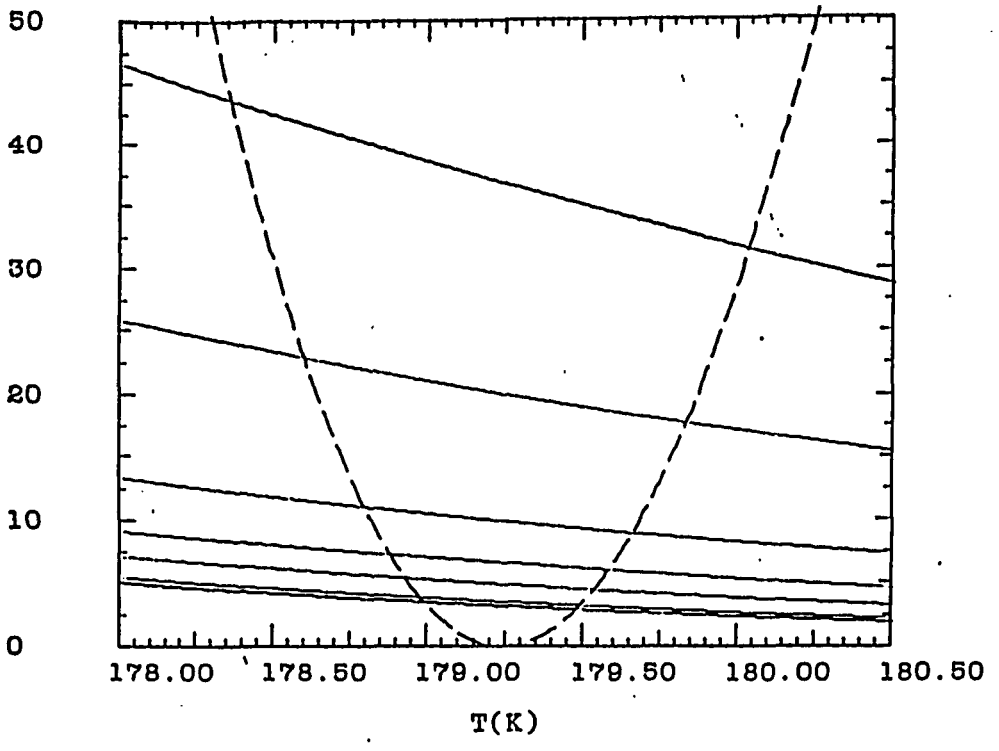

Fig. 1.16. Competition between "lock-in" energy and "elastic energy" for the 1/8 commensurate phase with different biasing E-field levels. Broken line -- the elastic energy cost for 1/8 lock-in. Solid line -- the lock-in energy with different biasing E-field levels. From top to bottom: E = 1000, 500, 200, 100, 50, 10, 0 V/cm .

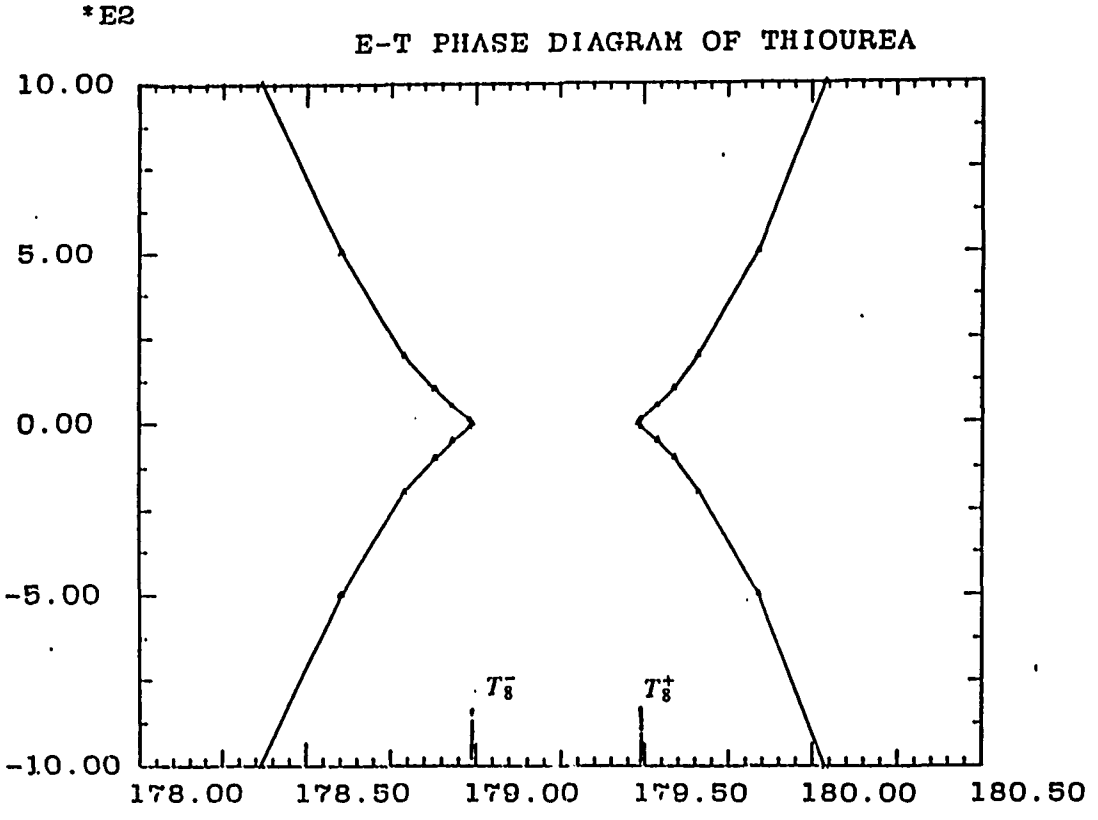

Fig.1.17. (E-T) phase diagram of thiourea near 1/8 lock-in region obtained from numerical calculation of Landau theory under the plane wave approximation.

measuring and biasing fields. Then this $\frac{1}{8}$ commensurate phase should be considered as field-induced. On the other hand, if $\nu\eta^8$ is not small in comparison with an experimentally accessible E-field, the existence of an intrinsic $\frac{1}{8}$ should be experimentally observable and can be tested by a low-field dielectric constant measurement.

The value of $\nu\eta^8$ can be determined by measuring the electric polarization in the $\frac{1}{8}$ phase. The electric polarization in the $\frac{1}{8}$ phase is given by (1.63) and can be rewritten as

$$<P> = \eta_0 = R(E \pm 2\nu\eta^8). \tag{1.67}$$

In fact, the existence of an experimentally measurable spontaneous polarization $2\nu R\eta^8$ with $E = 0$ already implies that $\nu\eta^8$ is not negligibly small in comparison with the measuring field. Our experimental data gives

$$\nu\eta^8 = \frac{\eta_0}{2R}\Big|_{E=0} = 47 \ \ (V/cm)$$

which is certainly not unmeasurably small.

We have performed dielectric constant measurements with measuring fields three orders of magnitude lower than $\nu\eta^8$ and observed a non-zero temperature interval for the $\frac{1}{8}$ phase. We also found that this temperature interval does not significantly increase with a biasing E-field until the biasing field reaches a level comparable to the level of $\nu\eta^8$ (see sec.I.3), as predicted by the above theoretical calculation.

When the applied field is much higher than $\nu\eta^8$, it can be shown from (1.22) and (1.66) that the temperature interval of the $\frac{1}{8}$ commensurate phase will be approximately proportional to the square root of the applied electric filed, which agrees with experimental results [G2][J1].

It is interesting to note that the value of $\nu\eta^8$ is considerably smaller in the case

of d-thiourea. Consequently, the temperature interval ΔT of the intrinsic $\frac{1}{8}$ phase is considerably smaller in d-thiourea. Therefore, the $\frac{1}{8}$ lock-in phase in d-thiourea appears to be closer to the "field-induced" picture.

Up till now, the above discussions are based on the single plane wave approximation. However, the structural modulation is known to deviate from the plane wave form as the temperature approaches a lock-in transition [M12]. Besides, the presence of an external electric field will deform the modulation structure, which can substantially affect the dielectric properties of the crystal [I1]. In the next section, we will go beyond the plane wave approximation and discuss the dielectric behavior of thiourea in the modulated phases.

I.2.4. Dielectric Behavior and Corrections to the IPW Approximation

a) Harmonics of the primary order parameter

Thiourea is a proper ferroelectric material. The successive phase transitions are characterized by a spatially varying electric polarization. Therefore, it is particularly important to study the dielectric behavior which directly probes the nature of the phase transitions.

In order to analyze the dielectric properties in the modulated phases correctly, the single plane wave approximation that we have been using as far must be corrected. The dielectric constant $\varepsilon_a(T)$ derived from the Landau theory under the single plane wave approximation is given by:

$$\varepsilon_a = \frac{d<P>}{dE}\Big|_{E=0} = \varepsilon_b + \frac{4\pi}{A+(6B+4\gamma q_0^2)\eta^2}, \qquad (1.68)$$

where ε_b is the background value due to degrees of freedom other than the order parameter. The temperature-dependent dielectric constant $\varepsilon_a(T)$ from eq.(1.68) and from experimental measurement are plotted in fig.1.18. Obviously, the profound dielectric anomaly of the $\frac{1}{8}$ lock-in transition observed in experiments cannot be explained by the theory in the plane wave approximation. Besides, the plane approximation predicts that the dielectric constant $\varepsilon_a(T)$ decreases monotonically with decreasing temperature in the incommensurate phase whereas the experimental data shows that $\varepsilon_a(T)$ increases significantly on approaching the final lock-in transition, which is also observed in $NaNO_2$ [Q1]. These disagreements are not unexpected because the harmonics of the primary order parameter, which is neglected in the plane wave approximation, play an important role in the dielectric response behavior, especially near incommensurate to ferroelectric phase transitions [I1][P3].

As pointed out by Moncton *et al* The ground state of an incommensurate phase

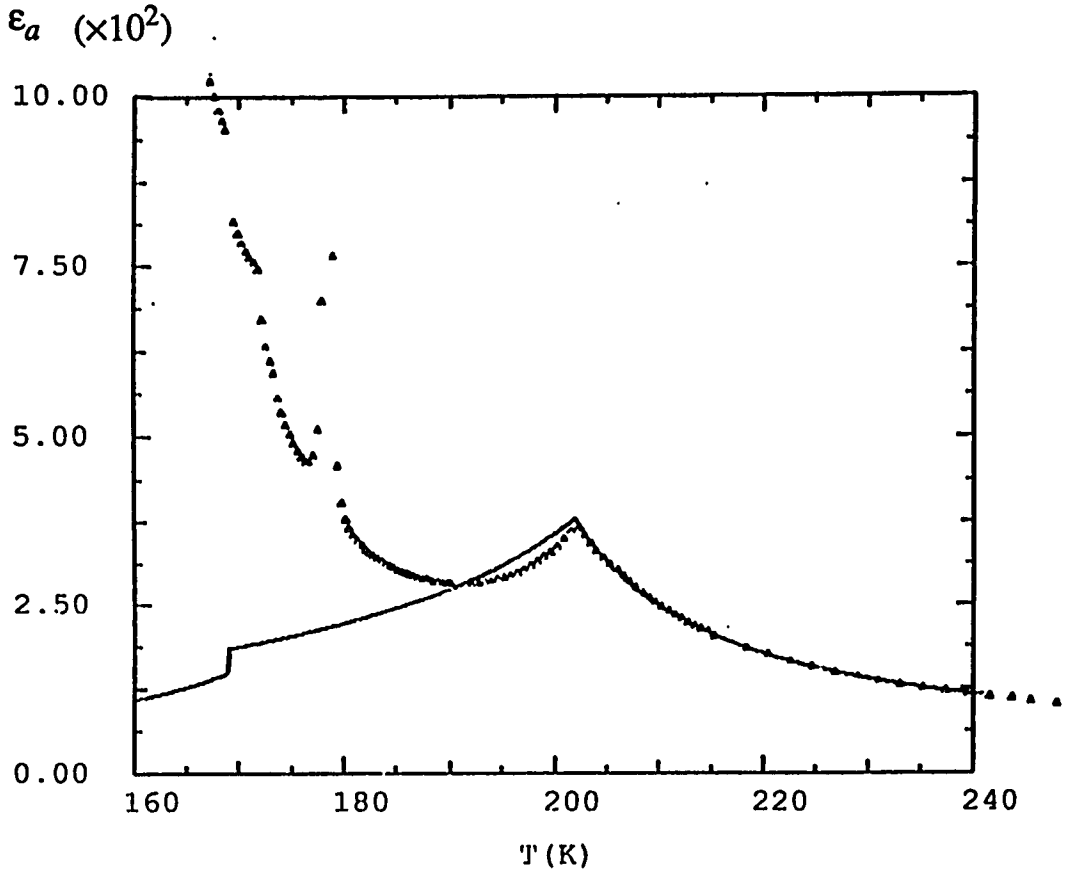

Fig.1.18. Dielectric constant of thiourea. triangular points: experimental data. Solid line: numerical calculation from the the base form of the Landau free energy (under plane wave approximation).

does not consist of a single plane wave distortion [M14], particularly near incommensurate-commensurate transitions. The lock-in terms in the free energy always ensure the existence of secondary distortions that are the harmonics of the primary order parameter [M13][A2]. A plane-wave structural distortion with an incommensurate wavevector close to some commensurate value will locally have rather large region in which the wave experiences an attractive potential (in-phase region), but these are followed by equally large out-of-phase regions where the lock-in potential is repulsive. Therefore, the average of the Umklapp energy is zero. One way to take advantage of the lock-in potential is to modulate the phase of the modulation wave, locally stretching or shrinking the wavelength to produce larger in-phase regions. In other words, the Umklapp terms are allowed in the incommensurate phase and will lower the free energy by deforming the structural distortion from the plane wave form. The deformation caused by an Umklapp term is more and more profound and phase soliton structures will be developed as the commensurate transition point is approached [B6].

It has been shown by Bruce *et al* that the above picture can be applied to type I incommensurate materials which have $q_c \neq 0$ commensurate lock-in transitions, but cannot be applied to type II incommensurate materials which do not have $q_c \neq 0$ commensurate lock-in transitions (like $NaNO_2$) [B4]. Sometimes thiourea is considered as a type II incommensurate material because the overall N-Inc-F transitions have much stronger effects than the $\frac{1}{8}$ and $\frac{1}{9}$ commensurate lock-in transitions. However, since the $\frac{1}{8}$ and $\frac{1}{9}$ phases do exist, the corresponding lock-in terms will ensure harmonics in the structural distortion, which will affect the dielectric behavior.

Moreover, as shown by Ishibasi and Shiba [I1][S10], even without the lock-in terms the harmonics of the structural distortion have a substantial contribution to the dielec-

tric response properties. An applied electric field, such as a measuring field, not only increases the homogeneous part of the electric polarization, but also deforms the spatially varying part from the plane wave form and creates the harmonics. Typically, the amplitude of the second harmonic component is proportional to the applied field [I1][L3]. Consequently, including the harmonics changes the temperature dependence of the dielectric constant in the incommensurate phase substantially.

b) Dielectric properties near the $\frac{1}{9}$ lock-in transition

One way to modify the plane wave approximation is to describe the structural modulation under the constant amplitude approximation [A2]. Assuming it takes less energy to create a phase distortion than an amplitude distortion, the order parameter in the modulated phases can be described by a condensed normal mode at a commensurate wavevector q_c with constant amplitude and an additional spatially varying phase factor $e^{i\phi(y)}$

$$P_x(Y) = \eta_0+\eta e^{iq_c y} e^{i\phi(y)}+\eta e^{-iq_c y} e^{-i\phi(y)} \tag{1.69}$$

where $\phi(y)$ is a slowly varying function of y so that the crystal lattice can be viewed as a continuum.

It is reasonable to first consider the lowest-order lock-in term which is the $\frac{1}{9}$ term (1.46), and neglect the higher-order ones. Then the free energy functional for the modulated phases can be written as:

$$F = \int f[\,\phi(y)\,]\,dy, \tag{1.70}$$

$$f[\,\phi(y)\,] = A\eta^2+\frac{3}{2}B\eta^4+[\alpha(q_c+\phi')^2+\frac{1}{2}\beta(q_c+\phi')^4+\frac{1}{2}\beta(\phi'')^2]\eta^2+ 2\gamma(q_c+\phi')^2\eta^4+2b_9\eta^9\cos(9\phi), \tag{1.71}$$

where $q_c = \frac{b^*}{9}$. Minimizing the free energy by the Euler-Lagrangian equation [B7]

$$f_\phi - \frac{d}{dy} f_{\phi'} + \frac{d^2}{dy^2} f_{\phi''} = 0. \tag{1.72}$$

yields:

$$-18b_9\eta^9\sin(9\phi) - 2[\alpha+3\beta(q_c+\phi')^2+2\gamma\eta^2]\eta^2\phi''+\beta\phi^{(4)} = 0. \tag{1.73}$$

Again, since $\phi(y)$ is a slowly varying function, the forth derivative $\phi^{(4)}(y)$ can be neglected and $(\phi'+q_c)$ can be simplified as q_0 which the wavevector of the IPW approximation. Thus we have the sine-Gordon equation:

$$-18b_9\eta^9\sin(9\phi) = 4\beta q_0^2\eta^2\phi''. \tag{1.74}$$

Integrating (1.74) yields:

$$(\phi')^2 = \frac{-b_9\eta^9}{\beta q_0^2\eta^2}\left[1-2\sin^2(\frac{9}{2}\phi+\frac{\pi}{2})\right] + C \tag{1.75}$$

The integration constant C can be determined by the condition that the structural modulation would go back to the plane wave form when the lock-in term is zero. i.e.,

$$\phi'+q_c = q_0 \qquad (when\ \ b_9 = 0) \tag{1.76}$$

Then

$$(\phi')^2 = (q_0-q_c)^2\left[1-a_9^2\sin^2(\frac{9}{2}\phi+\frac{\pi}{2})\right], \tag{1.77}$$

where

$$a_9^2 = \frac{-2b_9\eta^7}{\beta q_0^2(q_0-q_c)^2} < 1. \tag{1.78}$$

Therefore, the solution of the sine-Gordon equation (1.74) can be expressed in terms of elliptic integral of the first kind:

$$y = y_0 + \frac{1}{|q_0-q_c|}\int_{\phi_0}^{\phi}\left[1-a_9^2\sin^2(\frac{9}{2}u+\frac{\pi}{2})\right]^{-\frac{1}{2}} du, \tag{1.79}$$

The results of (1.79) for $\phi(y)$ from numerical calculations for several selected temperatures are shown in fig.1.19.

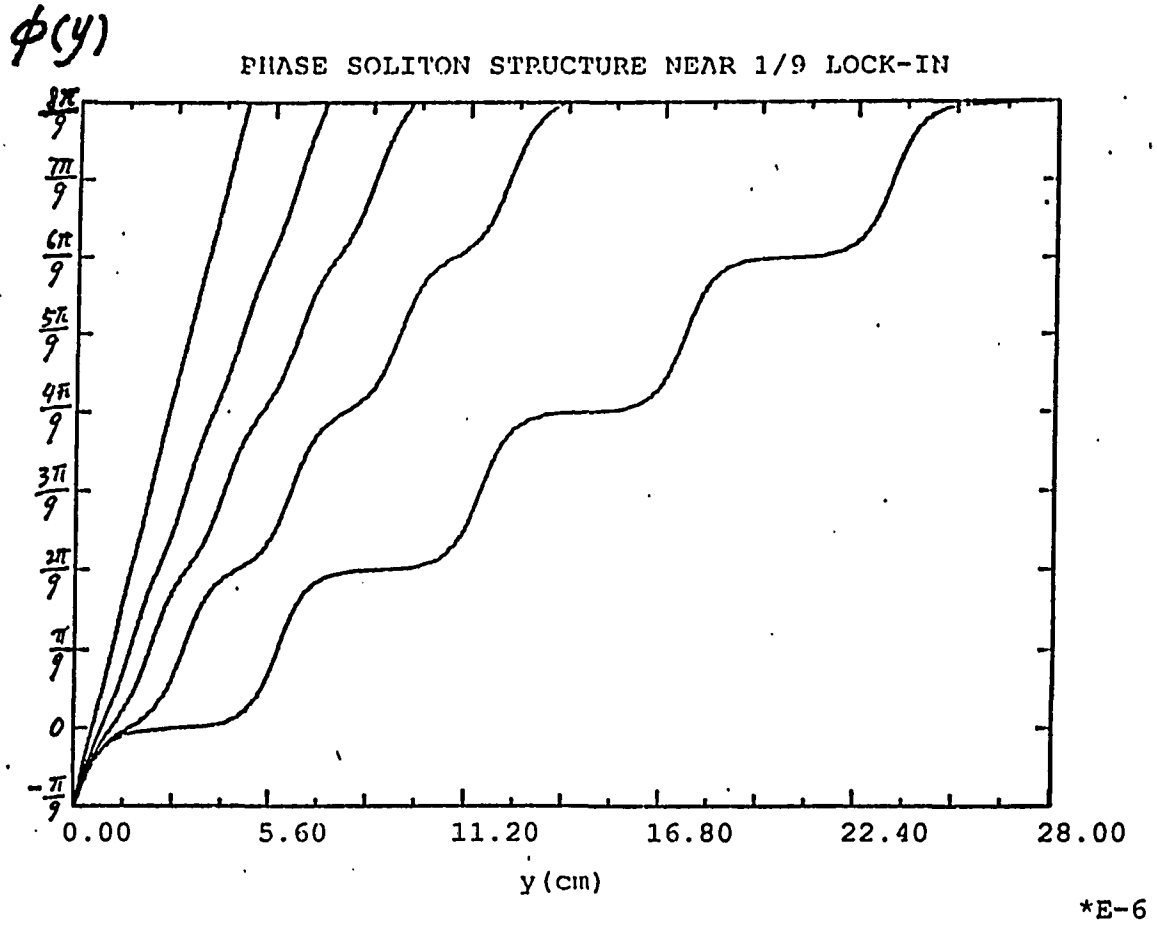

Fig.1.19. Phase soliton structure near the 1/9 lock-in temperature T_9. From left to right: $T = T_9 + 3.3, 1.3, 0.5, 0.1, 0.0005$ K.

When the temperature is lowered toward the $\frac{1}{9}$ commensurate transition point, a_9^2 increases and $\phi'(y)$ becomes more and more space-dependent. Near the $\frac{1}{9}$ transition point, $a_9^2 \approx 1$ and the plane wave form of the structural modulation is substantially distorted. The modulated structure consists of large commensurate regions of essentially constant ϕ that are separated by narrow regions of rapidly varying ϕ which are termed discommensurations or phase solitons [M12]. The soliton width d can be defined by

$$d = \frac{2\pi}{9(q_0-q_c)} \tag{1.80}$$

where $q_0-q_c = \phi'_{max}$ is the slope of $\phi(y)$ at $\phi = \frac{m\pi}{9}$ with m an integer. The intersoliton distance x_0 is defined by

$$x_0 = \frac{K(a_9)}{q_0-q_c}, \tag{1.81}$$

where $K(a_9)$ is the complete elliptic integral of the first kind with modulus a_9. On approaching the transition point, the intersoliton distance x_0 increases, diverging to infinity at $a_9^2 = 1$, which gives a more precise transition temperature T_9 (see fig.1.20):

$$\frac{-2b_9\eta^7(T_9)}{\beta q_0^2(T_9)[q_0(T_9)-q_c]^2} = 1. \tag{1.82}$$

The numerical value of T_9 determined by (1.82) is

$$T_9 = 171.71\ K,$$

which is slightly higher than the value given by the plane wave approximation.

The incommensurate to commensurate lock-in transition can be considered as a process of melting the discommensurations. The reverse transition can be viewed as a process of nucleation of the discommensurations [M12].

The average modulation wavevector is

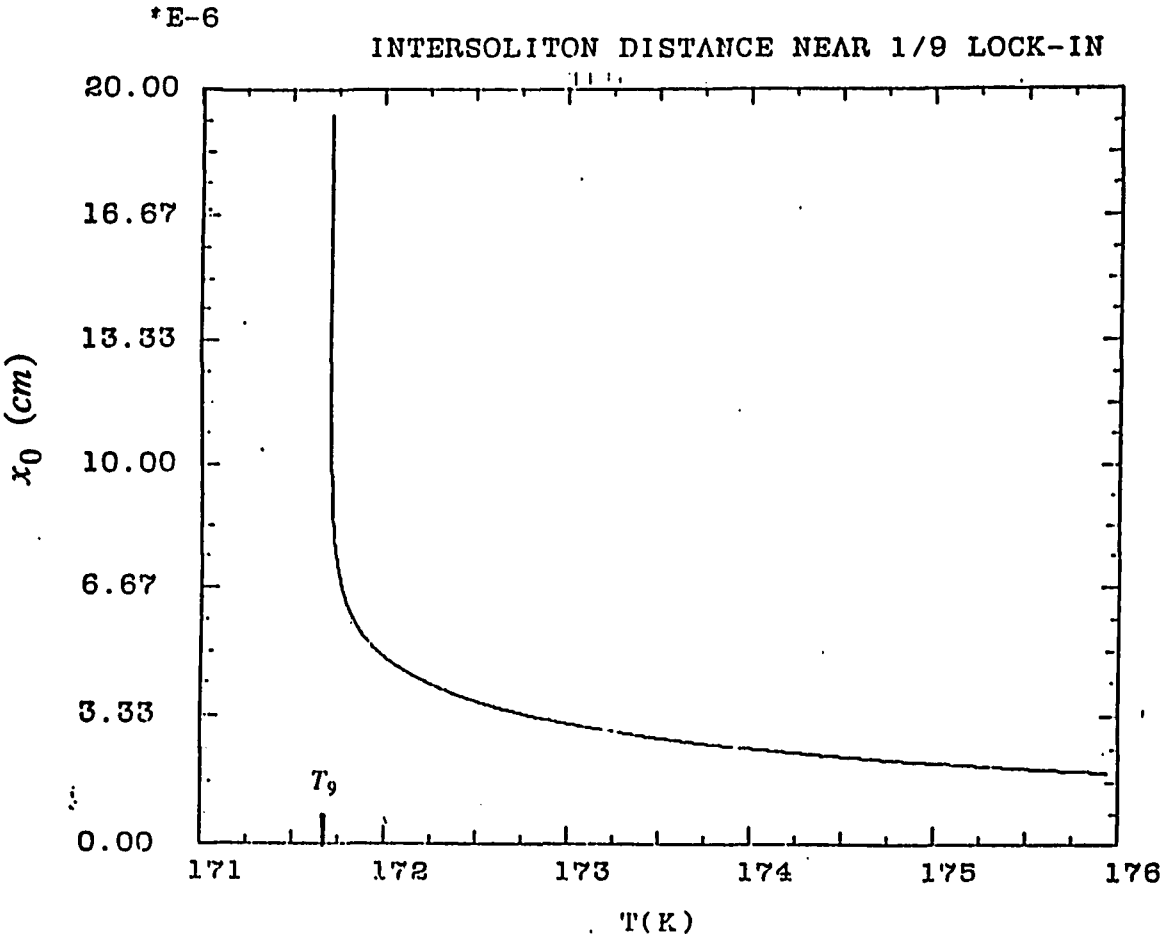

Fig.1.20. Intersoliton distance vs. temperature. T_9 — 1/9 lock-in transition temperature.

$$q_{av} = q_c + \phi'_{av}, \tag{1.83}$$

where ϕ'_{av} is the average slope of $\phi(y)$ given by

$$\phi'_{av} = \frac{2\pi}{9x_0}. \tag{1.84}$$

It can be shown from (1.84) and (1.81) that the average modulation wavevector q_{av} drops to q_c rapidly as the transition point T_9 is approached. This rapid decrease in q_{av} has been observed in experiments, but cannot be explained by the plane wave approximation.

For temperatures well above T_9, a_9^2 is small, $\phi(y)$ is practically a linear function of y, $\phi(y) = (q_0 - q_c)y$, which is the single plane wave form with wavevector q_0. It can be seen from fig.1.19 that the harmonics due to the $\frac{1}{9}$ lock-in term can surely be neglected for $T \geq 175.0K$.

Although the modulation structure is distorted from the plane wave form near the $\frac{1}{9}$ lock-in transition, it can be easily shown that this deformation does not have substantial effects on the dielectric properties. In the presence of an electric field E, the free energy can be written as:

$$F = \int \left[f[\,\phi(y)\,] + \frac{1}{2}A\eta_0^2 + \frac{1}{4}B\eta_0^4 - E[\eta_0 + 2\eta\cos(\frac{b^*}{9}y + \phi)] \right] dy, \tag{1.85}$$

where $f[\,\phi(y)\,]$ is given by (1.71). It can be seen from the last term of (1.85) that the effects of the E-field on the slowly varying phase function $\phi(y)$ is smeared out due to the rapidly varying argument $\frac{b^*}{9}y$ in the sine function. Therefore, the dielectric constant as a function of temperature is essentially given by the same expression as without the $\frac{1}{9}$ lock-in term, except that the value of the modulation wave vector is changed (not dramatically but observably).

c) Dielectric properties near the $\frac{1}{8}$ lock-in phase boundary

As shown above, to discuss the structural distortion near the $\frac{1}{8}$ commensurate phase which is well above 175K, the $\frac{1}{9}$ lock-in term can be neglected. Then the free energy can be written as:

$$F = \int f[\,\phi(y)\,]\,dy \tag{1.86}$$

$$f[\,\phi(y)\,] = A\eta^2+\frac{3}{2}B\eta^4+[\alpha(q_c+\phi')^2+\frac{1}{2}\beta(q_c+\phi')^4+\frac{1}{2}\beta(\phi'')^2\,]\eta^2+$$
$$2\gamma(q_c+\phi')^2\eta^4-2Rv^2\eta^{16}\cos^2(8\phi), \tag{1.87}$$

where $q_c = \frac{b^*}{8}$. Again $\phi(y)$ is a slowly varying function and the crystal lattice can be viewed as a continuum. Similar to the $\frac{1}{9}$ case, minimizing the free energy functional yields:

$$Rv^2\eta^{14}\sin(16\phi) = \frac{1}{4}\beta q_0^2\phi'' \tag{1.88}$$

$$\phi' = |\,q_0-q_c\,|\left[1 - a_8^2\sin^2(8\phi+\frac{\pi}{2})\right]^{\frac{1}{2}}, \tag{1.89}$$

where

$$a_8^2 = \frac{Rv^2\eta^{14}}{\beta q_0^2(q_0-q_c)^2}. \tag{1.90}$$

The solution of (1.89) is:

$$y = y_0 + \frac{1}{|\,q_0-q_c\,|}\int_{\phi_0}^{\phi}\left[1 - a_8^2\sin(8u+\frac{\pi}{2})\right]^{-\frac{1}{2}}du \tag{1.91}$$

The phase soliton structures are developed near both the upper and lower boundaries of the $\frac{1}{8}$ commensurate phase. Since a_8^2 is proportional to η^{14}, it is vary small except in the immediate vicinity of the phase boundaries where $q_0 \approx q_c$. Therefore, the phase soliton structure appears significantly only when the temperature is very close to the transition points (see fig.1.21). The upper and lower transition temperatures $T_8^{\dagger}$ and

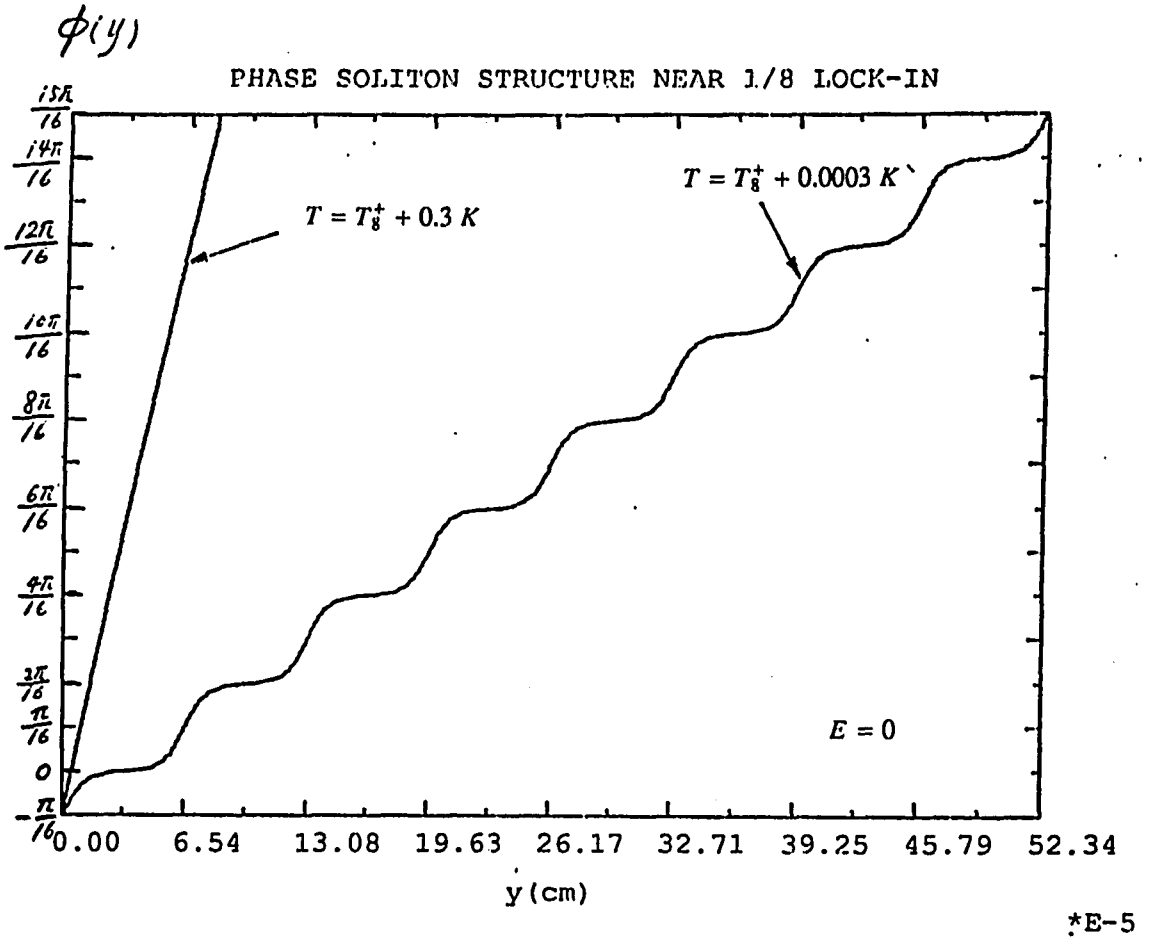

Fig.1.21. Phase soliton structure near T_8^+. T_8^+ -- the upper transition point of the 1/8 ferroelectric lock-in phase.

T_8^- determined by $a_8^2 = 1$ are obtained by numerical calculations:

$$T_8^+ = 179.5$$
$$T_8^- = 179.0$$

(In fact, they differ from the results given by the plane wave approximation by a negligible amount).

In contrast to the $\frac{1}{9}$ lock-in case, the harmonics due to the $\frac{1}{8}$ lock-in term make a substantial contribution to the dielectric properties. In the presence of an electric field E, the free energy functional is:

$$F = \int \left[f[\,\phi(y)\,] - EP(y) \right] dy \tag{1.92}$$

where $f[\,\phi(y)\,]$ is given by (1.87). Minimizing the free energy (1.92) leads to a double sine-Gordon equation:

$$Rv^2\eta^{14}\sin(16\phi) + RvE\eta^6\sin(8\phi) = \frac{1}{4}\beta q_0^2\phi'' \tag{1.93}$$

The solution to (1.93) is:

$$y = y_0 + \frac{1}{|\,q_o - q_c\,|}\int_{\phi_0}^{\phi} \left[1 - a_8^2\sin^2(8u+\frac{\pi}{2}) - a_E^2 E\sin(8u+\frac{\pi}{2}) \right]^{-\frac{1}{2}} du \tag{1.94}$$

where

$$a_E^2 = \frac{Rv\eta^6}{\beta q_0^2 (q_o - q_c)^2}, \tag{1.95}$$

and a_8^2 is given by (1.90). The ϕ *vs* y curve in the presence of an applied E-field obtained from numerical calculation is shown in fig.1.22.a. The electric field deforms the phase solitons in such a way that the commensurate regions with $cos(8\phi) = +1$ are stretched while the other commensurate regions with $cos(8\phi) = -1$ are shrunk. In other words, the external E-field extends the regions with polarization parallel to the E-field but compresses the regions antiparallel to E (see fig.1.22.b). When the E-field is high enough so that the size of the "parallel" regions diverges to infinity, an incommensurate-commensurate transition occurs. This is the "field-induced" phase

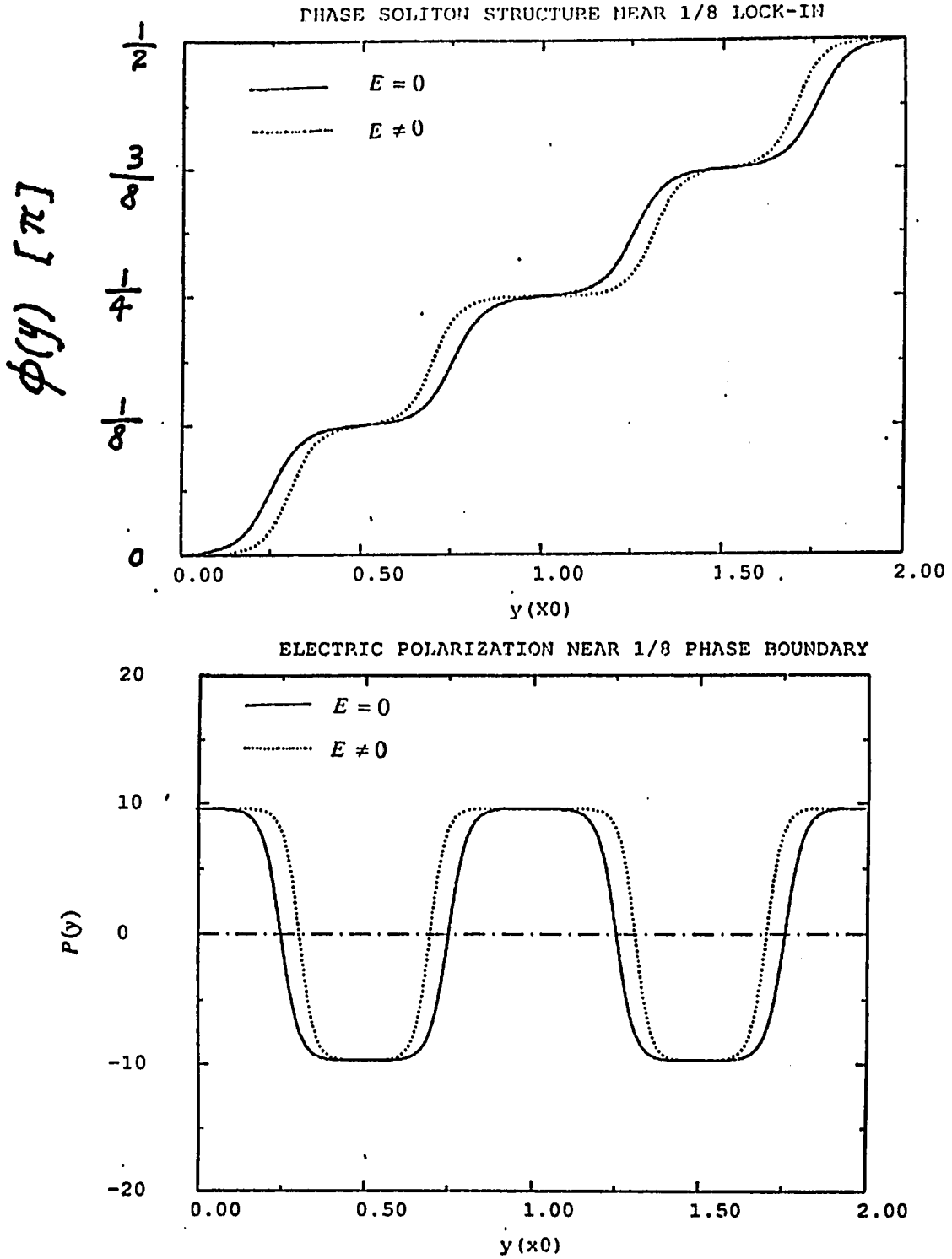

Fig. 1.22. Effects of an applied E-field near the 1/8 phase boundary.
Solid line -- without E-field, Dotted line -- with E-field.
(a). -- Deformation of the phase soliton structure under an E-field.
(b). -- Electric polarization $P_x(y)$.

transition mechanism.

The period of the function $\phi(y)$ is now

$$X_0 = \frac{1}{|q_0-q_c|}\int_0^{\frac{\pi}{4}}\left[1-a_8^2\sin^2(8u+\frac{\pi}{2}) - a_E^2 E\sin(8u+\frac{\pi}{2})\right]^{-\frac{1}{2}}du. \tag{1.96}$$

Then the macroscopic electric polarization $<P>$ is given by

$$\begin{aligned}
<P> &= \frac{1}{X_0}\int_0^{X_0}\eta_0[\,\phi(y)\,]dy \\
&= \frac{1}{X_0}\int_0^{\frac{\pi}{4}}\eta[\,\phi(y)\,]\,\frac{dy}{d\phi}d\phi \\
&= \frac{1}{X_0}\int_0^{\frac{\pi}{4}}\frac{RE+2R\nu\eta^8\cos(8\phi)}{|q_0-q_c|\left[1-a_8^2\sin^2(8\phi+\frac{\pi}{2}) - a_E E\sin(8\phi+\frac{\pi}{2})\right]^{\frac{1}{2}}}d\phi \\
&= RE + \frac{1}{X_0|q_0-q_c|}\int_0^{\frac{\pi}{4}}\frac{2R\nu\eta^8\cos(8\phi)\,d\phi}{\left[1-a_8^2\sin^2(8\phi+\frac{\pi}{2})-a_E^2E\sin(8\phi+\frac{\pi}{2})\right]^{\frac{1}{2}}}
\end{aligned} \tag{1.97}$$

The dielectric constant is given by

$$\varepsilon_a = \varepsilon_b + 4\pi\frac{d<P>}{dE} \tag{1.98}$$

where

$$\begin{aligned}
\frac{d<P>}{dE} &= R + \frac{Rva_E^2\eta^8}{X_0|q_0-q_c|}\int_0^{\frac{\pi}{4}}\frac{\eta^8\cos^2(8\phi)\,d\phi}{\left[1-a_8^2\cos^2(8\phi) - a_E^2E\cos(8\phi)\right]^{\frac{3}{2}}} - \\
&- \frac{Rva_E^2\eta^8}{X_0^2(q_0-q_c)^2}\int_0^{\frac{\pi}{4}}\frac{\eta^8\cos(8\phi)\,d\phi}{\left[1-a_8^2\cos^2(8\phi) - a_E^2\cos(8\phi)\right]^{\frac{1}{2}}}\int_0^{\frac{\pi}{4}}\frac{\cos(8\phi)\,d\phi}{\left[1-a_8^2\cos^2(8\phi) - a_E^2E\cos(8\phi)\right]^{\frac{3}{2}}}
\end{aligned} \tag{1.99}$$

The dielectric constant as a function of temperature at different biasing E-field obtained from numerical calculation of (1.98) and (1.99) is shown in fig.1.23.

At zero biasing field, the two sharp peaks are well separated, indicating a non-zero temperature interval of the $\frac{1}{8}$ commensurate phase. The width of the

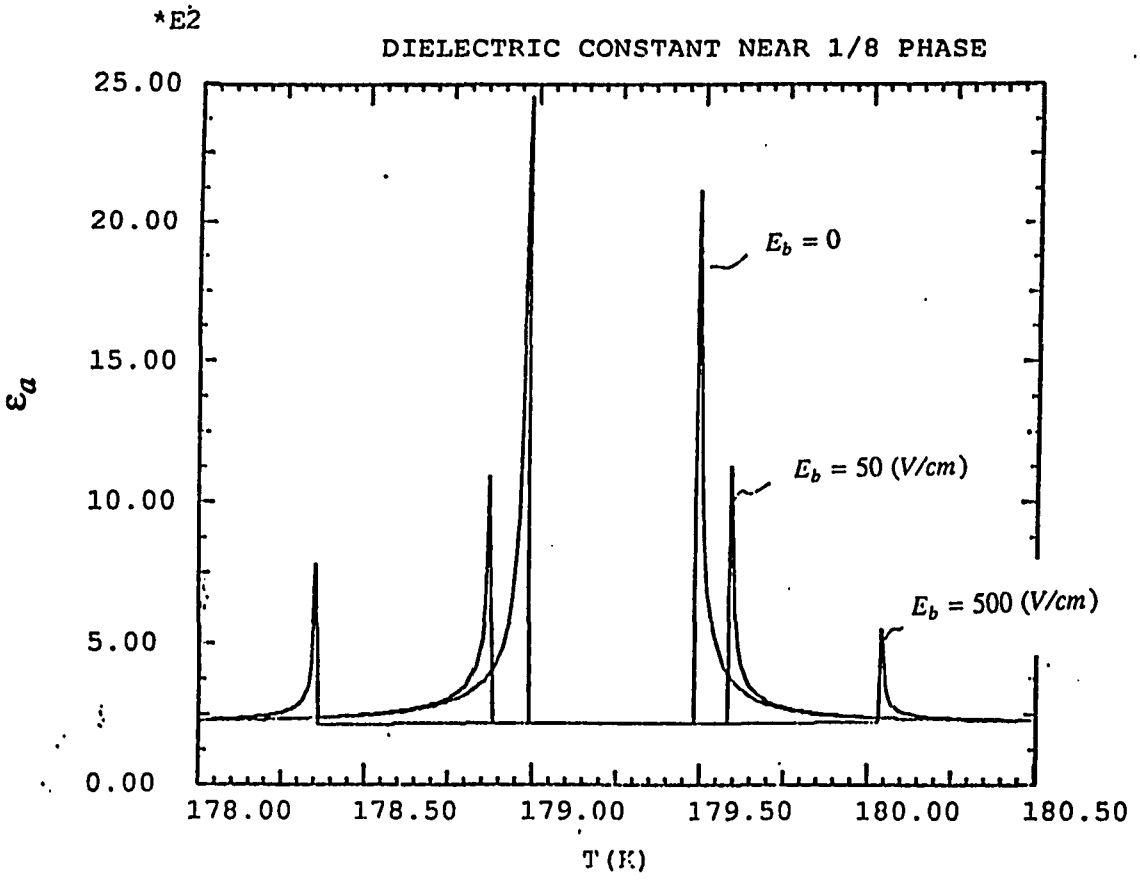

Fig.1.23. Dielectric constant of thiourea in the vicinity of the 1/8 lock-in phase at different biasing E-fields (from numerical calculation). $E_{biasing}$ = 0, 50, 500, *V/cm*.

temperature interval increases with the applied biasing electric field. The height of the peaks decreases with increasing biasing E-field. These predictions are consistent with experimental observations [G4].

d) Dielectric properties without the lock-in terms

As shown by Ishibashi and Shiba in 1978 [I1], the harmonics of the primary order parameter make a substantial contribution to the dielectric properties even without the commensurate lock-in terms. As a lowest order correction to the single plane wave approximation, we take the second harmonic component into account and describe the structural modulation as [L3]:

$$P_x(y) = \eta_0 + 2\eta cos(q_0 y) + 2\eta_2 \cos(2q_0 y). \tag{1.100}$$

Substituting the order parameter (1.100) into the base form of the free energy in the presence of an electric field E :

$$F = \frac{1}{v}\int \left[\frac{1}{2}AP_x^2+\frac{1}{4}BP_x^4+\frac{1}{2}\alpha\left[\frac{dP_x}{dy}\right]^2+\frac{1}{4}\beta\left[\frac{d^2P_x}{dy^2}\right]^2+\gamma\left[P_x\frac{dP_x}{dy}\right]^2 - EP_x\right] dv \tag{1.101}$$

yields:

$$\begin{aligned} F = {} & \frac{1}{2}A\eta_0^2+\frac{1}{4}B\eta_0^4+A_1\eta^2+A_2\eta_2^2+(\frac{3}{2}B+2\gamma\frac{3}{2}B+2\gamma\frac{3}{2}B+2\gamma q_0^2)\eta^4+(\frac{3}{2}B+8\gamma q_0^2)\eta_2^4 \\ & +(3B+2\gamma q_0^2)\eta_0^2\eta^2+(3B+8\gamma q_0^2)\eta_0^2\eta_2^2+(6B+20\gamma q_0^2)\eta^2\eta_2^2+(6B+12\gamma q_0^2)\eta_0\eta^2\eta_2 - E\eta_0 \end{aligned} \tag{1.102}$$

where

$$A_1 = A+\alpha q_0^2+\frac{1}{2}\beta q_0^4, \tag{1.103}$$

$$A_2 = A+\alpha(2q_0)^2+\frac{1}{2}\beta(2q_0)^4. \tag{1.104}$$

Minimizing the free energy (1.101) with respect to η_2 gives:

$$\eta_2 \approx -\frac{(3B+6\gamma q_0^2)\eta_0\eta^2}{A_2+(6B+2\gamma q_0^2)\eta^2}. \tag{1.105}$$

In the absence of Umklapp terms η_0 is basically proportional to the electric field E

(in the incommensurate phase). Therefore, the second harmonic component is induced by the E-field. The dielectric susceptibility in the zero field limit is given by;

$$\chi = \left[\frac{\partial^2 F}{\partial \eta_0^2}\right]^{-1} \Big|_{E=0} = \left[A+(6B+4\gamma q_0^2)-\frac{2(3B+6\gamma q_0^2)^2\eta^4}{A_2+(6B+20\gamma q_0^2)\eta^2}\right]^{-1} \qquad (1.106)$$

As shown in fig.1.24, the dielectric constant calculated from (1.106) predicts the substantial increase near the final ferroelectric transition point T_c, which is commonly observed in type II incommensurate materials. In other words, the difficulty of the single plane wave approximation in predicting the dielectric behavior in the incommensurate phase can be overcome by taking into account the harmonics of the primary order parameter.

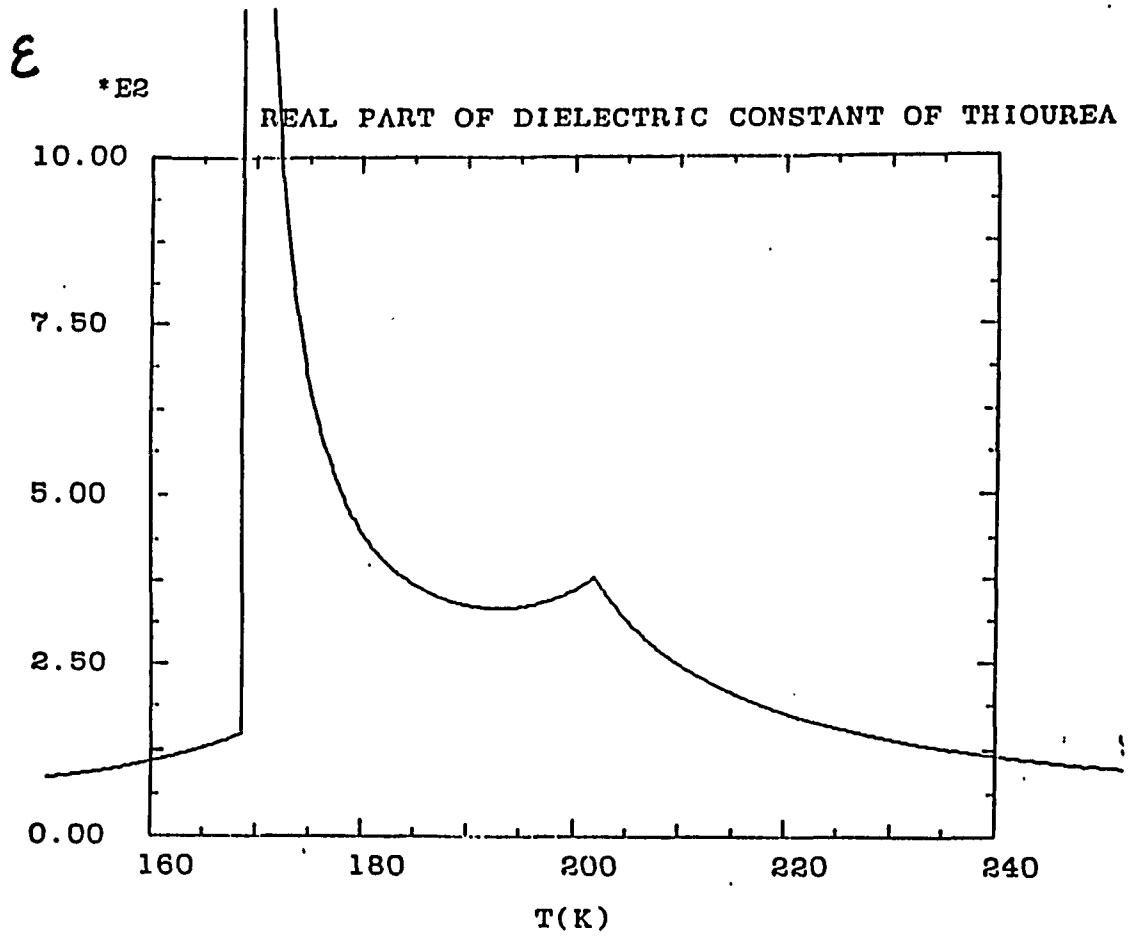

Fig.1.24. Dielectric constant of thiourea obtained from the base form of the free energy. Second harmonic has been included.

I.2.5. Dielectric Relaxation Mechanism Near the 1/8 Phase

a) The equation of motion of the phase mode

From the previous section it is clear that an applied electric field deforms the phase soliton structure which results in the dielectric anomaly near the boundary of the $\frac{1}{8}$ ferroelectric phase. To make theoretical prediction on the frequency dependence of the dielectric constant, we need to study the dynamic behavior of the phase soliton structure. The following discussion will still be under the constant-amplitude continuum approximation.

With a time-dependent phase factor, the order parameter can be rewritten as:

$$P_x(y,t) = \eta_0 + Q(y,t) + Q^*(y,t), \tag{1.107}$$

where the primary order parameter $Q(y,t)$ is given by:

$$Q(y,t) = \eta e^{iq_c y} e^{i\psi(y,t)} \tag{1.108}$$

where $q_c = \frac{b^*}{8}$. The free energy density can be considered as the potential energy density:

$$V(y,t) = A\eta^2 + \frac{3}{2}B\eta^4 + \left[\alpha(q_c+\psi')^2 + \frac{1}{2}\beta(q_c+\psi')^4\right]\eta^2 + 2\gamma(q_c+\psi')^2\eta^4$$
$$-2\nu RE\eta^8\cos(8\psi) - 2\nu^2 R\eta^{16}\cos^2(8\psi) - \frac{1}{2}RE, \tag{1.109}$$

where η_0 has been eliminated by minimizing the free energy with respect to η_0, which means that η_0 is assumed to follow the primary order parameter $Q(y,t)$ adiabatically,

$$\eta_0 = R\left[E + 2\nu\eta^8\cos(8\psi)\right] \tag{1.110}$$

where R and ν are defined by (1.51) and (1.57), and prime represents derivatives with respect to y.

The kinetic energy density can be written as:

$$T(y,t) = \frac{1}{2}m_1\dot{Q}\dot{Q}^* = \frac{1}{2}m_1\eta^2\dot{\psi}^2. \tag{1.111}$$

where m_1 is the effective mass of the $Q(y,t)$ mode and dot represents time derivatives. The Lagrangian density can be constructed as:

$$L(y,t) = T(y,t) - V(y,t) \tag{112}$$

Since the dielectric dissipation is a key aspect in the dynamic susceptibility studies, the relevant generalized friction force must be taken into account when the equation of motion is derived. The energy dissipation of the $Q(y,t)$ mode can be described by the Rayleigh dissipation function [G5]:

$$R = \frac{1}{2}\gamma_1 \dot{Q}\dot{Q}^* = \frac{1}{2}\gamma_1 \eta^2 \dot{\psi}^2. \tag{1.113}$$

Then the Lagrange equation is given by [G5]:

$$\frac{d}{dt}\left[\frac{\partial L}{\partial \dot{\psi}}\right] + \frac{d}{dy}\left[\frac{\partial L}{\partial \psi'}\right] - \frac{\partial L}{\partial \psi} = -\frac{\partial R}{\partial \dot{\psi}}. \tag{1.114}$$

Therefore, the equation of motion of the phase mode $\psi(y,t)$ is given by:

$$m_1\ddot{\psi} + \gamma_1\dot{\psi} - \beta q_0^2\psi'' + 16Rv E\eta^6 \sin(8\psi) + 16Rv^2\eta^{14}\sin(16\psi) = 0. \tag{1.115}$$

The above derivation is equivalent to Horioka and Sawada's approach for K_2SeO_4 based on the phenomenological theory of thermodynamic irreversible processes [H1][L7]. The dispersion relation of the phase-fluctuation mode can be obtained by solving eq.(1.115) with $\gamma_1 = 0$ and $E = 0$ [H1][M12], which is not included in the present study.

b) The dynamic susceptibility

When the external electric field E is small and alternating,

$$E = E_0 e^{i\omega t}, \tag{1.116}$$

$\psi(y,t)$ will oscillate around the zero-field static solution $\phi(y)$. i.e.,

$$\psi(y,t) = \phi(y) + \theta(y)e^{i\omega t} \tag{1.117}$$

where $\phi(y)$ is given by (1.91) and $\theta(y)$ describes the complex amplitude of the small

oscillations. Then the equation of motion (1.115) can be linearized as:

$$(-\omega^2 m_1 + i\omega\gamma_1)\theta - 4\beta q_0^2\theta'' + (16\nu)^2 R\eta^{14}\cos(16\phi)\theta + 16\nu R\eta^6 E_0\sin(8\phi) = 0, \tag{1.118}$$

which can be rewritten as:

$$-\theta'' + \left[-\Omega^2 + i\tau_1 + \lambda^2\cos(16\phi)\right]\theta = -\sigma E_0\sin(8\phi) \tag{1.119}$$

where

$$\Omega^2 = \frac{m_1\omega^2}{4\beta q_0^2}, \qquad \tau_1 = \frac{\omega}{4\beta q_0^2},$$
$$\lambda^2 = \frac{64\nu^2 R\eta^{14}}{\beta q_0^2}, \qquad \sigma = \frac{4\nu R\eta^6}{\beta q_0^2}$$

The solution is [H1]:

$$\theta(y) = HE_0\sin(8\phi) \tag{1.120}$$

where

$$H = \frac{\sigma}{\lambda^2\left[\frac{1-a_8^2}{a_8^2}\right] - \Omega^2 + i\tau_1} \tag{1.121}$$

The macroscopic electric polarization can be obtained by averaging over a period of intersoliton distance x_0. i.e.,

$$P(t) = \frac{1}{x_0}\int_0^{x_0}\eta_0\, dy, \tag{1.122}$$

where

$$x_0 = \frac{K(a_8)}{|q_0 - q_c|} \tag{1.123}$$

The result of (1.122) is

$$P(t) = <P>\, e^{i\omega t} \tag{1.124}$$

$$<P> = RE_0 + \frac{8H(1-a_8^2)E_0}{a_8^2}\left[\frac{E(a_8)}{K(a_8)(1-a_8^2)} - 1\right]. \tag{1.125}$$

where $K(a_8)$ and $E(a_8)$ stand for complete elliptic integral of the first and second kind respectively. Therefore, the frequency-dependent susceptibility is obtained as:

$$\chi(\omega) = R + \frac{8H(1-a_8^2)}{a_8^2}\left[\frac{E(a_8)}{K(a_8)(1-a_8^2)} - 1\right]. \tag{1.126}$$

which can be rewritten in a simpler form:

$$\chi(\omega) = \chi(\infty) + \frac{\chi(0)-\chi(\infty)}{1-\left[\frac{\omega}{\omega_1}\right]^2 + i\frac{\omega\Gamma_1}{w_1^2}}. \tag{1.127}$$

where $\chi(\infty) = R$.

The static susceptibility is given by:

$$\chi(0) = \frac{R\ E(a_8)}{(1-a_8)\ K(a_8)}, \tag{1.128}$$

which is consistent with the result from the static approach discussed in the previous section.

The resonance frequency ω_1 and the damping Γ_1 are given by:

$$\omega_1^2 = \frac{256\beta q_0^2(q_0-q_c)^2(1-a_8^2)}{m} \tag{1.129}$$

$$\Gamma_1 = \frac{\gamma_1}{m_1} \quad . \tag{1.130}$$

As the temperature approaches the $\frac{1}{8}$ phase from either the high or low temperature side, the resonance frequency decreases and tends to zero. Near the transition points T_8^+ and T_8^- $\Gamma_1 \gg \omega_1$, i.e., the phase mode is overdamped, and the dynamic susceptibility $\chi(\omega)$ reduces to the Debye relaxation form:

$$\chi(\omega) = \chi(\infty) + \frac{\chi(0)-\chi(\infty)}{1+i\omega\tau}. \tag{1.131}$$

The relaxation time τ is given by:

$$\tau = \frac{\Gamma_1}{\omega_1^2} = \frac{\gamma_1}{256\beta q_0^2(q_0-q_c)^2(1-a_8^2)}. \tag{1.132}$$

The relaxation time τ as function of temperature is shown in fig.1.25. It is clear that the relaxation time increases rapidly as the temperature approaches the $\frac{1}{8}$ lock-in transition points from the incommensurate phase (from both sides) and diverges to

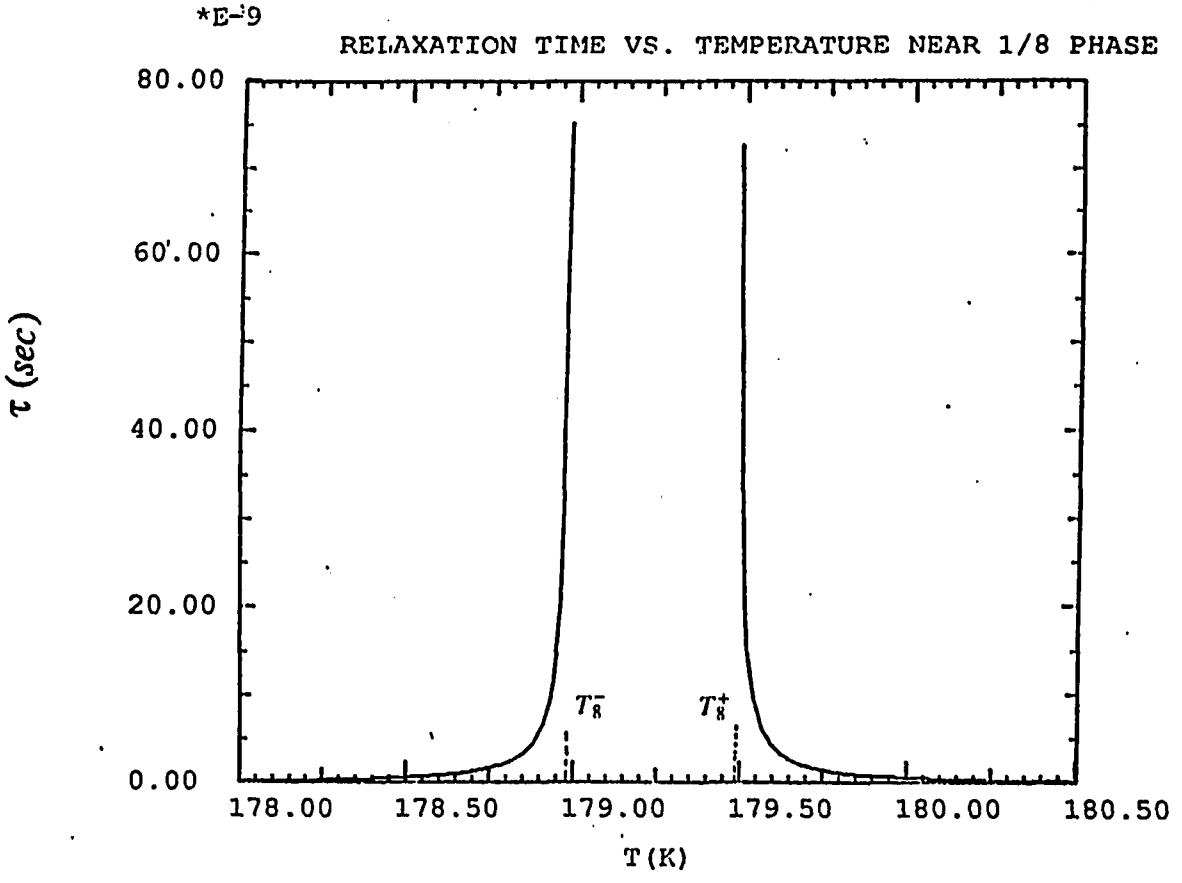

Fig.1.25. Relaxation time vs. temperature (from numerical calculation). γ is chosen as 2.0×10^{-13} (cgse units).

infinity at the upper and lower transition points where $a_8^2 = 1$. Namely, critical slowing-down of relaxation processes at T_8^+ and T_8^- are predicted. The frequency-dependent real and imaginary part of the complex dielectric constant near the $\frac{1}{8}$ transition points calculated from this model are shown in fig.1.26 ($\gamma_1 = 2.0\times10^{-13}$ was used to generate the numerical data).

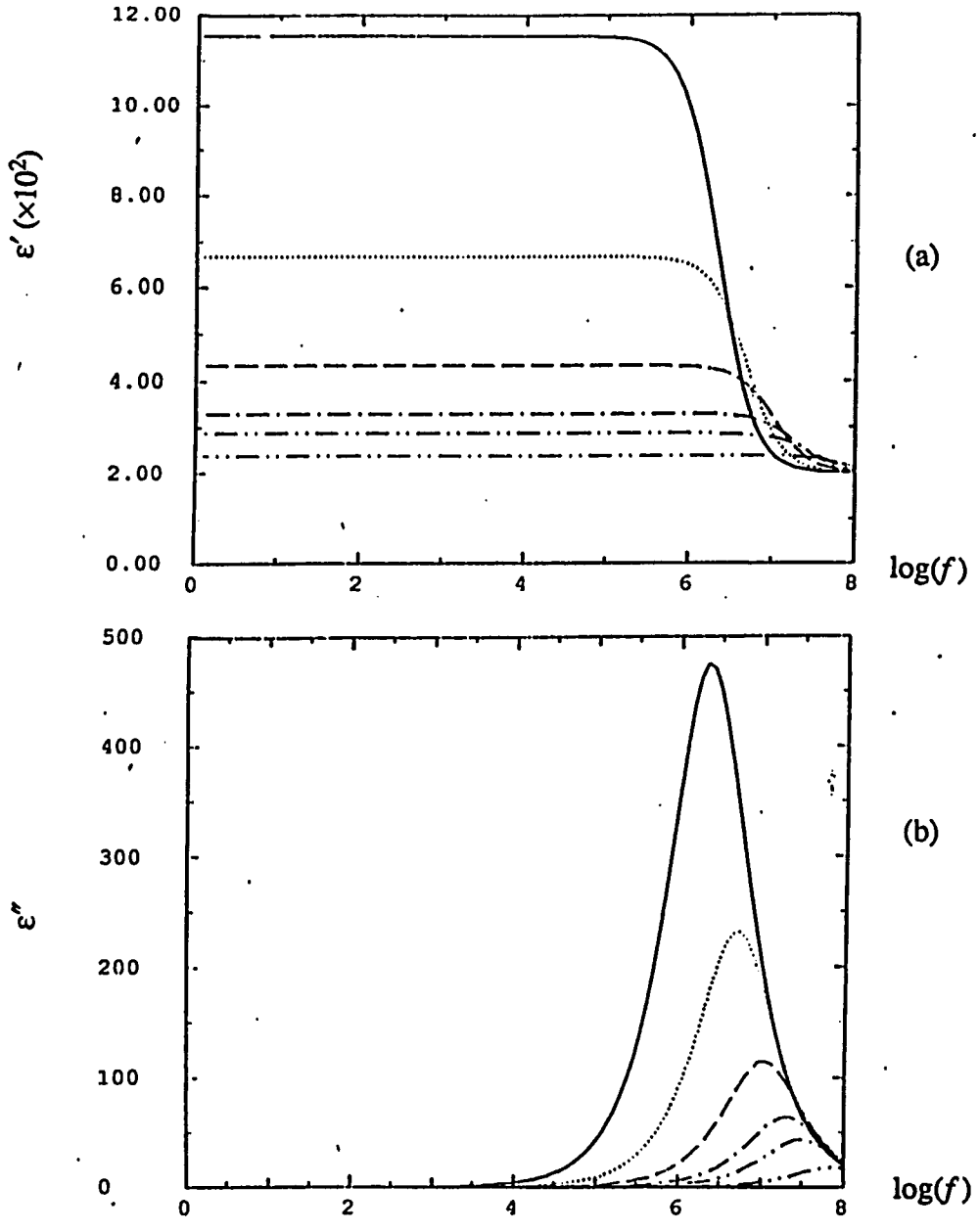

Fig.1.26. The real (a) and imaginary (b) part of dielectric constant as a function of frequency near the 1/8 lock-in transition point T_8^+. From top to bottom: $T = T_8^+ + 0.01, 0.02, 0.04, 0.07, 0.1, 0.2\ K$.

Chapter I.3

Dielectric Constant Measurements

I.3.1. Sample Preparation and Experimental Apparatus

a) Crystal growth and sample preparation

Thiourea single crystals were grown from saturated methanol solution by slow evaporation at a constant temperature of 38°C. The solution was purified by repeated crystallization. The evaporation rate was adjusted so that crystals of centimeter size were formed in a period of several weeks. Only clearly transparent crystals without visible clouds or defects were used for dielectric constant measurements.

A single crystal forms a six-side prism as shown in fig.1.27. The orientation was determined by X-ray diffraction along with optical birefringence observations and confirmed by Raman spectra. The ferroelectric direction is along **a**.

Specimens were cut on a string saw and dry polished for dielectric measurements. Aluminium electrodes were evaporated on the surfaces perpendicular to the ferroelectric axis and lead wires were attached with silver paint. To obtain the lowest possible measuring field in the sample, a 2.7 *mm* thick sample ($a \times b \times c = 2.7 \times 6.0 \times 8.0\ mm^3$) was prepared. Most of the low-field dielectric constant data were obtained from this sample. A thinner sample with dimensions $a \times b \times c = 0.5 \times 3.2 \times 6.0\ mm^3$ was prepared for relative high-field measurements.

b) Dielectric constant measurement apparatus

The dielectric constant of thiourea was measured by conventional impedance

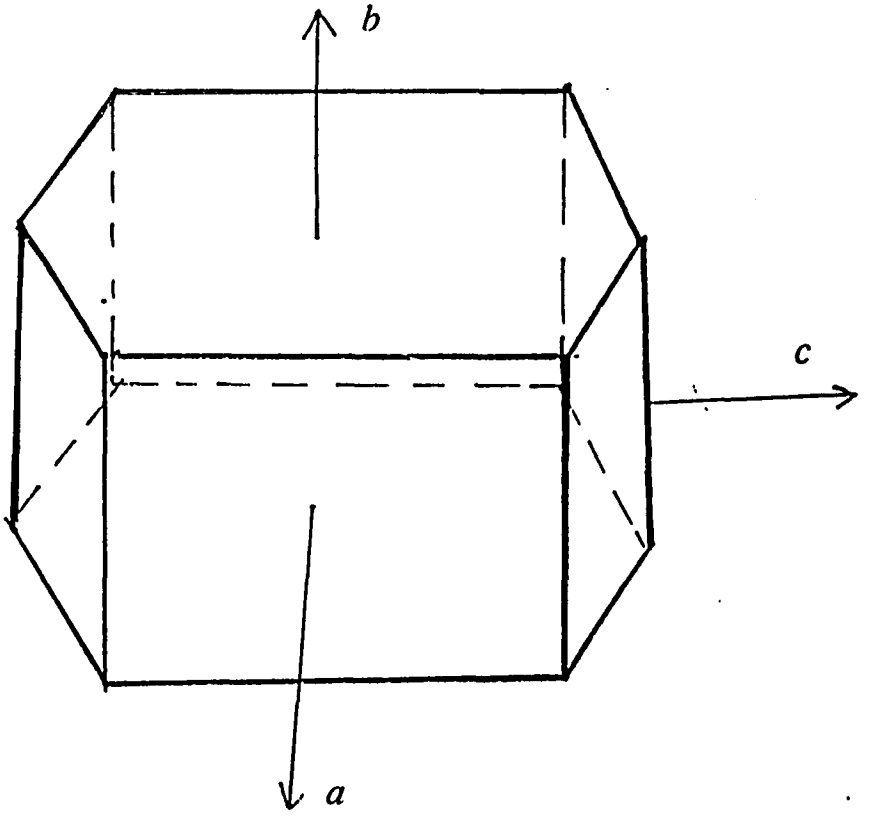

Fig.1.27. Thiourea single crystal.

analysis. The experimental apparatus is schematically shown in fig.1.28.

The sample was mounted loosely in a brass housing which was attached to the cold finger of an Oxford DN1754 nitrogen cryostat equipped with a platinum resistance thermometer, and controlled by an Oxford ITC-4 digital temperature controller.

The capacitance C and the dissipation factor D of the sample were measured with a Hewlett Packard 4192A automatic impedance analyzer which provides AC measuring voltages between $5\ mV$ and $1.1\ V$, $5\ Hz - 13\ MHz$ measuring frequencies, and $-35 - 35\ V$ DC biasing voltages. The impedance analyzer was interfaced to an IBM PS2 computer via a Hewlett Packard 82990A HP-IB interface board.

During an experiment, the temperature was scanned continuously by the Oxford temperature controller at a programmed scanning rate. At selected times (corresponding to a set of temperatures) the HP impedance analyzer automatically measured C and D of the sample with given measuring voltages V_m, frequencies f and biasing voltages V_b. The data of C, D, V_m and f were recorded and stored in the computer along with the time and temperature. A typical BASIC data acquisition program is listed in Appendix A. After the data acquisition, the raw data which are in ASCII code were transferred to a Vax780 mainframe computer and converted to numerical data.

The complex dielectric constant

$$\varepsilon^* = \varepsilon' - i\varepsilon'' \tag{1.133}$$

was determined from the C and D data along with the frequencies of the measuring AC voltage. The sample with electrodes can be considered as a capacitor and the dielectric constant of the sample is complex. The complex capacitance is given by:

$$C = \frac{\varepsilon^* S}{d} = \frac{S}{d}(\varepsilon' - i\varepsilon''). \tag{1.134}$$

where S is the sample area and d the thickness. Then the relationship between the

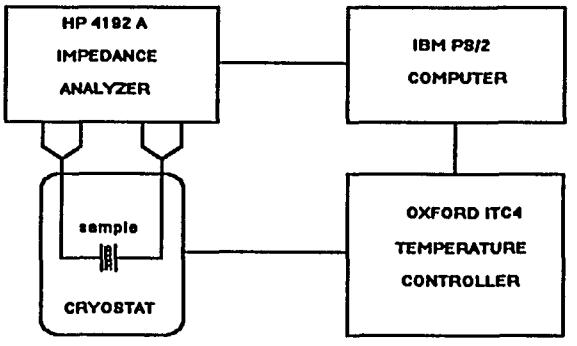

Fig. 1.28. Block diagram of the dielectric constant measurement apparatus.

complex current $\tilde{I}$ and voltage $\tilde{V}$ is

$$\tilde{I} = i\omega C\ \tilde{V} = \omega\frac{S}{d}(i\varepsilon' + \varepsilon'')\tilde{V}. \tag{1.135}$$

where ω is the angular frequency. On the other hand, what the impedance analyzer measures is the capacitance and the dissipation factor of the equivalent circuit shown in fig.1.29. i.e.

$$\tilde{I} = (i\omega C + \frac{1}{R})\tilde{V} \tag{1.136}$$

and the dissipation factor is defined by

$$D = \frac{Re(\tilde{I})}{Im(\tilde{I})} = \frac{1}{\omega RC} \tag{1.137}$$

Therefore, the relationship between (C, D) and $(\varepsilon', \varepsilon'')$ is:

$$\varepsilon' = \frac{Cd}{S} \tag{1.138}$$

$$\varepsilon'' = D\varepsilon'. \tag{1.139}$$

With our experimental setup, we can measure the real and imaginary part of the dielectric constant as a function of temperature, frequency, time, biasing electric field, and measuring E-field. We are able to investigate the effects of measuring E-fields at low levels (the lowest measuring field we used was 18 *mV/cm*), which is particularly important in studying the mechanism of the $\frac{1}{8}$ ferroelectric lock-in transition.

Because there is a temperature gradient between the sample and the thermometer which was placed outside the sample holder, the absolute value of the temperature measured in the experiments could have a systematic error of about 2 K. However, since the temperature was scanned continuously with a constant cooling (or warming) rate, the error due to the temperature gradient should be a constant for a slow run in a narrow temperature range. Therefore, it will not affect the measurements of the temperature interval of the $\frac{1}{8}$ lock-in phase.

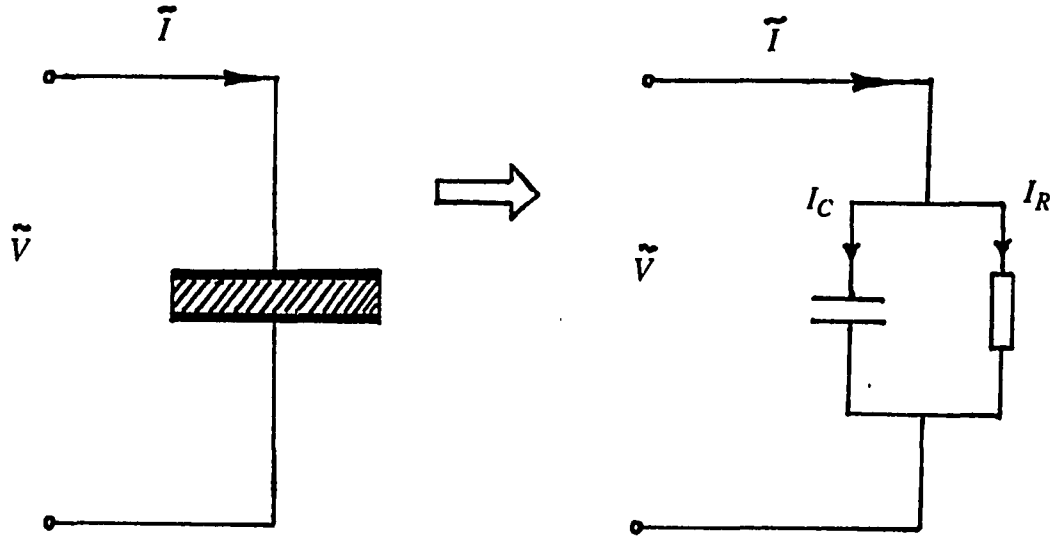

Fig.1.29. Equivalent circuit of the sample capacitor.

I.3.2. The Observed Anomalies

The real part of the dielectric constant of thiourea along the a axis as a function of temperature, $\varepsilon'(T)$, measured with 185 mV/cm measuring field at 1 KHz and 100 KHz is shown in fig.1.30. The dielectric constant is essentially frequency independent except for the temperature regions in or close to the two ferroelectric phases. Therefore, the static dielectric constant is equal to ε' measured at 1 KHz except for the frequency-dependent regions.

On cooling at atmospheric pressure, five anomalies were observed.

The first peak at 202 K corresponds to the normal-incommensurate transition. The continuous change in $\varepsilon'(T)$ indicates that the phase transition is a second order transition. The shape of the peak is correctly predicted by the Landau theory (eq.(1.68)).

The second anomaly at about 177K actually consists of two sharp peaks separated by a temperature interval about 0.7 K, indicating the upper and lower transition points of the $\frac{1}{8}$ ferroelectric phase. We will present a detailed discussion of the dielectric behavior in this region in the next section.

The third anomaly is a small plateau from 171 K to 169 K, which corresponds to the $\frac{1}{9}$ commensurate phase range. This small change in $\varepsilon'(T)$ is consistent with the Landau theory discussed in section I.2.4. Namely, the $\frac{1}{9}$ lock-in term does not couple to the electric field so that it has little effect on the dielectric behavior; the small plateau comes from small change in the modulation wavevector and amplitude.

The fourth anomaly at T_c = 169 K is a sudden jump in $\varepsilon'(T)$ which indicates the first order transition from the $\frac{1}{9}$ commensurate phase to the final ferroelectric phase.

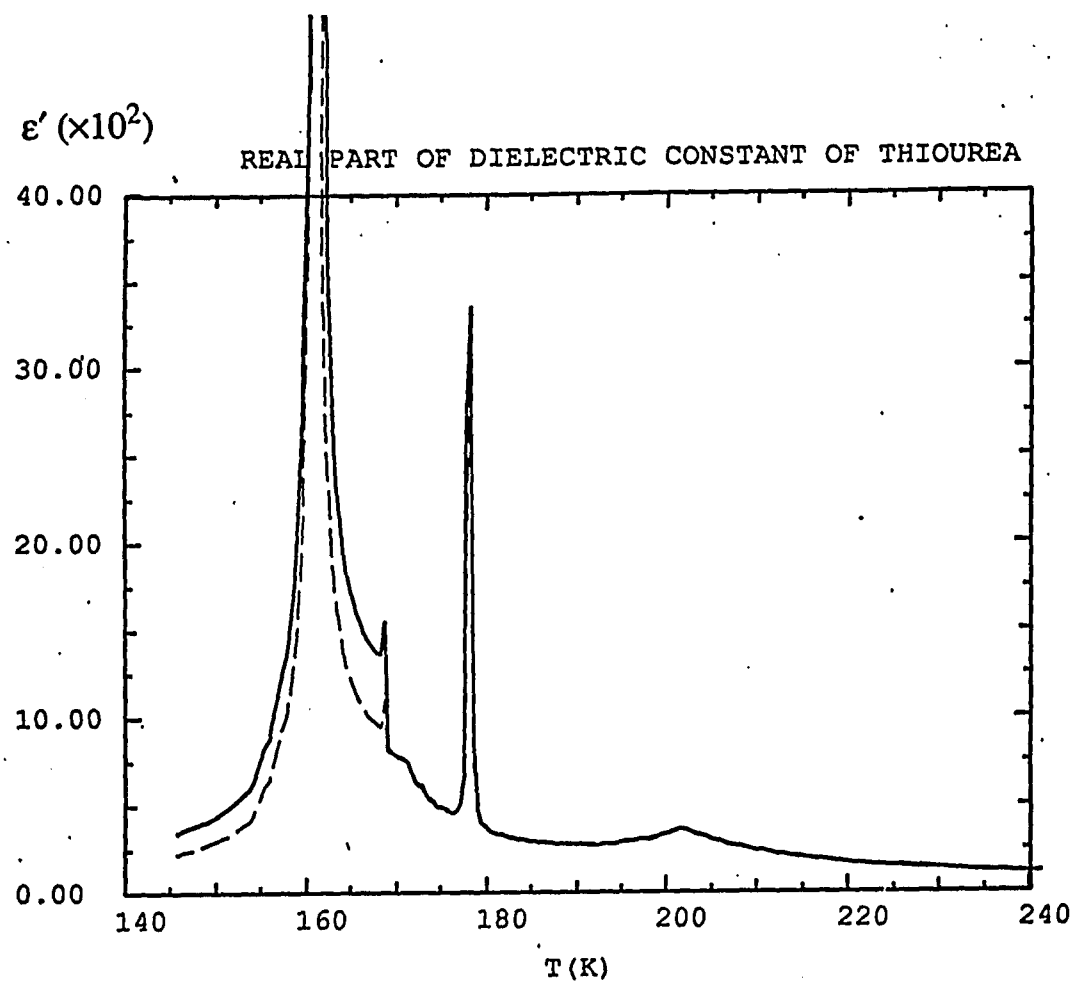

Fig.1.30. Real part of the dielectric constant vs. temperature with different frequencies. Solid line: f = 1 KHz. Broken line: f = 100 KHz.

The dielectric constant $\varepsilon'(T)$ below T_c exhibits somewhat complicated properties. It depends on frequency, measuring field, time, etc. In particular, both the real and imaginary parts of the dielectric constant decrease with decreasing measuring field. In fact, when the measuring field is lower than $\sim 50mV/cm$, the dielectric constant just below T_c is smaller than that just above T_c. The dielectric constant just bellow T_c should be explained along with the last anomaly at $160\,K$.

The last anomaly is a huge peak at about $160\,K$ which does not correspond to any known phase transition. Mashiyama *et al* proposed an interpretation of this peak based on the interaction mechanism between the residual discommensurations in the final ferroelectric phase [M6]. They observed diffuse X-ray scattering in the temperature region between $160\,K$ and $169\,K$, which indicates the existence of residual discommensurations in this temperature region. They also investigated the E-field effects on the dielectric constant in this temperature region and concluded that the interaction between the residual discommensurations changes from oscillatory to exponentially at $\sim 160\,K$, which gives rise to the extra dielectric anomaly.

The temperature dependence of the real part of dielectric constant $\varepsilon'(T)$ in the normal phase can be well described by a Curie-Weiss law. The experimental data were fitted to the result of Landau theory (see. eq.(1.68)):

$$\varepsilon'(T) = \varepsilon_b + \frac{4\pi}{a(T-T_0)} \tag{1.140}$$

The best fit gives:

$$\varepsilon_b = 12.968$$
$$a = 2.286\times10^{-3}\ (K^{-1})$$
$$T_0 = 186.73\ K$$

The temperature dependence of the inverse of the electric susceptibility predicted by Landau theory is a straight line:

$$\chi^{-1}(T) = \frac{\partial^2 F}{\partial \eta_0^2}\Big|_{E=0} = a(T - T_0) \tag{1.141}$$

The $\chi^{-1}(T)$ data from experimental measurements and the theoretical result of (3.6) are in very good agreement (see fig.1.31).

As discussed in sec.I.2.4, the overall shape of $\varepsilon'(T)$ in the incommensurate phase can be described by the Landau theory with the second harmonic of the primary order parameter taken into account. In particular, the substantial increase in $\varepsilon'(T)$ near T_c can be explained. However, a quantitative agreement could not be obtained when the ε_b, a, and T_0 were kept at the values determined from $\varepsilon'(T)$ in the normal phase. On the other hand, reasonable agreement was obtained by treating ε_b, a, ,T_0 and $\frac{B}{\gamma}$ as free parameters in a compromise fit for the dielectric constant in the temperature range covering both the normal and incommensurate phases ($171 \sim 242\ K$ except for $176 \sim 180\ K$). The fitting result is shown in fig.1.32.

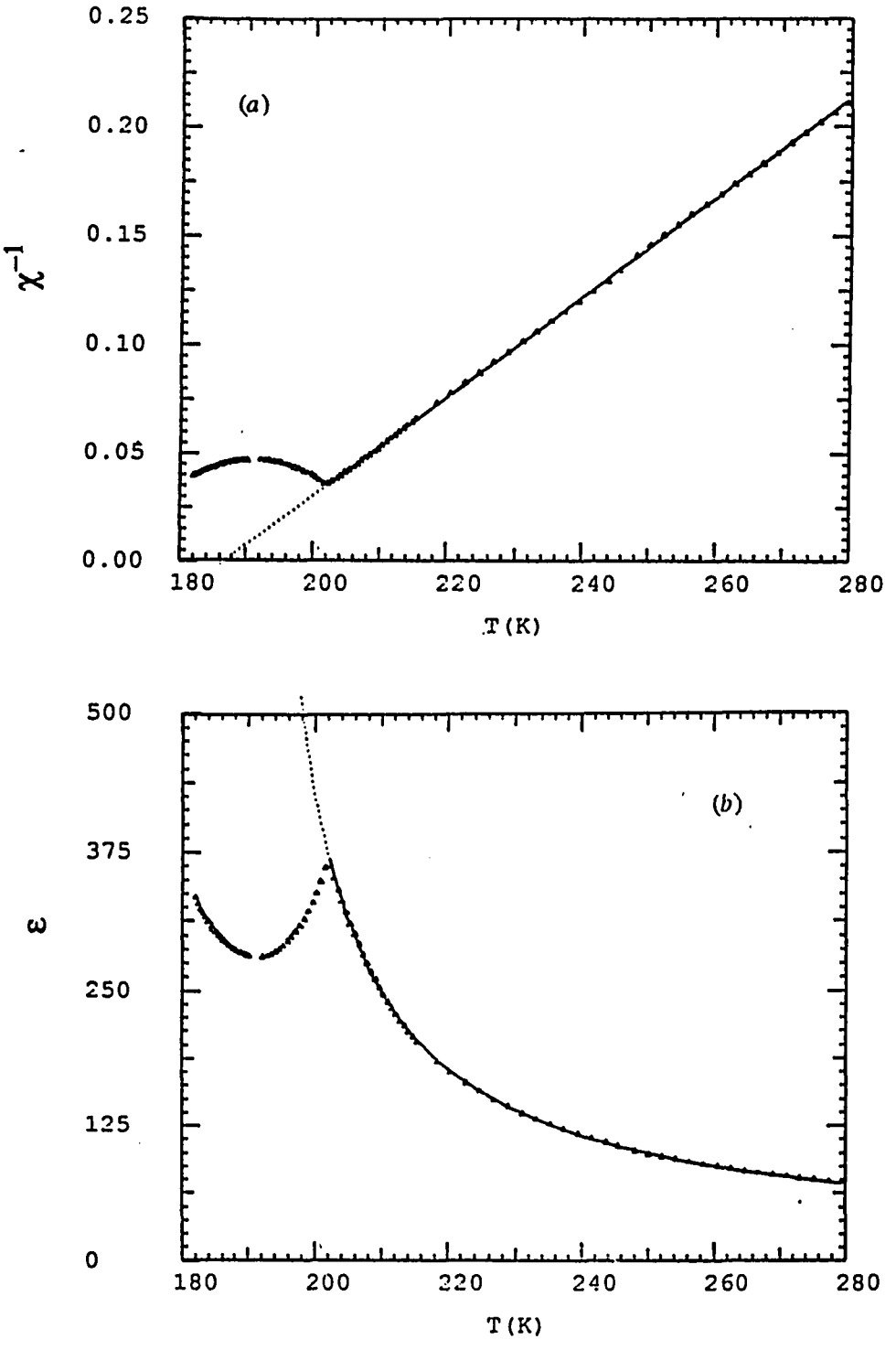

Fig.1.31. (a): χ^{-1} vs. T in the normal phase. (b): ε vs. T. Triangular points -- from experimental data. Solid line: theoretical fit.

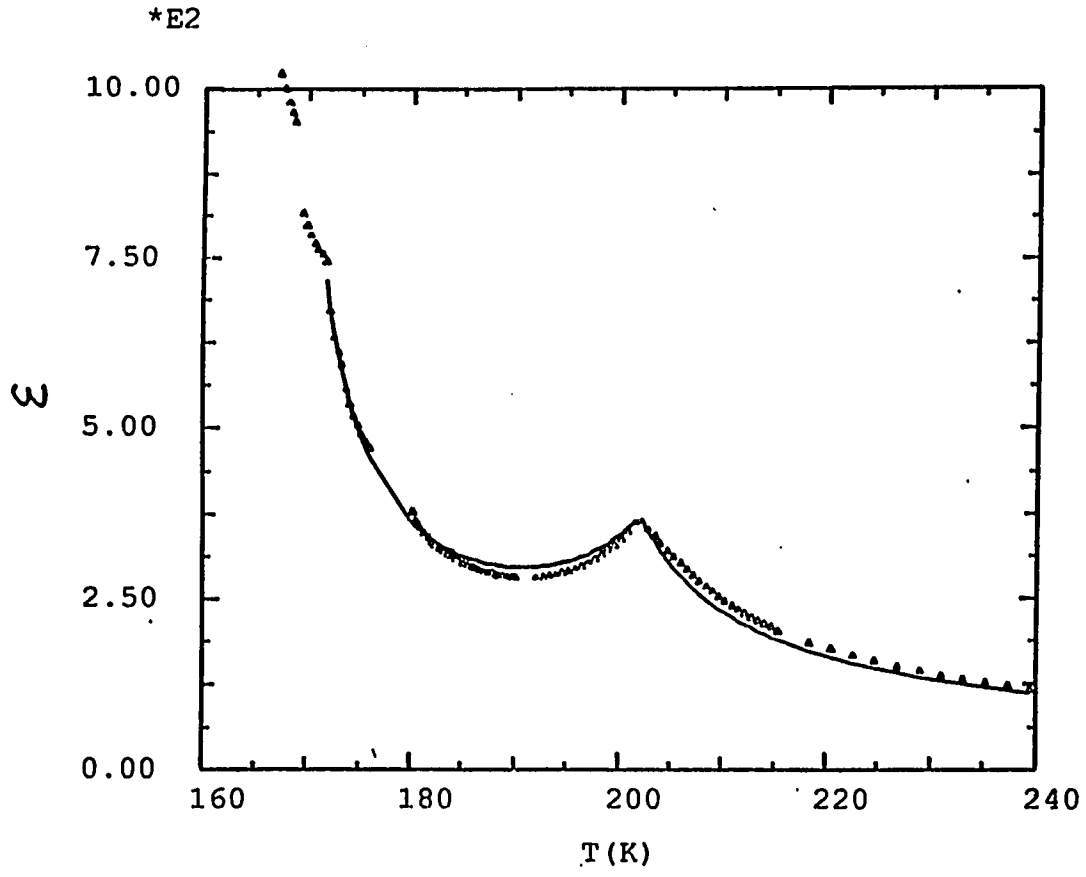

Fig.1.32. 4-parameter fit of $\varepsilon'(T)$ in the normal and incommensurate phases. Second harmonic is included. $a = 3.415 \times 10^{-3}$, $T_0 = 190.90$, $\frac{B}{\gamma} = 2.223 \times 10^{14}$, $\varepsilon_b = 46.8$ (in cgse units).

I.3.3. Dielectric Behavior Pertaining to the 1/8 lock-in transition

a) $\varepsilon'(T)$ at different measuring field levels

As discussed in sec.I.2.4, the temperature interval of the intrinsic $\frac{1}{8}$ ferroelectric phase can be determined by dielectric constant measurements with measuring fileds much lower than $v\eta^8$ which is 47 *V/cm*. The measuring fields we used for these dielectric constant measurements were from 18 *mV/cm* to 3.7 *V/cm*.

Fig.1.33 shows a typical result for the real part of the dielectric constant as a function of temperature near the $\frac{1}{8}$ phase region. The measuring field was 18 *mV/cm*, the cooling rate 0.2 *K/min*, the frequency 1 *KHz* and the temperature resolution was 0.07 *K*. The two peaks indicating the boundary of the $\frac{1}{8}$ lock-in phase are clearly well separated. The temperature interval was found to be about 0.7*K*. The temperature interval and the shape of the peaks are essentially frequency-independent for frequencies lower than 100 *KHz* (see fig.1.34). Therefore, it is reasonable to consider the dielectric constant measured with frequencies lower than 100 *KHz* as the static dielectric constant. The non-zero temperature interval and the shape of the two peaks corresponding to the upper and lower transition points of the $\frac{1}{8}$ ferroelectric phase are consistent with the Landau theory discussed in sec.1.2.4.

As seen in fig.1.35, when the measuring field is below 0.7 *V/cm*), the dielectric anomaly near the $\frac{1}{8}$ phase is essentially independent of the level of the measuring field. Specifically, ΔT_8 does not tend to decrease with decreasing measuring field at all. For $E_m > 0.7$ *V/cm*, ΔT_8 even increases slightly with decreasing measuring fields, but the peak heights decreases with decreasing measuring field. This measuring-field-dependence can be interpreted as the result of polarization reversal. When the

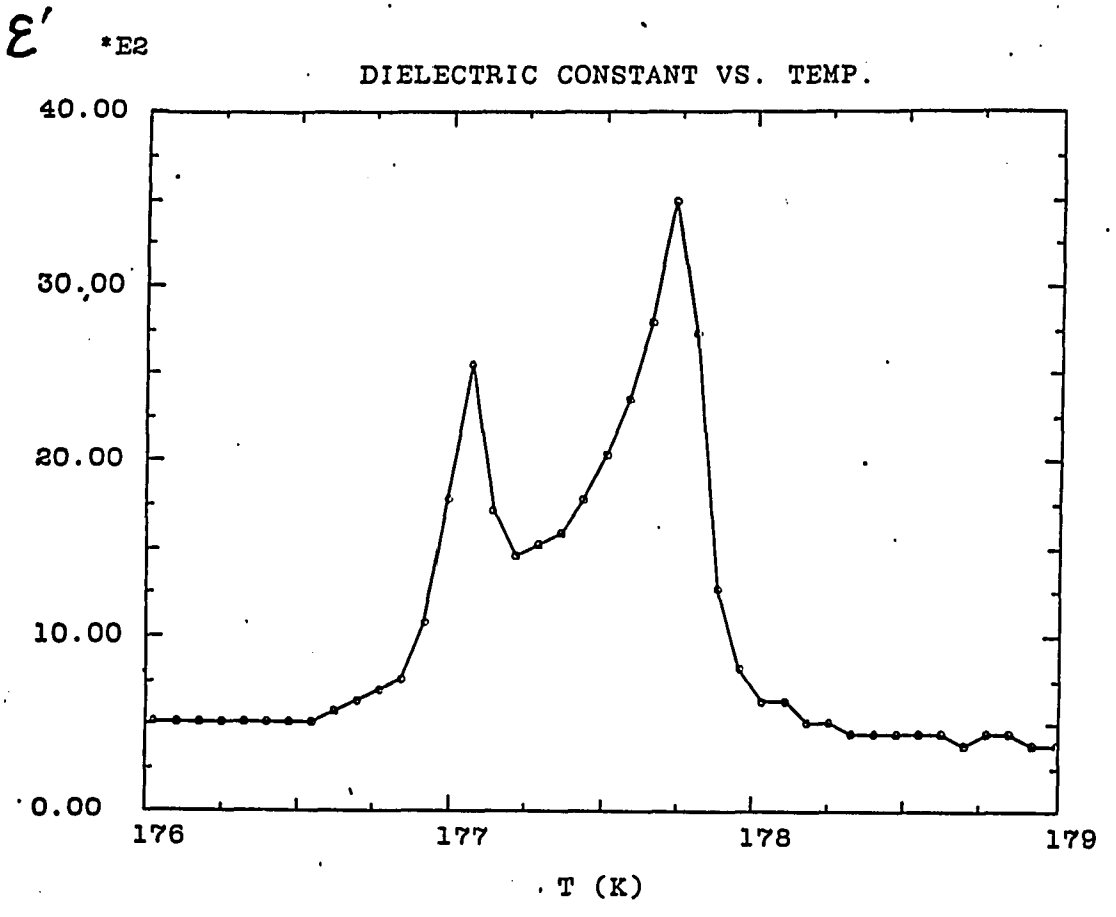

Fig.1.33. Experimental data of ε′ vs. T in the vicinity of the $\frac{1}{8}$ phase. Measuring field: E_m = 18 *mV/cm*.

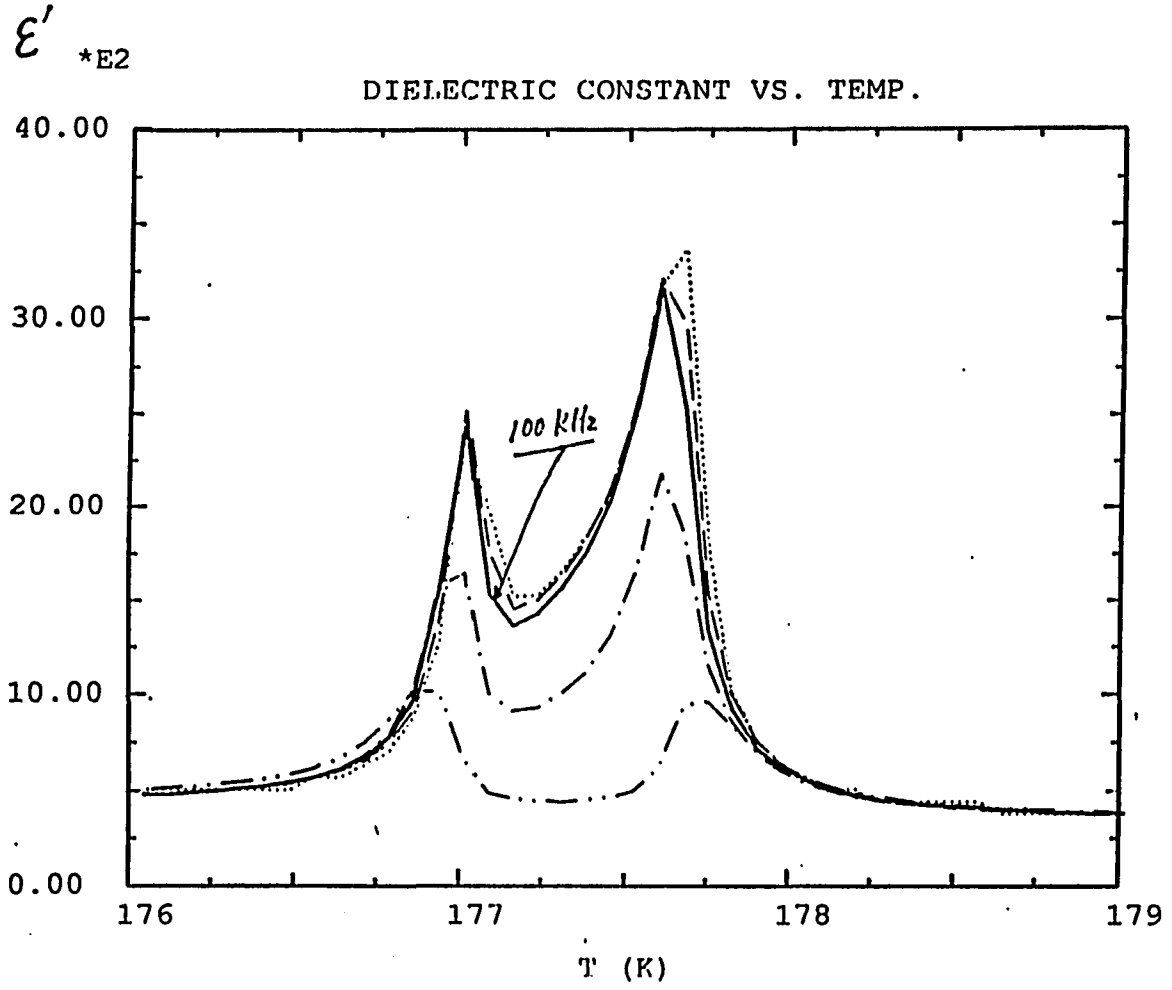

Fig.1.34. Experimental data of ε′ vs. T at different frequencies. From top to bottom: $f = 0.5\,K,\ 10\,K,\ 100\,K,\ 1\,M,\ 10\,M$ *Hz*. The measuring field is 100 *mV/cm*.

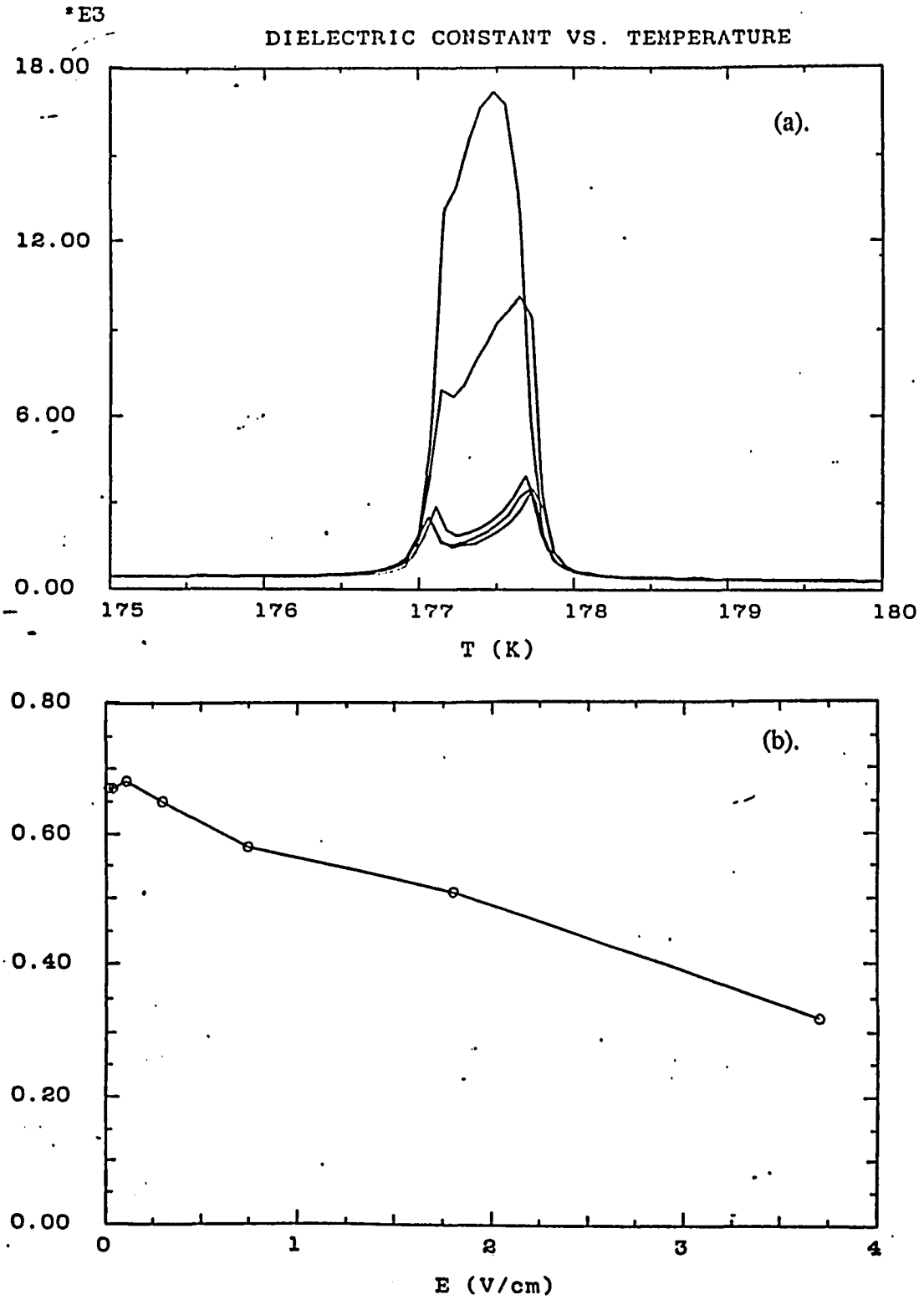

Fig.1.35. The effects of measuring field E_m. (a). ε' vs. T at different measuring fields (from top to bottom: E_m = 3.7, 1.8, 0.74, 0.30, 0.018 *V/vm*). (b). ΔT_g vs. E_m. ΔT_g does not extrapolate to zero at zero measuring E-field.

AC measuring field is high enough to reverse the spontaneous polarization, the sample exhibits a dramatic increase in dielectric response [L7]. From our experiments, it was found that the coercive field for reversing the spontaneous polarization in the $\frac{1}{8}$ ferroelectric phase is about 1 *V/cm*. When the measuring field is higher than the coercive field, the observed dielectric constant depends strongly on the the value of the spontaneous polarization so that the peaks in the $\varepsilon'(T)$ curve do not correspond to the transition points. In fact, as the measuring field was increased (above 1 *V/cm*), the observed two peaks of $\varepsilon'(T)$ tend to join into one strong peak where the spontaneous polarization has the maximum value.

On the other hand, even with the measuring field considerably higher than the coercive field, the separated two peaks were still observed in high frequency measurements. (see fig.1.36) In this case, the polarization reversal process presumably cannot follow the rapidly varying measuring field so that the observed dielectric response still reveals some of the basic features of the static dielectric constant.

b) Thermal hysteresis

To study the thermal hysteresis effects of the $\frac{1}{8}$ lock-in transition, we measured the cool-down and warm-up $\varepsilon(T)$ curves in slow temperature scans (0.1 *K/min*). The curves are shown in fig.1.37. Although it was difficult to determine the small difference of the transition temperatures for the two runs, the significant difference in the shape of the curves certainly indicates thermal hysteresis. We found that the peaks corresponding to approaching the lock-in phase are considerably stronger than the ones corresponding to receding from the lock-in phase.

From the soliton structure point of view, the incommensurate-to-commensurate

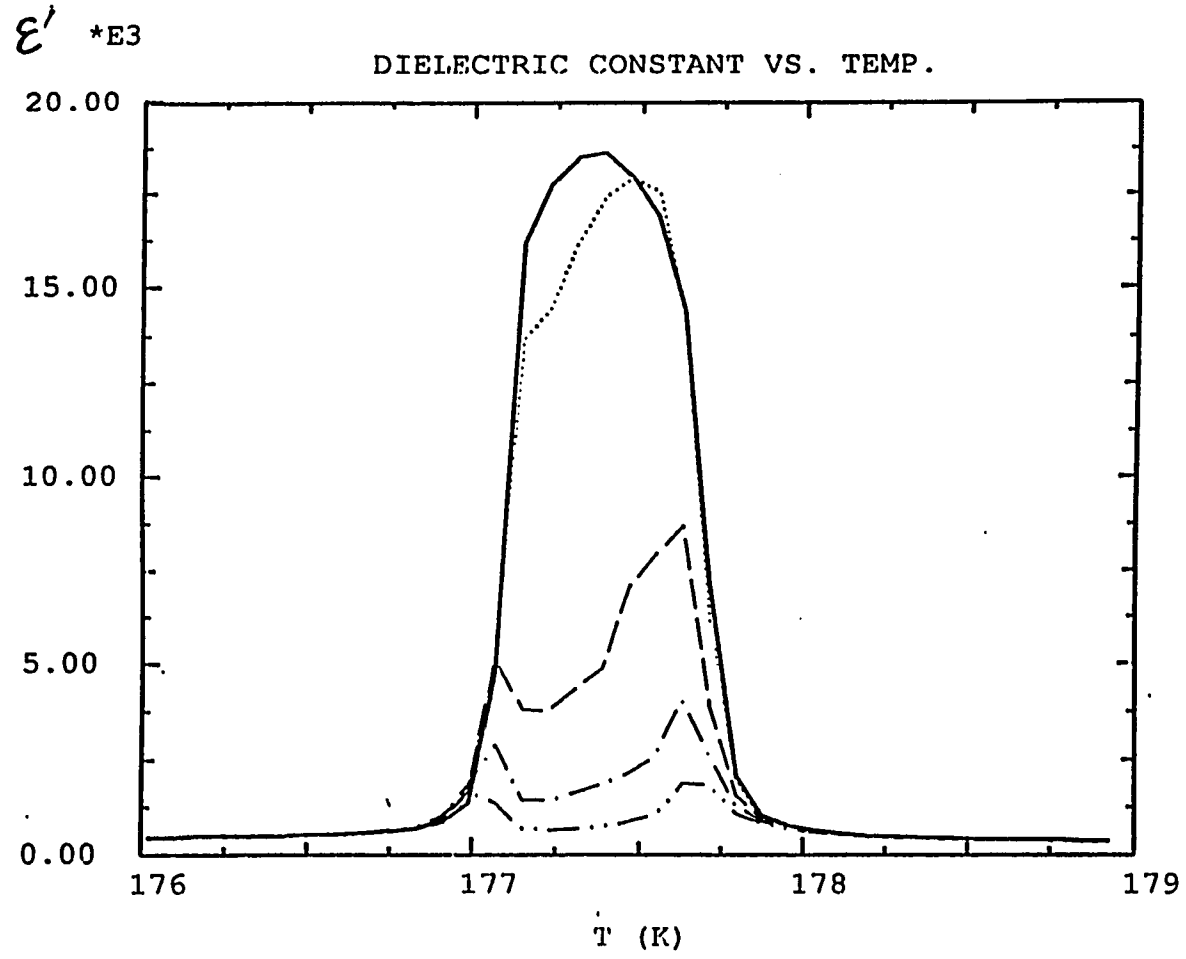

Fig.1.36. $\varepsilon'(T)$ measured with $E_m = 3.7$ *V/cm* at different frequencies. From top to bottom: 0.5, 1, 10, 100, 1000 *KHz*.

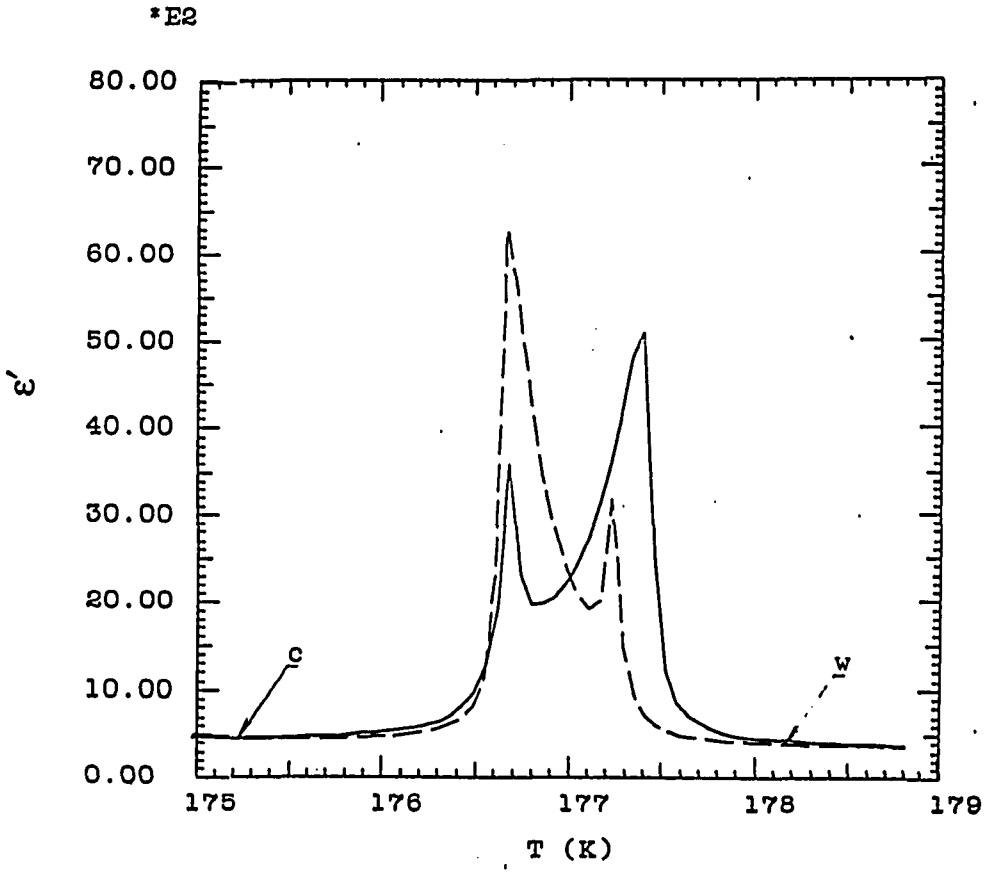

Fig.1.37. Thermal hysteresis of $\varepsilon'(T)$ near the $\frac{1}{8}$ phase. Solid line: cooling down. Broken line: warming up.

transition corresponds to a process of soliton melting; and the commensurate-to-incommensurate transition corresponds to the nucleation of solitons. Consequently, they are very close to second-order phase transitions [B7]. The substantial difference between the "in" and "out" transitions observed in our experiments may result from defects which could pin the solitons and play a significant role in the dielectric properties [H2][H3].

c) Frequency dependence of the complex dielectric constant

We investigated the frequency dependence of the complex dielectric constant near the $\frac{1}{8}$ ferroelectric phase. With a 0.1 *V/cm* measuring field, we were able to obtain reliable data for the real and imaginary part of $\varepsilon^*(T,\omega)$ in the frequency range 5 *KHz* – 10*MHz*. The imaginary part of $\varepsilon^*(T,\omega)$ is too small to be measured reliably for frequencies lower than 5 *KHz* with our instrument.

The real and imaginary parts of the dielectric constant as a function of frequency at different temperatures are shown in fig.1.38. The curves qualitatively resemble the results of the theoretical prediction given in sec.I.2.5. In particular, the slowing-down of relaxation processes was observed near both the upper and lower transition points of the $\frac{1}{8}$ lock-in phase.

However, the theory predicts that the relaxation time τ should diverge to infinity at the transition points, but the experimental data shows that τ stops increasing at about 10^{-6} *sec.* , remains constant in the $\frac{1}{8}$ phase and then decreases again on leaving the $\frac{1}{8}$ phase. This "incomplete slowing down" of the relaxation could be explained by the "pinned soliton" picture proposed by Holakovsky and Dvorak in 1988 [H2]. The

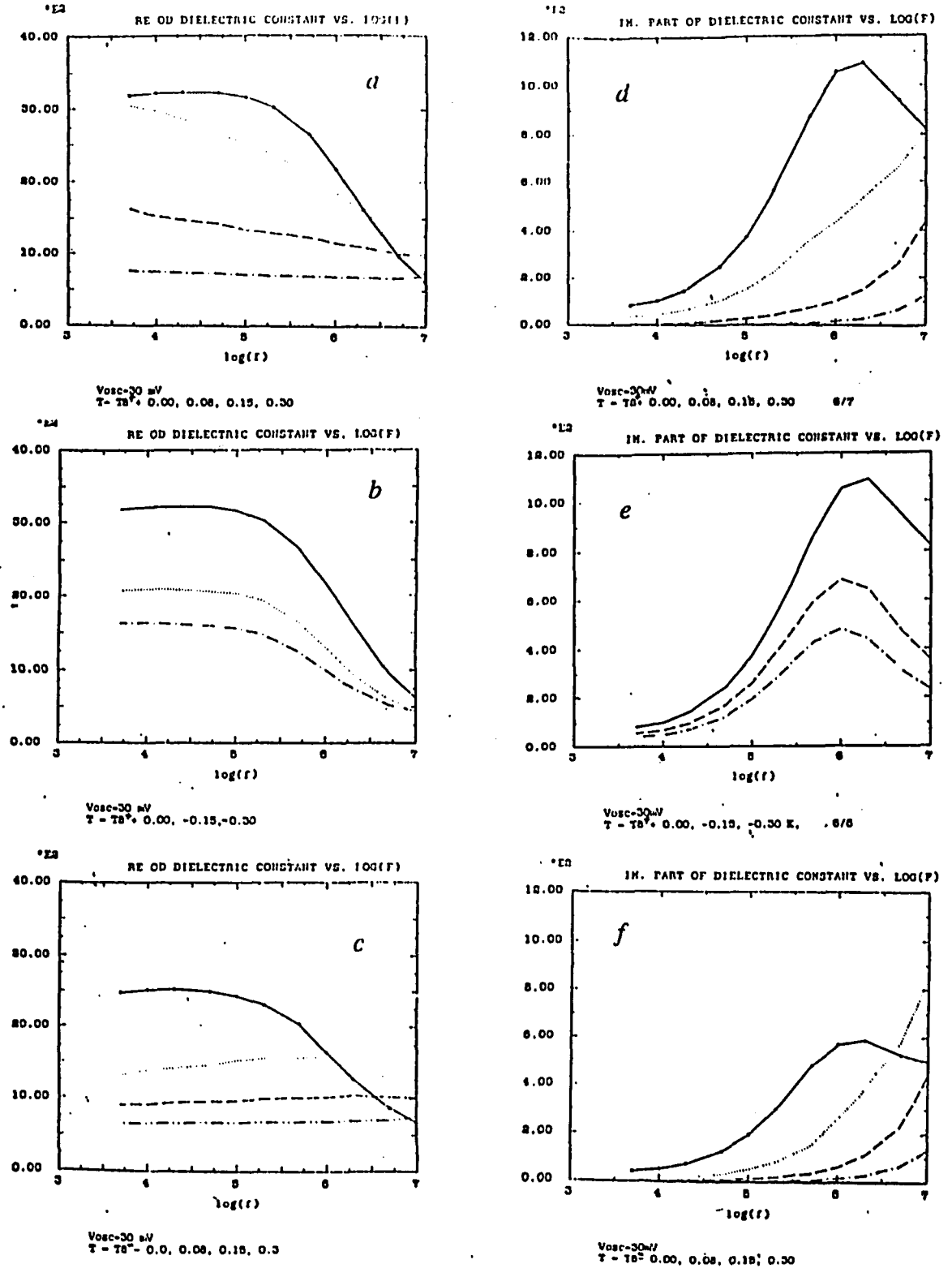

Fig.1.38. Real and imaginary part of the dielectric constant as a function of frequency at different temperatures. (a), (b) and (c): real part; (d), (e) and (f): imaginary part. (a) and (d): above the 1/8 phase; (b) and (e): within the 1/8 phase; (c) and (f): below the 1/8 phase.

relaxation processes probed by dielectric constant measurements correspond to the motions of the solitons about their equilibrium configurations. Since the intersoliton distance increases as the temperature approaches the transition points, the relaxation processes slow down because of the weakening of the intersoliton interactions. Ideally, the intersoliton distance $x_0(T)$ diverges at the transition points $T_8^{\ddagger}$, which leads to the diverging relaxation-time prediction (see sec.I.2.5). However, in a real crystal, solitons can be pinned by various defects [J6][B8]. Consequently, the intersoliton distance is always smaller than its ideal value [H2]. Due to the pinning effects, some residual solitons can persist even in the commensurate lock-in phase, which presumably leads to relaxation processes with a finite relaxation time at the lock-in transition points.

d) The effects of biasing fields

We measured the dielectric constant near the $\frac{1}{8}$ phase under different biasing electric fields E_b from 0 to 700 *V/cm*. The high biasing field data were obtained from the 0.5 *mm* thin sample. The real part of the dielectric constant as a function of temperature under several selected biasing fields is shown in fig.1.39a. The biasing field suppresses the two peaks and increases the temperature interval ΔT_8.

The values of ΔT_8 at different values of E_b obtained from these experimental measurements are listed in table 1.4 (also see fig.1.39b). When the biasing fields are lower than 7 *V/cm*, no changes in ΔT_8 were observed within the experimental accuracy. When E_b is higher than 30 *V/cm*, ΔT_8 start to increase with E_b significantly. This behavior is consistent with the Landau-theory prediction given in sec.I.2.3.

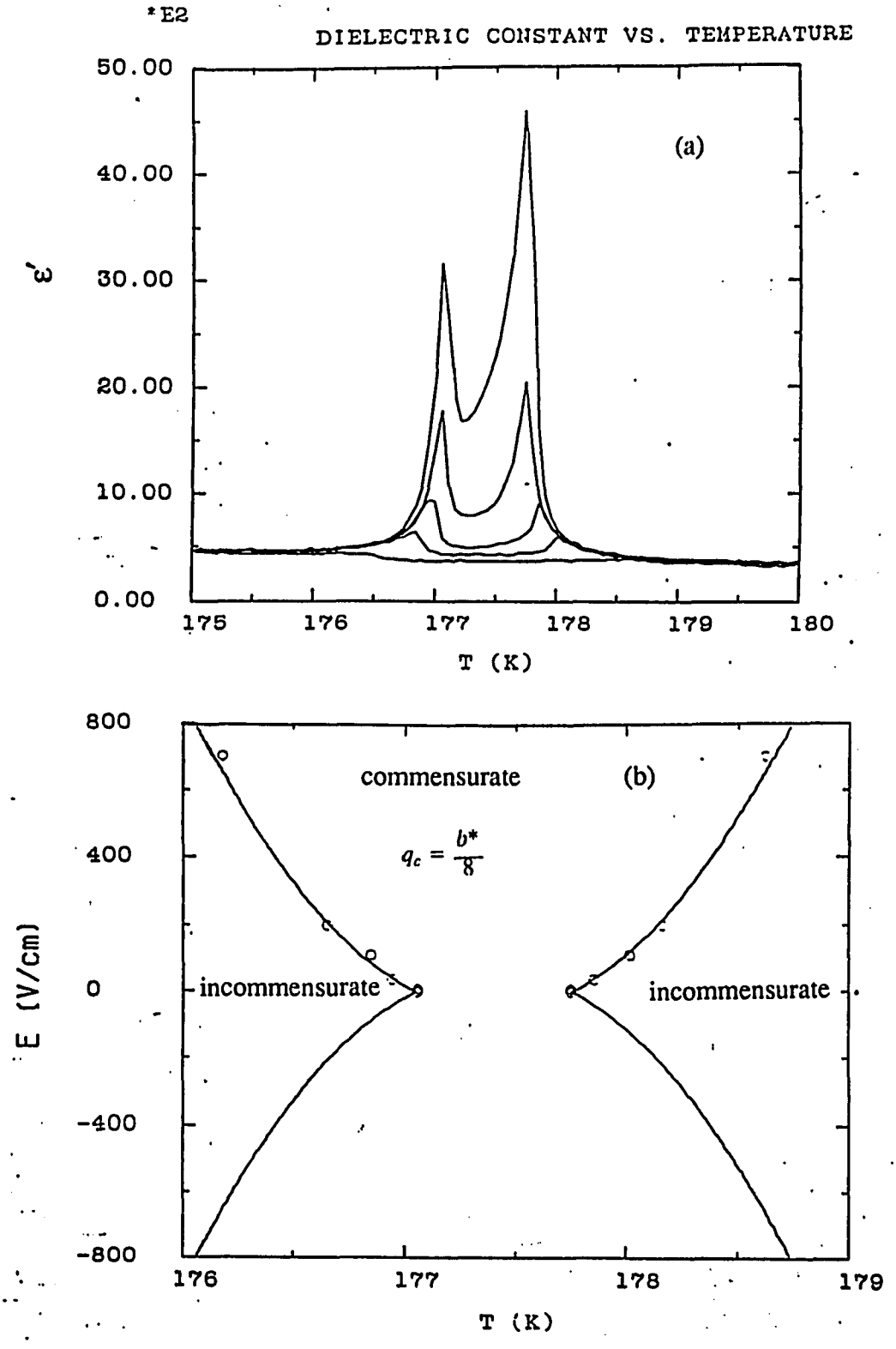

Fig.1.39. Effects of biasing E-fields. (a). $\varepsilon'(T)$ under different biasing E-filed levels E_b, from top to bottom: E_b = 700, 200, 110, 37.0, 7.40, 0.00 (*V/cm*). (b). (E-T) phase diagram near $\frac{1}{8}$ region obtained from dielectric constant data.

table 1.4 ΔT_8 at different biasing fields

E_b (V/cm)	0.0	1.85	7.41	37.0	111	200	700
ΔT_8 (K)	0.69	0.69	0.69	0.91	1.2	1.5	2.3

The (E-T) phase diagram mapped out by these experimental results can be fitted to a simplified formula derived from the Landau theory given in sce.I.2.3. When $q_0 \approx \frac{1}{8}$, eq.(1.22) can be approximated by

$$q_0^2(T) = q_i^2 - \frac{2a(T_I - T)}{\beta(3\frac{B}{\gamma} + 4q_i^2)} \tag{1.142}$$

Then, under the plane wave approximation, the $\frac{1}{8}$ phase boundary can be determined by (see 1.66):

$$T_8^{\pm} = T_8 \pm \sqrt{s\eta^6(|E| + \nu\eta^8)} \tag{1.143}$$

where

$$s = \frac{2\nu R(3\frac{B}{\gamma} + 4q_i^2)}{a}$$

T_8 is the temperature at which the modulation wavevector given by the base form of the free energy is equal to $\frac{b^*}{8}$. Since the temperature range is small, we treated the modulation amplitude η as temperature independent, and T_8^c was fixed at 177.4 K which was the average value of the center point of the two $\varepsilon'(T)$ peaks. Then we have two free fitting parameters $s\eta^6$ and $\nu\eta^8$. As shown in fig.1.39b, a good fit has been obtained.

The other major effect of biasing fields is that the height of the two peaks decreases with increasing biasing fields, which qualitatively agrees with the theoreti-

cal prediction given in sec.1.2.4. However, as noticed by Fousek and Kroupa in the case of Rb_2ZnCl_4 [F5], the experimental $\varepsilon'(T)$ curves with different biasing fields do not cross, which is not predicted by the theory (see fig.1.23 and fig.1.39a). As shown by Holakovsky and Dvorak, this non-crossing phenomena can be attributed to the commensurate-structure nucleation and soliton pinning effects due to lattice defects [H2].

e) Summary

In summary, we have measured the real and imaginary part of dielectric constant with different frequencies, different measuring and biasing fields in the temperature range covering the $\frac{1}{8}$ ferroelectric phase and its vicinity. First, we found that the temperature interval of the two well separated peaks does not extrapolate to zero at zero measuring field, which strongly indicates that the $\frac{1}{8}$ ferroelectric phase is intrinsic. Second, we found that the dynamic susceptibility near and in the $\frac{1}{8}$ phase can be qualitatively described by a Debye relaxation model. The observed slowing-down of the relaxation precess indicates the existence and the development of the soliton structure due to the $\frac{1}{8}$ lock-in term, which is consistent with the intrinsic lock-in mechanism. We also confirmed Gesi's result that biasing fields can increase the temperature interval of the $\frac{1}{8}$ phase and suppress the peak of the dielectric constant at the $\frac{1}{8}$ phase boundary [G4].

All the above results are predicted by the phenomenological Landau theory discussed in sec.I.2. However, there are some quantitative disagreements in details, which in principle can be explained by taking into account the defects that pin the

solitons and lead to the deviation from the ideal model.

Chapter I.4

D-E Hysteresis Loop Observations and Spontaneous Polarization Measurements

I.4.1. Predictions of the D-E Hysteresis Loops

The basic feature of ferroelectrics is the existence of a spontaneous polarization that can be reversed by an applied electric field. According to the Landau theory, the $\frac{1}{8}$ commensurate lock-in phase in thiourea is ferroelectric (see sec.I.2). Thus it is particularly important to verify the existence of the spontaneous polarization in this phase. Furthermore, since the polarization reversal process is different in an intrinsic ferroelectric than a field-induced one, the origin of the $\frac{1}{8}$ ferroelectric lock-in phase (field-induced or intrinsic) can be distinguished by D-E hysteresis observations.

In an intrinsic ferroelectric phase, there are two states of minimum free energy corresponding to the two equal-value but opposite-sign spontaneous polarizations (see fig.1.40a). To reverse the polarization and go from one equilibrium state to the other it is necessary to apply a coercive field to overcome the energy barrier between the two minima. Consequently, when an alternating E-field is applied along the ferroelectric axis, an open D-E hysteresis loop can be observed [D8]. A typical D-E hysteresis loop is shown in fig.1.40b. The spontaneous polarization and the coercive field can be measured from the loops. Ideally, the spontaneous polarization is equal to the electric displacement D divided by 4π at zero E-field since

$$\mathbf{D} = (1+4\pi\chi)\mathbf{E} + 4\pi\mathbf{P}_s \qquad (1.44)$$

where χ is the linear susceptibility. However, in practice domains of reversed

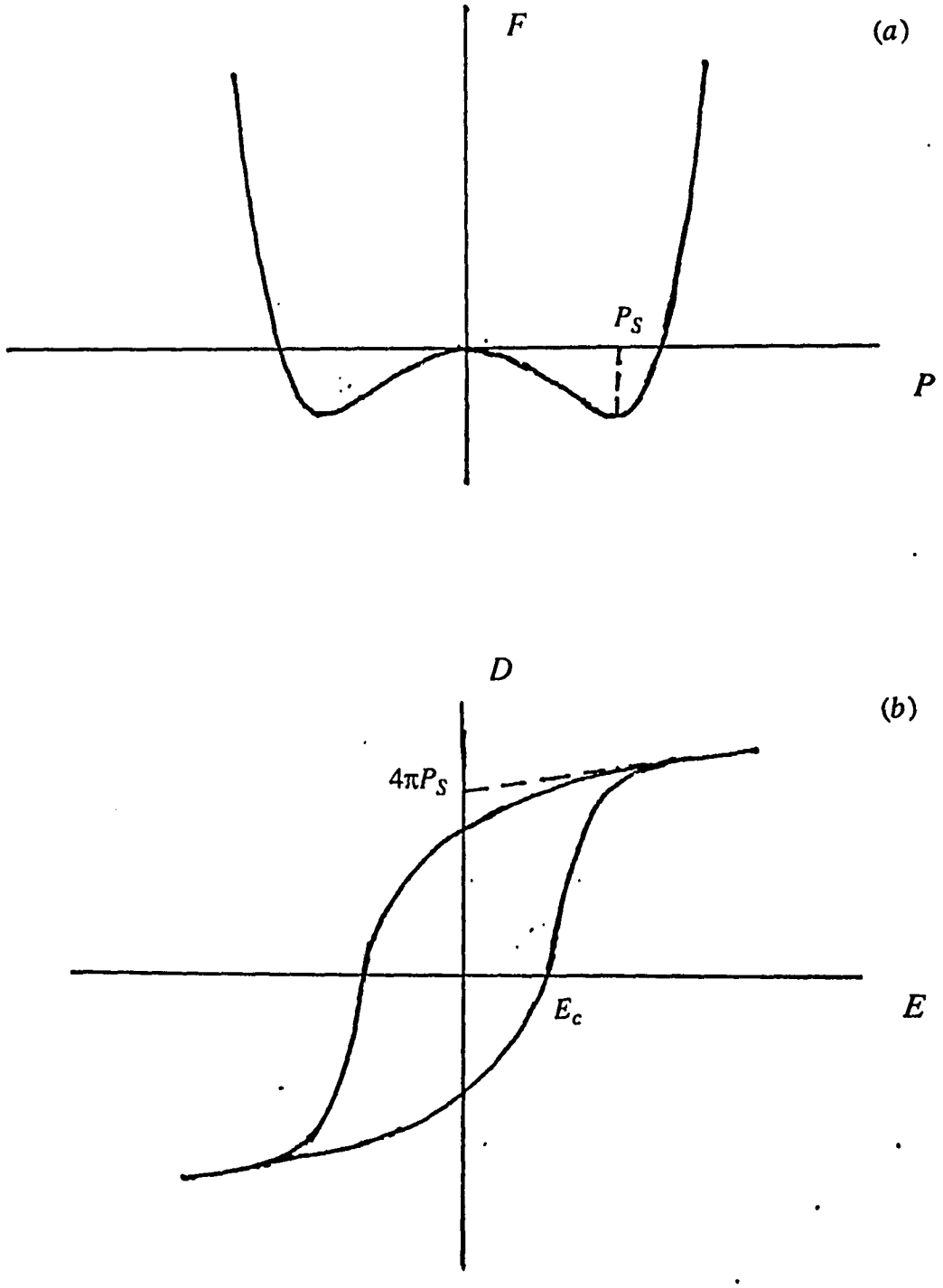

Fig.1.40. D-E hysteresis of intrinsic ferroelectrics. (a). Free energy as a function of electric polarization. (b). Single D-E hysteresis loop.

polarization start to nucleate before the applied E-field changes sign. Therefore, the spontaneous polarization should be determined by extrapolating the saturated electric dispacement to zero E-field, as shown in fig.1.40b.

In the case of field-induced ferroelectrics, in the absence of an applied electric field the lowest minimum free energy corresponds to a non-ferroelectric state, as seen in fig.1.41a. The other two minima corresponding to ferroelectric states are local minima (This picture is applicable only for first-order transitions). When an electric field is applied and one of the $P \neq 0$ minima becomes lower than the $P=0$ minimum, a field-induced ferroelectric phase transition will occur. Because of the energy barriers between the $P=0$ state and the $P = \pm P_s$ states, double D-E hysteresis loops will be observed in these field-induced ferroelectrics (see fig.1.41b). In fact, this kind of double loop was observed in $BaTiO_3$ about forty years ago [M15].

According to our theoretical analysis and dielectric constant measurements, there is a non-zero temperature interval where the $\frac{1}{8}$ ferroelectric phase is intrinsic. Outside the intrinsic phase, there is a field-induced region on each side where the $\frac{1}{8}$ phase can be stablized by an applied electric field. Therefore, it is reasonable to expect that single D-E loops will appear in a non-zero temperature region corresponding to the intrinsic $\frac{1}{8}$ phase, and double loops will appear in the field-induced region on both sides.

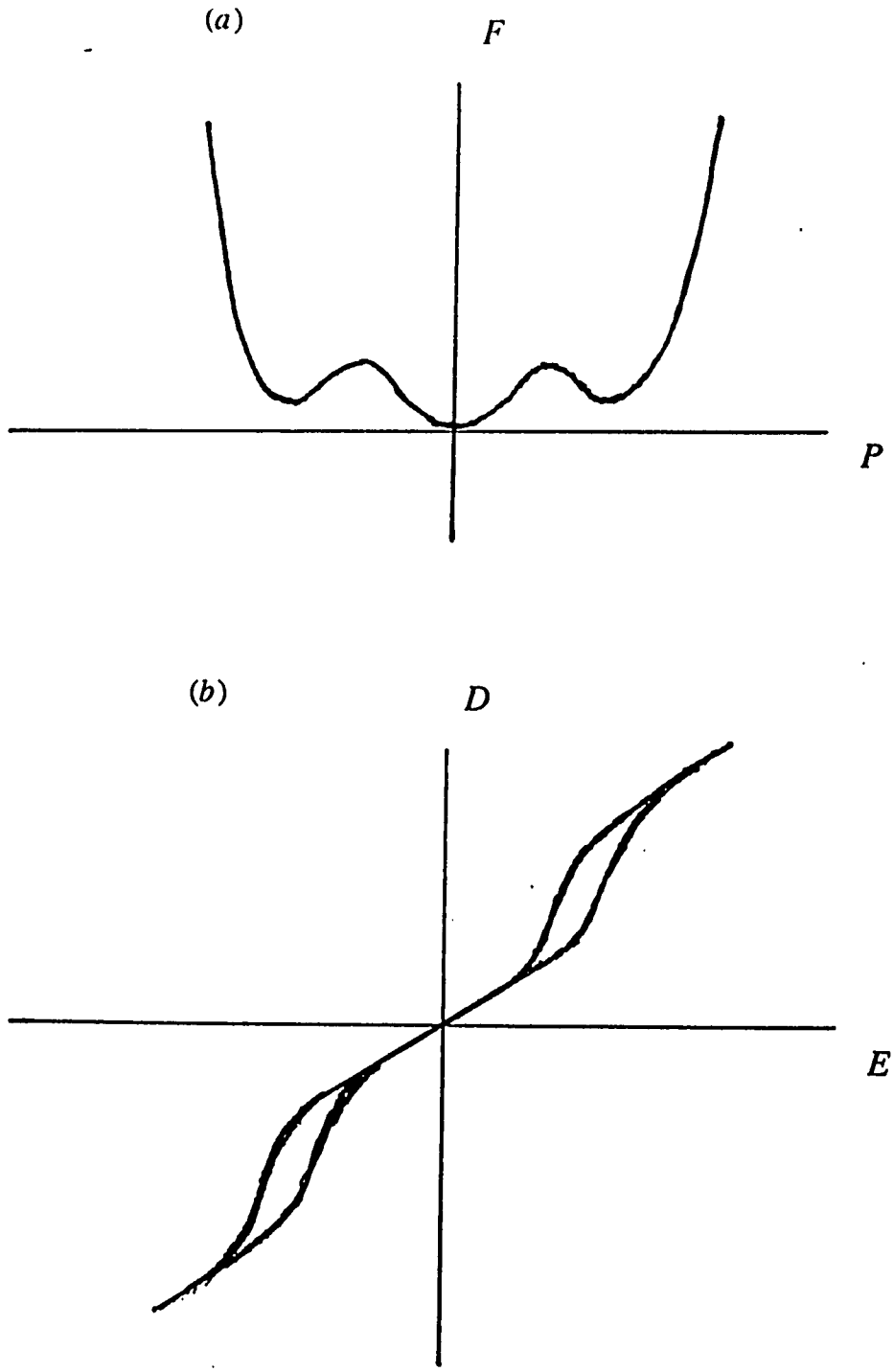

Fig.1.41. D-E hysteresis of "field-induced" ferroelectrics. (a). Free energy as a function of electric polarization. (b). Double D-E hysteresis loop.

I.4.2. The Computerized Sawyer-Tower Circuit

We observed the D-E hysteresis loops and measured the spontaneous polarization by using a modified Sawyer-Tower circuit which has been widely used for the identification of ferroelectrics [S9][L7]. Both the 2.7 *mm* and the 0.5 *mm* thick sample were measured and the results were consistent. As shown in fig. 1.42, the capacitor C_x formed by the sample with its evaporated electrodes was connected in series with a large capacitor C ($C \gg C_x$). The voltage across the sample is approximately equal to the measuring voltage V_x;

$$V_x - V_y = V_x - \frac{C_x}{C+C_x}V_x \approx V_x. \tag{1.145}$$

Then the applied electric field on the sample is given by:

$$E = \frac{V_x}{d} \tag{1.146}$$

where d is the sample thickness. The charge on the sample Q_x, which is equal to the charge on the capacitor C, is proportional to the voltage across the capacitor C:

$$Q_x = Q_C = CV_y.$$

The electric displacement in the sample is given by

$$D = 4\pi\sigma = \frac{4\pi C}{S}V_y \tag{1.147}$$

where S is the sample area. Therefore, the values of E and D in the sample can be determined by the voltages V_x and V_y. In an experiment, the measuring voltage V_x is generated by an IBM PS2 computer via a D/A converter controlled by a data acquisition control board. The advantage of using a a computer as a voltage source is that the frequency can be made arbitrary low. When the frequency is sufficiently low, the dielectric dissipation will be negligibly small since thiourea is a good DC insulator. This is why our circuit does not contain a phase-shift compensation element. Moreover, a low frequency measuring voltage allows the sample to remain in its equili-

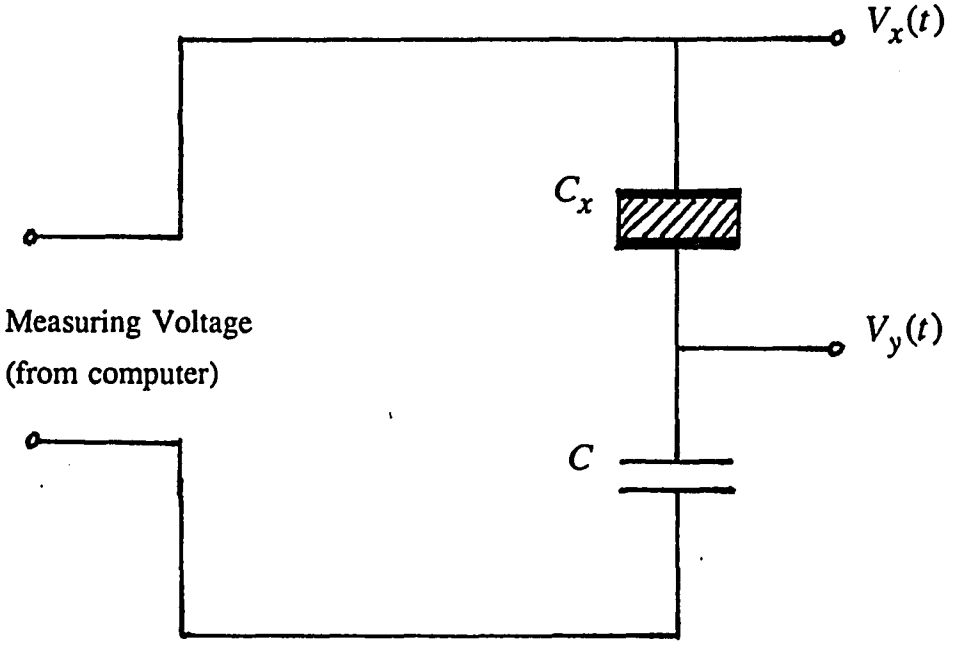

Fig.1.42. Modified Sawyer-Tower circuit. Usually $V_y(t)$ is amplified by an EG&G amplifier and recorded by the computer. The capacitor used in most of the experiments is 21 *nf*.

brium, which is important in distinguishing between field-induced and intrinsic spontaneous polarizations.

The voltage V_y is amplified by an EG&G isolated preamplifier and measured by the computer via the same data acquisition controller. The real-time D-E hysteresis loops can be plotted on the computer screen instantaneously and the data can be stored in the computer along with the experimental parameters.

To improve the thermal conduction, the sample holder was filled with dry nitrogen gas and sealed with a rubber o-ring. The temperature gradient between the sample and the thermistor was reduced by about 1.5 K.

I.4.3. Results

a) D-E hysteresis loops

Single D-E hysteresis loops were observed in the temperature range from 178.2 K to 178.9 K. Fig.1.43a shows a typical single loop measured at 178.4 K with a sinusoidally varying voltage at 0.1 Hz. The electric polarization clearly does not vanish at zero field.

However, as pointed out by Line and Glass [L8], ferroelectric-like D-E loops can be obtained from a nonlinear lossy material that is not ferroelectric. To eliminate this possibility, we repeated the observations with different measuring frequencies. No significant difference was observed when the frequency was changed from 0.5 Hz to 5 mHz. From the imaginary part of dielectric constant measured in our experiments, the dielectric loss decreases with decreasing frequency (for $f < 10KHz$) and vanishes at zero frequency, which is a common feature of insulators since the DC conductance is zero. Therefore, the observed single D-E hysteresis loops really indicate that the sample is in an intrinsic ferroelectric state.

Double loops were observed in both the upper and lower sides of the single-loop region, as expected. As seen in fig.1.43b, the loops open up as the value of the electric field increases. The electric polarization vanishes at zero E-field. This picture demonstrates the "field-induced" ferroelectric transitions, represented by a vertical line in fig.1.17 at $T > T_8^+$ or $T < T_8^-$ which would cross the phase boundary twice.

Clearly, the observation of D-E hysteresis loops directly confirms the results of theoretical analysis and dielectric constant measurements. Namely, the $\frac{1}{8}$ ferroelectric lock-in phase is intrinsic in a non-zero temperature range of about 0.7 K, and the temperature range of the $\frac{1}{8}$ phase can be increased by an external electric field.

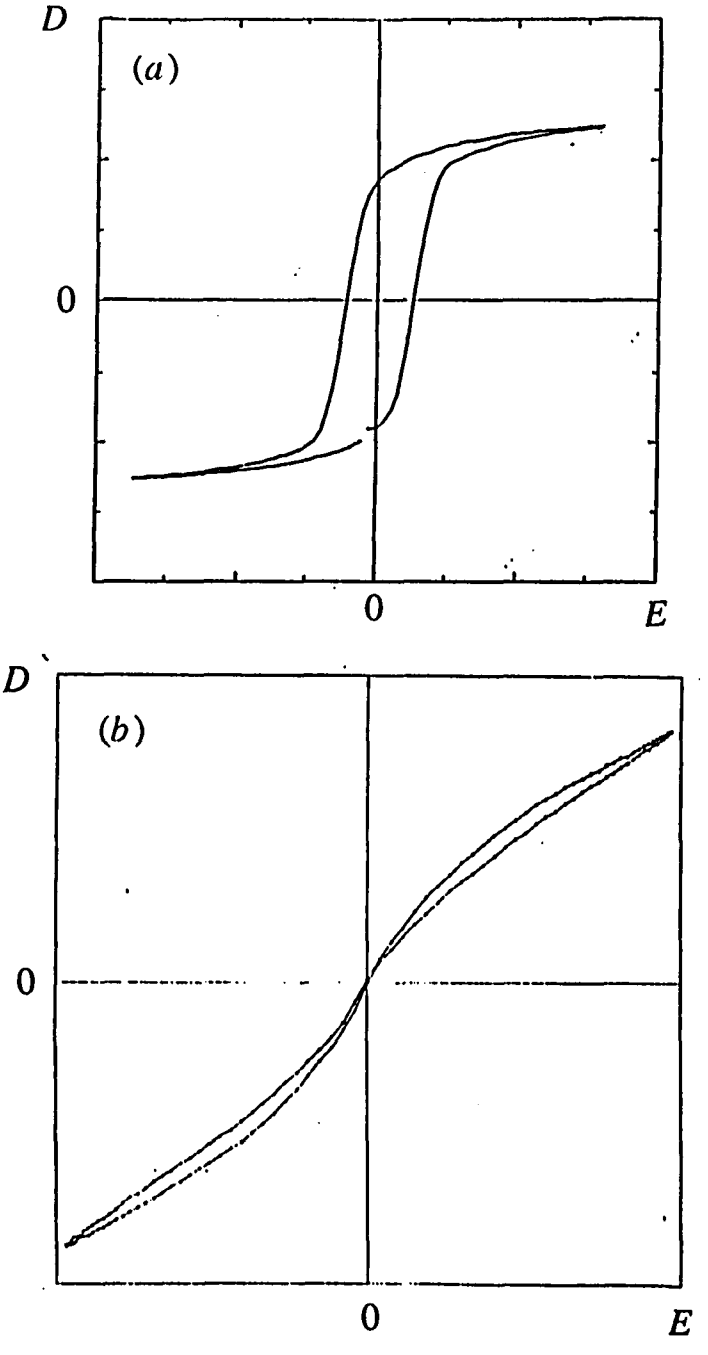

Fig.1.43. D-E hysteresis loops observed in the intrinsic and "field-induced" $\frac{1}{8}$ phase regions. (a). Single loop in the intrinsic region. (b). Double loop in the "field-induced" region.

b) spontaneous polarization and coercive field

The spontaneous polarization P_s as a function of temperature measured from the D-E hysteresis loops in the intrinsic $\frac{1}{8}$ ferroelectric phase is shown in fig.1.44. The fact that P_s increases with decreasing temperature is consistent with (1.50) (since η increases with decreasing temperature). The value of P_s is about 3×10^{-9} *coul/cm*^{2}, which is on the same order of magnitude as the previous result reported by Goldsmith and White [G1].

The coercive field E_c is roughly about 1 *V/cm*, which explains the fact that the dielectric constant is sensitive to the strength of the measuring field E_m when E_m is close to or higher than 1 *V/cm*. In fact, if the measuring field is not low enough, the two peaks of $\varepsilon'(T)$ at the $\frac{1}{8}$ phase transition points will be smeared out because of the effects of polarization reversal, which presumably is the reason why the two peaks were not well resolved in previous experiments by other groups [G1][G4].

The coercive field as a function of temperature $E_c(T)$ is shown in fig.1.45. The origin of this temperature dependence is not clear. It is not obvious that a reasonable interpretation can be given by the Landau theory.

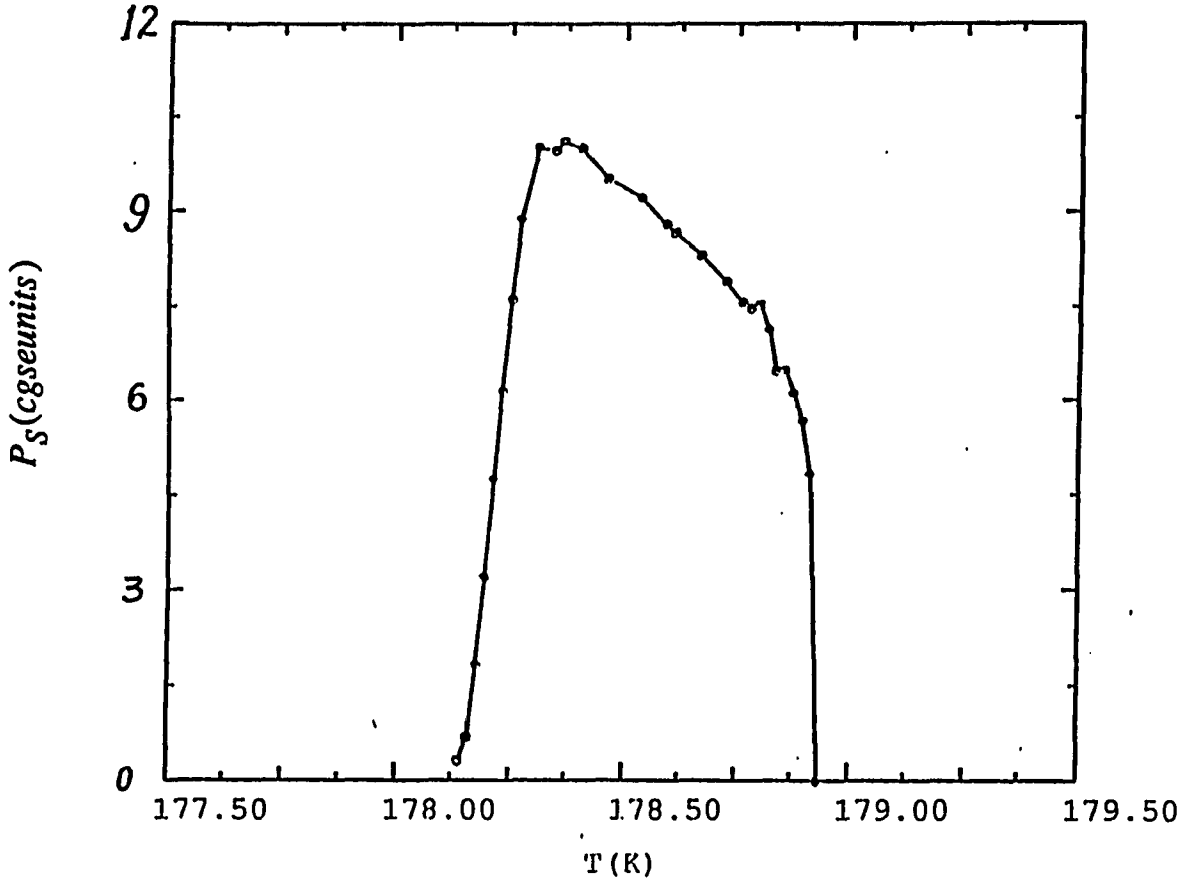

Fig.1.44. Spontaneous polarization vs. temperature in the $\frac{1}{8}$ ferroelectric phase.

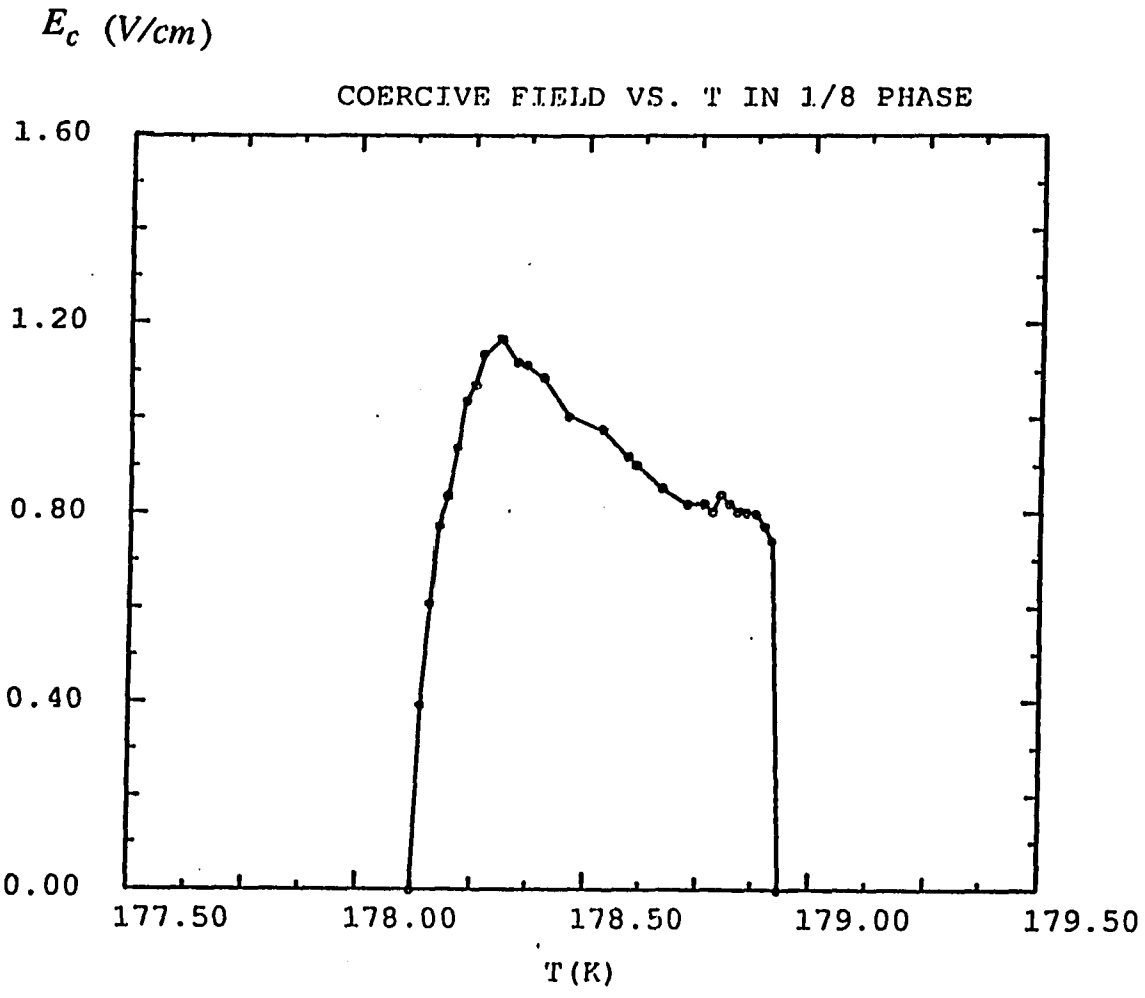

Fig.1.45. Coercive field vs. temperature in the $\frac{1}{8}$ ferroelectric phase.

Chapter I.5

Determination of the Coefficients in the Free Energy Expansion

I.5.1. The Constants a, T_0, α, β and $\frac{B}{\gamma}$

The phenomenological Landau theory has been widely used to describe the physical features of the structural phase transitions in thiourea [I1][D4][T5]. The Landau free energy has been successfully used to explain individual experimental results, but no attempt to determine the numerical values of the coefficients has yet been reported. It would be interesting to select one set of coefficients in the free energy expansion to explain various experimental results and predict the successive phase transitions self-consistently.

We started with the base form of the free energy (1.1). The constants a and T_0 could be determined by fitting the dielectric constant data in the normal phase to eq.(1.40). We fitted our experimental data and obtained:

$$a = 2.286 \times 10^{-3} \ (K^{-1})$$
$$T_0 = 186.73 \ (K).$$

Then, α and β were obtained by solving equations (1.21) and (1.25) since T_I and q_i are known to be 202 K and 0.141 b^* respectively (in *cgse* units):

$$\alpha = -6.48 \times 10^{-16}$$
$$\beta = 6.02 \times 10^{-30}$$

After that, the ratio $\frac{B}{\gamma}$ was obtained from the Inc-F transition condition

$$F_B^F(T_c) = F_B^{Inc}(T_c)$$

where T_c is known to be 169 K, $F_B^F(T)$ and $F_B^{Inc}(T)$ are given by (1.26) and (1.30) respectively.

$$\frac{B}{\gamma} = 8.79 \times 10^{13} \ (cgse \ units)$$

However, the modulation wavevector as a function of temperature $q_0(T)$ generated from eq.(1.22) by using these constants was considerably different from the reported experimental results. A serious problem was that the $q_0 = \frac{b^*}{8}$ temperature was 183.1 K, but experimental results indicate that it should be within the range between 176 ~ 180 K [G1].

To resolve this problem, we used all the above conditions including $q_0(T)$ and designed a fitting program to obtain a compromise result of a set of the above constants (in *cgse units):*

$$a = 2.55 \times 10^{-3}$$
$$T_0 = 188.1$$
$$\alpha = -6.29 \times 10^{-16}$$
$$\beta = 5.60 \times 10^{-30}$$
$$\frac{B}{\gamma} = 1.27 \times 10^{14}.$$

This set of constants gives $T_l = 202 \ K$ and $T_c = 169 \ K$. The numerical dielectric constant data $\varepsilon'(T)$ generated from this set of constants is still in reasonable agreement with experimental results as shown in fig.1.46. The modulation wavevector $q_0(T)$ from numerical calculation qualitatively agree with the experimental results (see fig.1.47). Particularly, the $q_0 = \frac{b^*}{8}$ temperature is 179.3 K which is within a reasonable range.

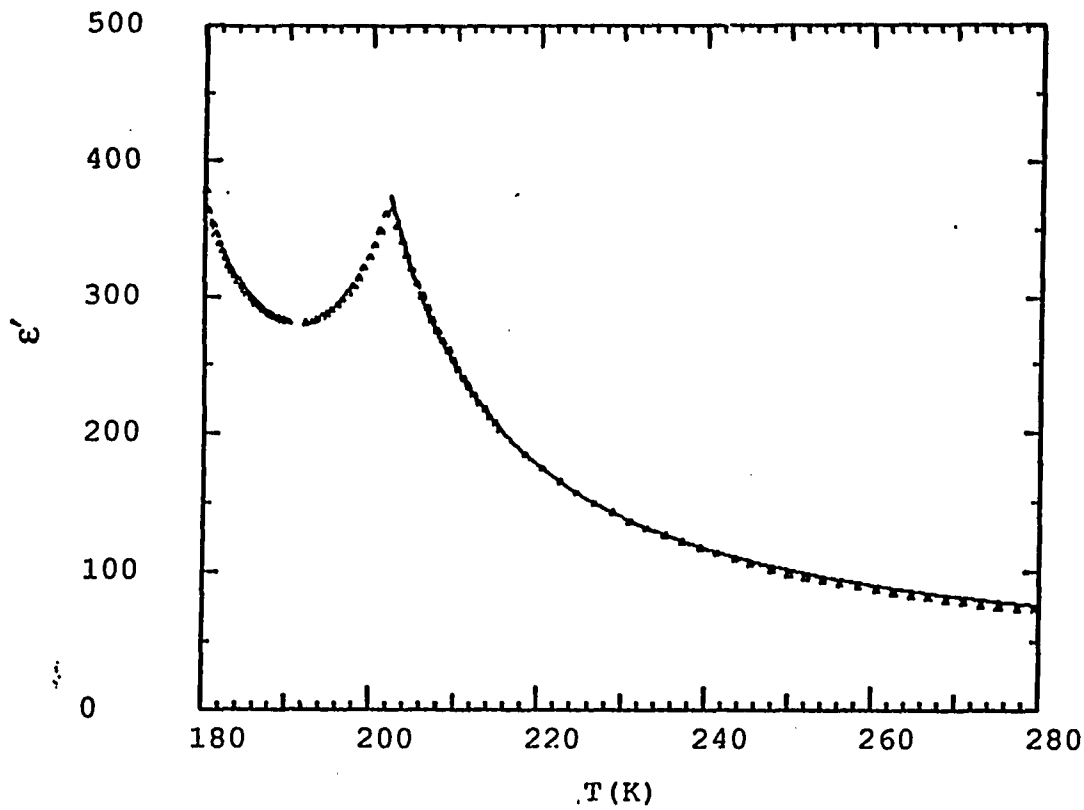

Fig.1.46. Dielectric constant $\varepsilon(T)$ generated from numerical calculation based on parameters obtained from the compromise fit. Triangular points: experimental data. Solid line: theoretical calculation.

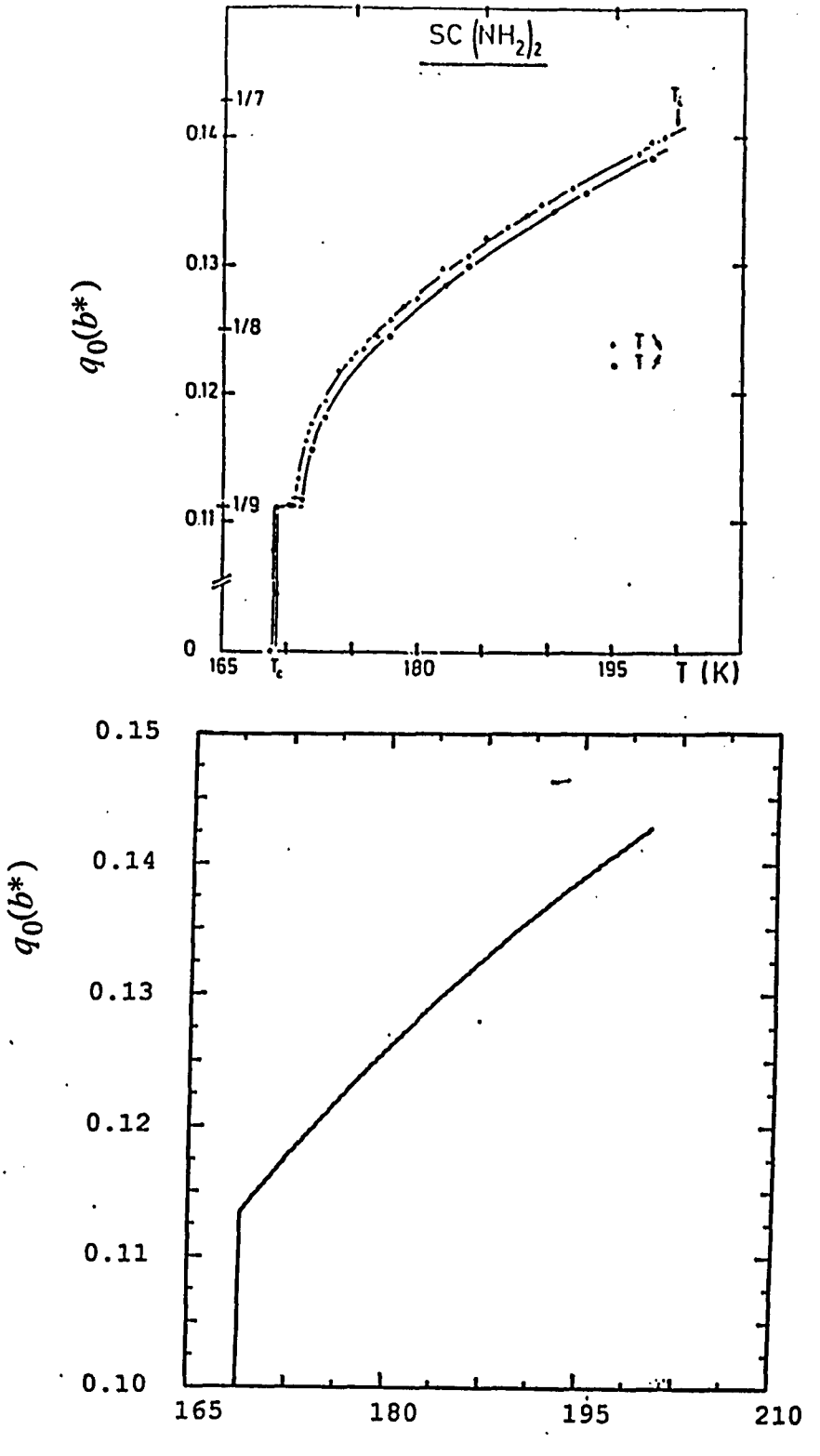

Fig.1.47. Modulation wavevector as a function of temperature. (a). experimental data (Denoyer and Currat 1986). (b). numerical calculation from Landau theory.

I.5.2. The Constants B, γ and b_9

a) B and γ

The constants B and γ can be determined from the value of the sudden increase in specific heat at T_I (see fig.1.9) along with the constants determined in the previous section. The relationship between the specific heat C_p and the free energy density F_T is given by:

$$C_p = -T\left[\frac{\partial^2 F_T}{\partial T^2}\right]_p \tag{1.148}$$

where

$$F_T = F_0 + F_B \tag{1.149}$$

F_B is the base form of the free energy (1.1) and F_0 is the "background" part corresponding to degrees of freedom other than the order parameter. The the specific heat jump at T_i is given by:

$$\begin{aligned}\Delta C_p &= -T_I\left[\frac{\partial^2 F_B}{\partial T^2}\right]_{T=T_I} \\ &= \frac{T_I \beta u}{4\gamma}\left[3\frac{B}{\gamma}\beta u + 8\beta u q_i^2 + 4(a+\alpha u)\right],\end{aligned} \tag{1.150}$$

where

$$u = \frac{2a}{\beta(3\frac{B}{\gamma}+4q_i^2)}.$$

The specific heat jump at T_I, which has been measured by Chang and Westrum, is

$$\Delta C_p = 1.17\ \frac{cal}{K\ mole} = 6.12\times 10^5\ \ (cgse\ units).$$

Substituting the numbers into (1.150) gives:

$$\gamma = 7.75 \times 10^{-24}\ \ (cgse\ units).$$

Then,

$$B = \gamma\frac{B}{\gamma} = 9.86 \times 10^{-10}\ \ (cgs\ units)$$

Now that the coefficients a, T_0, B, α, β and γ have been determined, the base form of the free energy $F_B(T)$ has been numerically defined.

b) b_9

The coefficient b_9 can be determined from the spontaneous polarization P_s measured in the $\frac{1}{8}$ phase (see eq.1.50). The maximum value of $P_s = \eta_0$ in the $\frac{1}{8}$ phase obtained from our experiments is

$$P_s = 10.1 \ \ (cgse\ units) = 3.36\times10^{-9} \ \ (\frac{coul}{cm^2}).$$

Substituting the numbers into (1.50) gives:

$$b_9 = -3.50 \times 10^{-30}$$

As discussed in sec.1.23, because b_{16} is estimated to be much smaller than $|b_9|^2$, it can be approximated as zero.

I.5.3. Discussions of the Stability of the Free Energy Expansion

The complete set of coefficients in the free energy expression determined in the sections I.5.1 and I.5.2 are listed in the upper part of the second column of table.1.5.

table 1.5 Coefficients of the free energy expansion (in cgse units)

	from compromise fit	+5%	-5%	experimental data
coefficients				
a	2.55×10^{-3}	2.68×10^{-3}	2.42×10^{-3}	
B	9.86×10^{-10}	1.03×10^{-9}	9.36×10^{-10}	
α	-6.29×10^{-16}	-6.61×10^{-16}	5.98×10^{-16}	
β	5.60×10^{-30}	5.88×10^{-30}	5.32×10^{-30}	
γ	7.75×10^{-24}	8.15×10^{-24}	7.35×10^{-24}	
b_9	-3.50×10^{-30}	-3.68×10^{-30}	3.33×10^{-30}	
T_0	188.1	188.1	188.1	
results				
T_1	202.0	202.0	202.0	202.0
T_c	168.7	168.7	168.5	169.0
T_9	170.6	170.9	170.5	171.0
T_8^+	179.5	179.8	179.3	$176 < T_8^+ < 180$
ΔT_8	0.5	0.6	0.5	0.7
$\frac{d\chi^{-1}}{dT} = a$	2.55×10^{-3}	2.68×10^{-3}	2.42×10^{-3}	2.286×10^{-3}
$q_0(T_1) = \sqrt{\frac{-\alpha}{\beta}}$	0.144 b^*	0.144 b^*	0.144 b^*	0.141 b^*
Δc_p	6.12×10^5	6.43×10^5	5.81×10^5	6.12×10^5
P_S	10.1	10.1	10.1	10.1

With the free energy numerically determined by the expansion coefficients, we are able to produce self-consistent explanations of the successive phase transitions in thiourea and the associated anomalies of a variety of physical quantities. In fact, all the numerical calculations given in sec.I.2 are based on this set of coefficients. The

calculated results are in reasonable agreement with our experimental data and some experimental results reported by other groups (see the discussions in the previous sections).

An important question is whether the theoretical results sensitively depend on the precision of the coefficients in the free expansion. We changed the absolute value of the coefficients $a, B, \alpha, \beta, \gamma$ and b_9 by $\pm 5\%$ and calculated some typical experimentally measurable quantities which are listed in the lower part of table 1.5. Noticing that changing T_0 basically only shifts the temperature scale, we selected the value of T_0 so that the incommensurate transition temperature T_I is $202.0\,K$, which has been precisely measured by various experiments.

As shown in table 1.5, the results obtained from the free energy expansion are reasonably stable with respect to small changes of the coefficients. In particular, small deviations in the numerical values of the coefficients would not substantially change the prediction about the temperature interval of the intrinsic $\frac{1}{8}$ ferroelectric phase.

Chapter I.6

Discussions

In summary, we have constructed a phenomenological Landau free energy expression with a complete set of numerically determined coefficients. Based on this free energy we have given a reasonably complete picture of the structural phase transitions in thiourea, particularly of the $\frac{1}{8}$ ferroelectric lock-in transition. We have sketched out the (E-T) phase diagram and predicted the static and dynamic dielectric behavior in the vicinity of the $\frac{1}{8}$ phase.

We have performed dielectric constant measurement experiments and examined the temperature, frequency, measuring-field and biasing-field dependence of the complex dielectric constant of thiourea, especially near the $\frac{1}{8}$ ferroelectric phase. We also investigated the D-E hysteresis loops in the intrinsic and "field-induced" regions of the $\frac{1}{8}$ phase and measured the spontaneous polarization and the coercive fields. Generally, the experimental results are consistent with the theoretical predictions.

Based on our experimental results and theoretical analysis, we conclude that there exists a non-zero temperature range in which the $\frac{1}{8}$ ferroelectric lock-in phase is intrinsic. The width of this intrinsic temperature range is about $0.7\,K$ which is experimentally measurable.

However, we are still unable to confirm our conclusion by other experimental evidence that does not involve an external electric field. Such experimental evidence would conclusively resolve the long-standing controversy about the origin of the $\frac{1}{8}$ ferroelectric lock-in phase.

Part II

Zone-Folding Raman Modes in TMATC-Zn

Chapter II.1

Introduction (TMATC-Zn)

Tetramethylammonium tetrachlorozincate ($[N(CH_3)_4]_2ZnCl_4$ = TMATC-Zn) belongs to the A_2BX_4 family of insulating crystals which exhibit incommensurate phase transitions. It has been extensively studied since the discovery of its ferroelectricity and successive structural phase transitions by Sawada *et al* in 1978 [S11] .

table 2.1. Phases of TMATC-Zn at atmospheric pressure

Phase	Transition Temp. T(K)	Modulation Wavevector $q_0(a^*)$	Z Formula Units per unit cell
I		normal phase (Pnam)	4
	297		
II		(2/5+δ) incommensurate	
	281		
III		2/5 ferroelectric	20
	277		
IV		1/3 ferroelastic	12
	177		
V		0	4
	159		
VI		1/3	12

The successive phases of TMATC-Zn at atmospheric pressure are listed in table 2.1. In the normal phase I above $297\,K$, The TMATC-Zn crystal is orthorhombic with the group D_{2h}^{16} (Pnam). On cooling at atmospheric pressure, it undergoes an incommensurate phase transition at 297 K to an incommensurate phase II with a structural modulation wavevector $q_0=(\frac{2}{5}+\delta)a^*$, followed by four successive lock-in transitions, to commensurate phase III at 281 K ($q_0=\frac{2}{5}a^*$), IV at 277 K ($q_0=\frac{1}{3}a^*$), V at 177 K ($q_0=0$) and finally to phase VI 159 K ($q_0=\frac{1}{3}a^*$). The temperature depen-

dence of the modulation wavevector, which has been measured by several groups by means of neutron scattering and X-ray diffraction [M15][T6][G6][M16][R2], is shown in fig.2.1. Much of the extensive experimental literature on TMATC-Zn has been reviewed recently by Cummins [C1]

One of the unusual properties of a structurally modulated crystal is that Raman inactive phonons at $\mathbf{q}=\mathbf{G}-m\mathbf{q}_0$ ($\mathbf{q}_0$ is the modulation wavevector , $\mathbf{G}$ is a reciprocal lattice vector and m is an integer) are "folded" into the Brillouin zone center by the modulation and may become Raman active [P4][P5][P6][L9]. The activation of such zone-folding modes can be utilized to study the phonon dispersion curves far from the Brillouin zone center and the structural changes of the crystal.

In 1989, Lee and Cummins reported the observation of large wavevector acoustic modes in the Raman spectra of several A_2BX_4 crystals activated by this zone-folding mechanism, and described these modes as folded acoustic modes (FAM's) [L9]. As an extension of this previous work, we carried out a detailed study of the FAM's in TMATC-Zn.

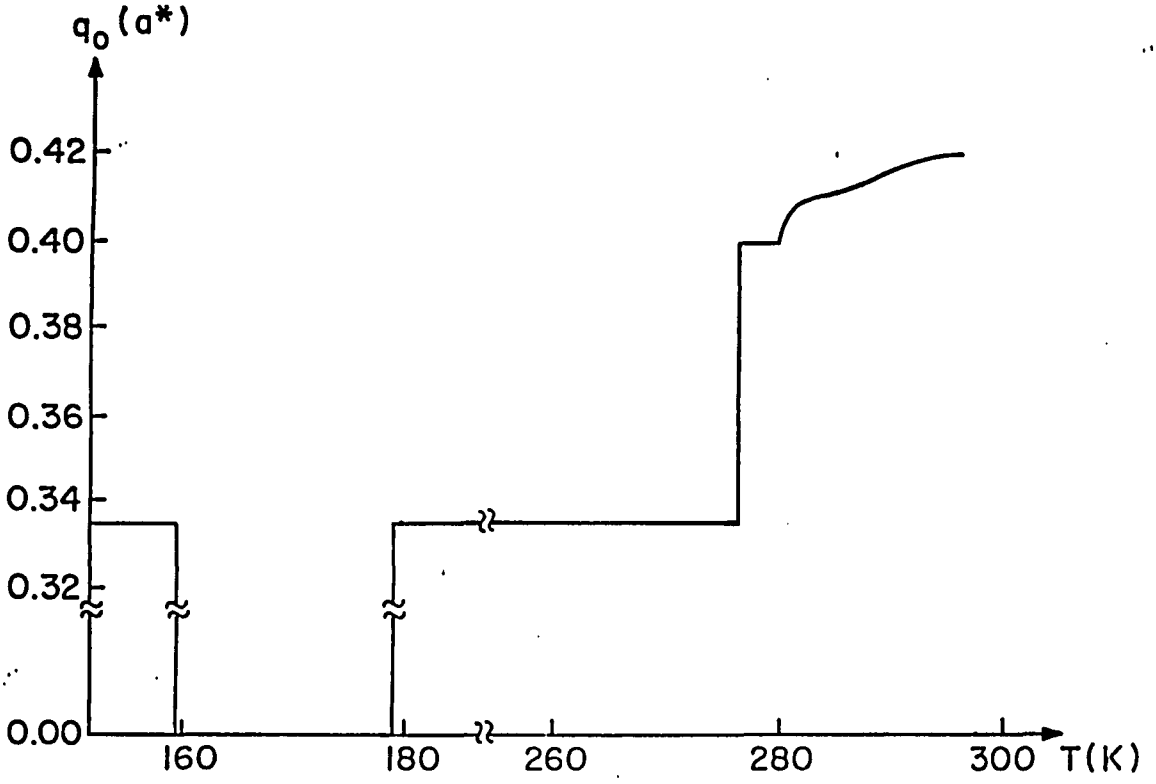

Fig.2.1. Temperature dependence of the modulation wavevector in TMATC-Zn

Chapter II.2

Theory of Zone-folding Raman Modes in TMATC-Zn

II.2.1. Raman Activation of Zone-folding Modes

Poulet and Pick discussed the general mechanism of light scattering in incommensurate crystals in 1986 [P6] . We will follow their approach to discuss Raman scattering from zone-folding modes of crystals in structurally modulated phases.

Generally, the static modulation can be considered as produced by a frozen-in phonon mode $Q_0(\mathbf{q}_0 j_0)$ where $\mathbf{q}_0$ is the wavevector and j_0 is the branch index indicating the symmetry property of the static distortion. Raman scattering from a zone-folding mode, which is a first order Raman process in the modulated phase, can be described as an nth-order Raman process in the normal phase with the frozen-in phonon entering $(n-1)$ times, and the vibrational mode $Q(\mathbf{q}j)$ generating the Raman shift entering once. The wavevector selection condition then follows from the translational symmetry requirement that the sum of the wavevectors of the n participating modes must be equal to a reciprocal lattice vector G (neglecting the Raman scattering vector $\mathbf{q}_k=\mathbf{k}_0-\mathbf{k}_s$ where $\mathbf{k}_0$ and $\mathbf{k}_s$ are the wavevectors of the incident and scattered light):

$$(n-1)\mathbf{q}_0+\mathbf{q}=\mathbf{G}. \qquad (2.1)$$

Consequently, the Raman shift of such a zone-folding mode ω can be estimated as the phonon frequency of the j branch at $\mathbf{q}=\mathbf{G}-(n-1)\mathbf{q}_0$ in the normal phase $\omega_1(\mathbf{q}j)$. This estimation has been successfully applied previously [L9]. However, this approach neglects the fact that the modulation induces gaps in the phonon dispersion curves at $\mathbf{q} = m\mathbf{q}_0$ [P4][P5].

The Raman shift of modes activated by zone-folding can be derived more precisely from lattice dynamics starting with a normal-mode expansion of the free energy. In the case of a second-order process (n=2), eq (1) gives $q=-q_0$. When the crystal has inversion symmetry in the normal phase, the two normal modes $Q_+(q,j)$ and $Q_-(-q,j)$ are degenerate. The relevant part of the free energy expansion in terms of Q_+ and Q_- has the form:

$$F = \frac{1}{2}A(T-T_i)Q_0Q^*_0+\frac{1}{4}BQ_0^2Q^{*2}_0+\omega_i^2(Q_+Q^*_++Q_-Q^*_-)$$
$$+DQ_0Q^*_0(Q_+Q^*_++Q_-Q^*_-)+C(Q_0Q_0Q_-Q^*_++Q_+Q^*_-Q^*_0Q^*_0) \quad (2.2)$$

where T_i is the transition temperature and ω_i is the degenerate frequency of $Q_+(q,j)$ and $Q_-(-q,j)$ at temperature T_i^+.

In the modulated phase, the order parameter of the phase transition $Q_0(q_0,j_0)$, describing the static distortion, can be written as

$$Q_0(q_0,j_0)=\eta e^{i\phi} \quad (2.3)$$

Eq.(2.2) becomes

$$F = \frac{1}{2}A(T-T_i)\eta^2+\frac{1}{4}B\eta^4+(\omega_i^2+D\eta^2)(Q_+Q^*_++Q_-Q_-)$$
$$+C\eta^2(e^{2i\phi}Q_-Q^*_++e^{-2i\phi}Q_+Q^*_-) \quad (2.4)$$

The last term in (2.4) couples the modes $Q_+(q,j)$ and $Q_-(-q,j)$ and will lift the degeneracy. The Lagrangian $L=T-V$ can be constructed by using F as a potential V:

$$L = -F_0+\frac{1}{2}\sum_{qq'}\dot{Q}_q\dot{Q}_{q'}-(\omega_i^2+D\eta^2)(Q_+Q^*_++Q_-Q^*_-)$$
$$-C\eta^2(e^{2i\phi}Q_-Q^*_++e^{-2i\phi}Q_+Q^*_-) \quad (2.5)$$

where F_0 is the part of free energy independent of Q_+ and Q_- .

Solving the Lagrangian equations of motion

$$\ddot{Q}_++(\omega_i^2+D\eta^2)Q_++C\eta^2e^{2i\phi}Q_-=0 \quad (2.6)$$
$$\ddot{Q}_-+(\omega_i^2+D\eta^2)Q_-+C\eta^2e^{-2i\phi}Q_+=0 \quad (2.7)$$

leads to an "even" mode with frequency ω_{even} and eigenvector Q_{even}

$$\omega_{even}= [\omega_i^2+(C+D)\eta^2]^{\frac{1}{2}} \tag{2.8}$$

$$Q_{even}= \frac{1}{\sqrt{2}}(e^{i\phi}Q_+ + e^{-i\phi}Q_-) \tag{2.9}$$

and an "odd" mode with frequency ω_{odd} and eigenvector Q_{odd}

$$\omega_{odd}= [\omega_i^2+(C-D)\eta^2]^{\frac{1}{2}} \tag{2.10}$$

$$Q_{odd}= \frac{1}{\sqrt{2}}(e^{i\phi}Q_+ - e^{-i\phi}Q_-). \tag{2.11}$$

It has been shown that the "odd" mode will be infrared active and the "even" mode will be Raman active [P5] .

Eqs. (2.8) and (2.10) indicate that the splitting of the degeneracy creates a gap in the phonon dispersion branch j at $\pm q_0$ (see fig.2.2). The magnitude of the gap is essentially proportional to the amplitude of the static distortion η.

The intensity of a zone-folded Raman mode via an nth-order process is given by

$$I(\omega) \sim R^2\eta^{2(n-1)}[n(\omega)+1]\mathrm{Im}[\chi(\omega)] \tag{2.12}$$

where $\chi(\omega)$ is the susceptibility associated with the dynamic mode Q_{even} and $n(\omega)$ is the Bose-Einstein factor. Since the amplitude of the static distortion η is small, the intensity of zone-folding modes, especially for high-order processes, is usually weak in comparison with ordinary Raman modes. Measurements of the temperature dependence of the Raman intensity provides the η^2 information needed to evaluate the gap in eqs.(2.8) and (2.10) as we shall see below.

Generally, the fact that optic mode dispersion curves are fairly flat makes it complicated to analyze the folded optic modes in a Raman spectrum because they fall in the same frequency rang of ordinary optical Raman modes. We will only concentrate on the folded acoustic modes, or FAM's, which occur at low frequencies.

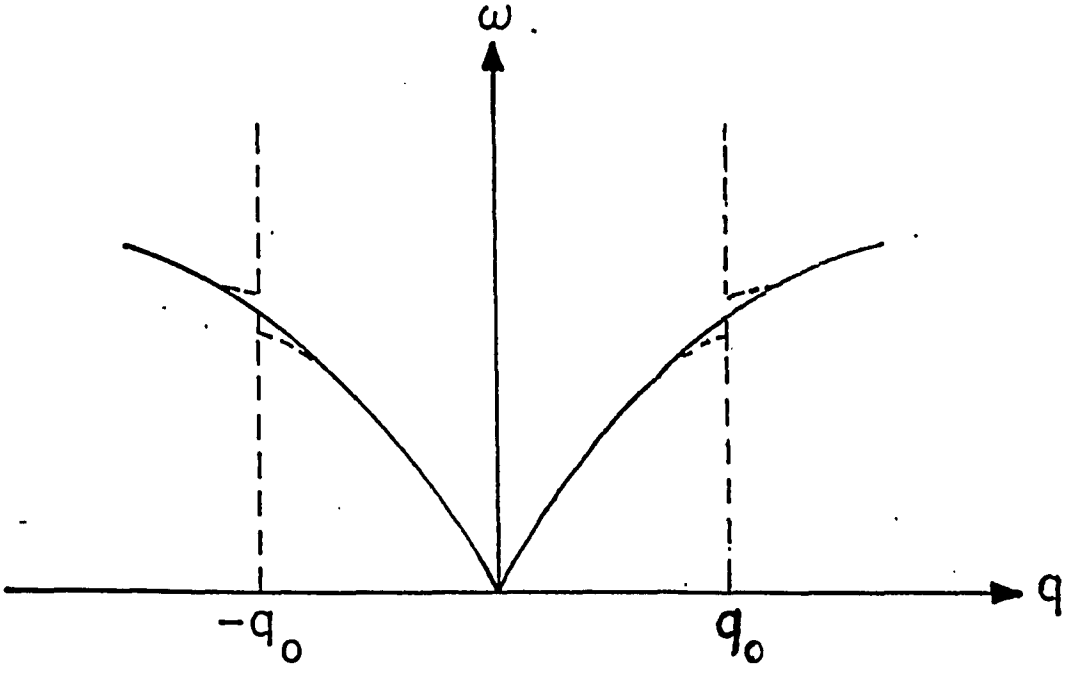

Fig.2.2. splitting of the degeneracy of $Q_+(q_0j)$ and $Q_-(-q_0j)$ acoustic modes due to the static modulation $Q_0(q_0,\Sigma_3)$.

II.2.2. Selection Rules of FAM's in TMATC-Zn

The polarization selection rules of FAM's associated with the Raman tensor structure are determined by the space group symmetry and the symmetry property of the static distortion [P6].

The space group of TMATC-Zn in the normal phase is D_{2h}^{16} . With Pnam notation, the irreducible representations of the acoustic phonons $Q(\Sigma_i, \mathbf{q})$ (i = 1, 3, 4. and $\mathbf{q}$ along $\mathbf{a}^*$) are given in table 2.2 [I3]. The irreducible representation of the frozen-in phonon $Q(\Sigma_3, \mathbf{q}_0)$ can be obtained from the second row by setting $\mathbf{q}$ as the modulation wavevector $\mathbf{q}_0$.

table 2.2 Irreducible representations of the acoustic phonons $Q(\Sigma_i, \mathbf{q})$ (i = 1, 3, 4) of TMATC-Zn in the normal phase

	$\{E \mid 0\}$	$\{C_{2x} \mid \frac{1}{2}(\mathbf{a}+\mathbf{bc})\}$	$\{\sigma_y \mid \frac{1}{2}(\mathbf{a}+\mathbf{b})\}$	$\{\sigma_z \mid \frac{1}{2}\mathbf{c}\}$
Σ_1 LA	1	$e^{i\frac{\mathbf{a}\cdot\mathbf{q}}{2}}$	$e^{i\frac{\mathbf{a}\cdot\mathbf{q}}{2}}$	1
Σ_3 TA	1	$-e^{i\frac{\mathbf{a}\cdot\mathbf{q}}{2}}$	$e^{i\frac{\mathbf{a}\cdot\mathbf{q}}{2}}$	-1
Σ_4 TA	1	$-e^{i\frac{\mathbf{a}\cdot\mathbf{q}}{2}}$	$-e^{i\frac{\mathbf{a}\cdot\mathbf{q}}{2}}$	1

For a second-order Raman process, the two participating phonons are the frozen-in phonon $Q(\Sigma_3, \mathbf{q}_0)$ and a dynamic phonon $Q(\Sigma_i, \mathbf{q}_i)$. Momentum conservation requires that $\mathbf{q}_i = -\mathbf{q}_0$. The selection rules are determined by the excitation symmetry obtained by taking the direct product of the irreducible representations of the two participating phonons [H5]. The results are given in table 2.3 (" × " represents direct product).

table 2.3 Excitation symmetry of two phonons: $\Sigma_3(q_0) \times \Sigma_i(-q_0)$

	$\{E \mid 0\}$	$\{C_{2x} \mid \frac{1}{2}(a+bc)\}$	$\{\sigma_y \mid \frac{1}{2}(a+b)\}$	$\{\sigma_z \mid \frac{1}{2}c\}$	basis
$\Sigma_1(-q_0) \times \Sigma_3(q_0)$	1	-1	1	-1	xz
$\Sigma_3(-q_0) \times \Sigma_3(q_0)$	1	1	1	1	x^2, y^2, z^2
$\Sigma_4(-q_0) \times \Sigma_3(q_0)$	1	1	-1	-1	yz

For a third-order Raman process, the frozen-in phonon $Q(\Sigma_3, q_0)$ enters twice and the dynamic phonon $Q(\Sigma_i, q_i)$ enters once. When $q_0 = \frac{a^*}{3}$ (in phase IV and VI), the momentum conservation requires that $q_i = q_0 = \frac{a^*}{3}$ (see eq.2.1). Similar to the second-order case, the selection rules can be determined by the direct product of the irreducible representations of the three participating phonons. The results are given in table 2.4 .

table 2.4 Excitation symmetry of three phonons: $\Sigma_3(q_0) \times \Sigma_3(q_0) \times \Sigma_i(q_0)$

	$\{E \mid 0\}$	$\{C_{2x} \mid \frac{1}{2}(a+bc)\}$	$\{\sigma_y \mid \frac{1}{2}(a+b)\}$	$\{\sigma_z \mid \frac{1}{2}c\}$	basis
$\Sigma_1(q_0) \times \Sigma_3(q_0) \times \Sigma_3(q_0)$	1	-1	1	-1	xy
$\Sigma_3(q_0) \times \Sigma_3(q_0) \times \Sigma_3(q_0)$	1	1	-1	-1	yz
$\Sigma_4(q_0) \times \Sigma_3(q_0) \times \Sigma_3(q_0)$	1	1	1	1	x^2, y^2, z^2

A necessary condition for a phonon excitation to be Raman active in geometry ($\alpha\beta$) is that it must transform in the same way as the polarizability component $\varepsilon_{\alpha\beta}$ ($\alpha, \beta = x, y, z$) [L11], where α and β are the incident and scattered polarization directions respectively. The selection rules of the FAM's in TMATC-Zn obtained by this condition are given in table 2.5.

table 2.5 Raman selection rules for FAM's in TMATC-Zn (static distortion = Σ_3).

Dynamic vibrational mode	Second-order process $n = 2$	Third-order process (phase IV and VI) $n = 3$
Σ_1 LA	(*ac*)	(*ab*)
Σ_3 TA	(*aa*) (*bb*) (*cc*)	(*ac*)
Σ_4 TA	(*bc*)	(*aa*) (*bb*) (*cc*)

II.2.3. Raman Shift of FAM's in TMATC-Zn

In TMATC-Zn, since phase V with no structural modulation (q_0=0) is sandwiched between phases IV and VI (both with a modulation wavevector $q_0=\frac{1}{3}a^*$), a zone-folding mode active in the modulated phases will appear in phase II, III, IV and VI, but disappear in phase V. The Raman shift of a FAM can be calculated from eq.(2.8).

To compute the Raman shift of a FAM, one needs the corresponding acoustic dispersion curve usually measured by inelastic neutron scattering experiment. However, there is no such neutron data available for $[N(CH_3)_4]_2ZnCl_4$.

However, Iizumi and Gesi measured the Σ_3 acoustic dispersion curve of $[N(CD_3)_4]_2ZnCl_4$ just above T_i (T_i+0.5K) by neutron scattering in 1983 [I4] . Assuming $[N(CH_3)_4]_2ZnCl_4$ has similar dispersion relations to $[NCD_3)_4]_2ZnCl_4$, we take the Σ_3 dispersion curve of $[N(CD_3)_4]_2ZnCl_4$ and scale the phonon energy such that the sound velocity derived from the dispersion curve is consistent with the corresponding sound velocity v_{55} of $[N(CH_3)_4]_2ZnCl_4$ measured from ultrasonic experiments [B9]. The Σ_3 acoustic dispersion curve of $[N(CH_3)_4]_2ZnCl_4$ obtained by this method is shown in fig.2.3.

The FAM of the Σ_3 branch via a second-order process will be active in the totally symmetric geometry as shown in table 2.3. The wavevector q determined by (1) is

$$q(T) = -q_0(T) \tag{2.13}$$

The Raman frequency shift as a function of temperature $\omega(T)$ computed from eq.(2.8) is shown in fig.2.4 by the solid line, where $\eta(T)$, being proportional to the intensity of the FAM (see eq.(2.12)), was obtained from of our Raman data.

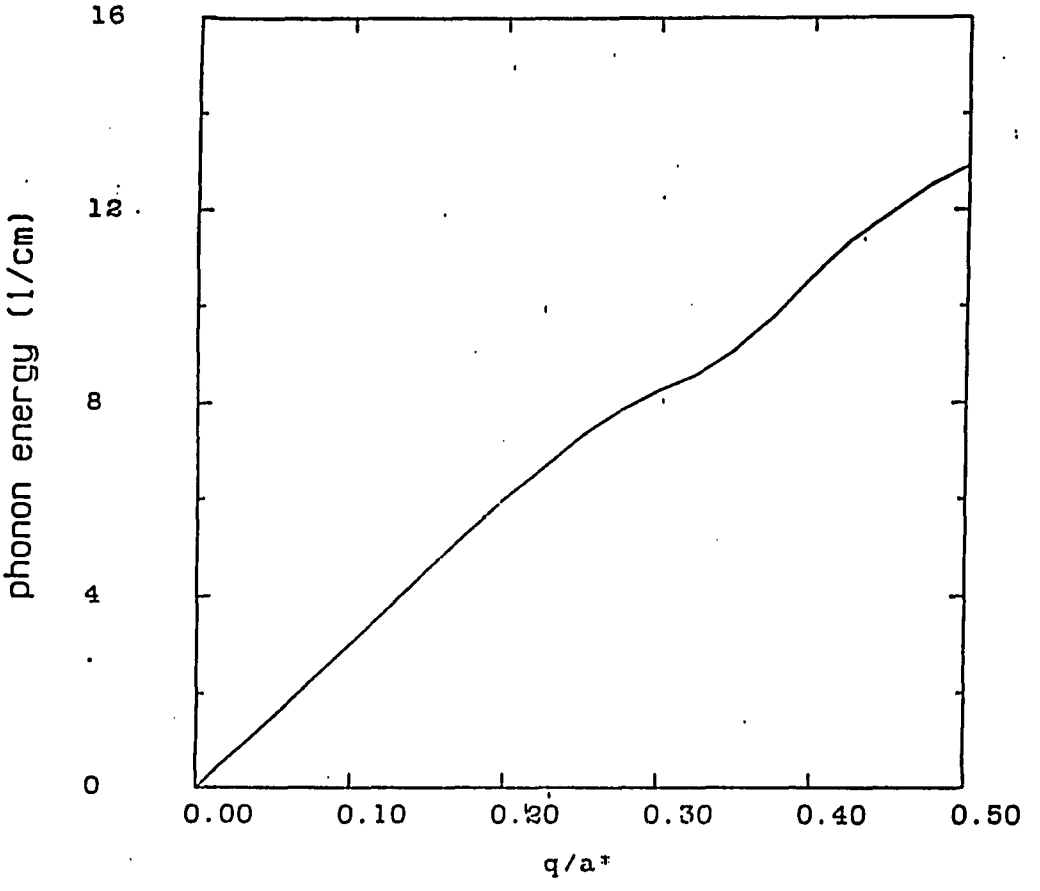

Fig.2.3. Σ_3 acoustic dispersion curve of $[N(CH_3)_4]_2ZnCl_4$.

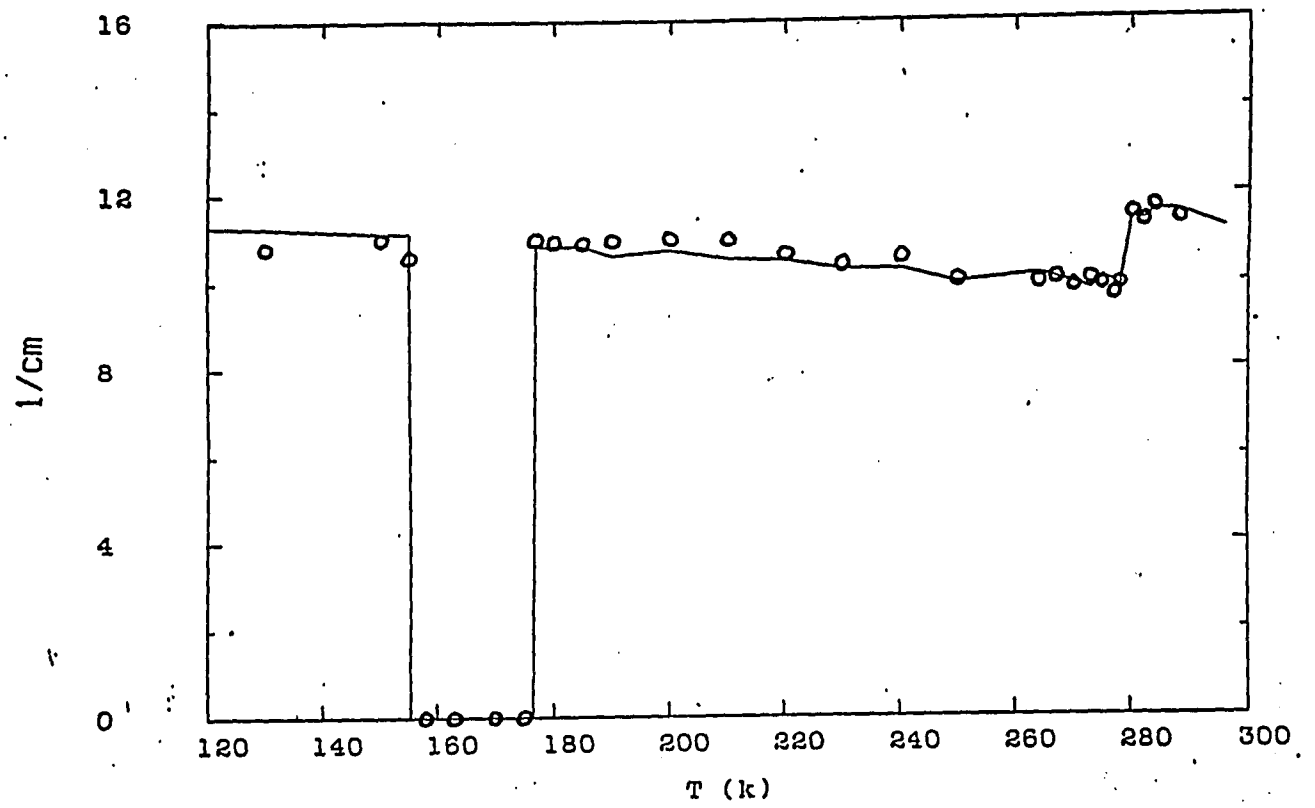

Fig.2.4. Frequency shift of the 11 cm^{-1} mode. Open circles -- experimental result. Solid line -- theoretical prediction.

Chapter II.3

Experiment

II.3.1. Crystal Growth and Raman Scattering Apparatus

Single crystals of $[NCH_3)_4]_2ZnCl_4$ were grown by slow evaporation at 25°C from an aqueous solution of $N(CH_3)_4Cl$ and $ZnCl_2$ in a molar ratio of 2:1. A sample about $3\times5\times8\ mm^3$ was polished and mounted in an Air Product LT-3-110 cryostat controlled by an Oxford ITC-4 digital temperature controller. A spectrum was taken after the temperature was stablized at a given value for one hour.

The Raman scattering apparatus is illustrated schematically in fig.2.5 . A Coherent 52 Argon-ion laser was operated at $4880\ \dot{A}$ (single-line multi-mode). The laser beam, with a constant power of $300\ mW$, was focused into the sample and the scattered light was collected and focused on an intermediate slit which eliminated the strong elastic scattering from the edges of the sample. The collected light was collimated and then refocused on the entrance-slit of the spex 1401 tandem grating spectrometer. To obtain a reasonable compromise between the throughput and resolution, the width of the three silts of the spectrometer was set at $80\text{–}120\text{–}60\ \mu m$. The resolution with this slit setting is $1.0\ cm^{-1}$. The scattered light was analyzed by a spex 1401 tandem grating spectrometer equipped with JY interferometrically ruled gratings. The transmitted light was detected by an I.T.T. FW-130 photomultiplier tube operated at a cathode voltage of $-1750\ V$. The PMT was cooled by a Te-104 (Products for Research Inc.) refrigerated chamber to reduced the background emission. The output electric pulses of the PMT were amplified and converted to TTL signal by a Canberra Industries model 813 discriminator/pre-amplifier, and then were acquired by an AT computer equipped with an EG&G Ortec ACE-MCS multi-scalar

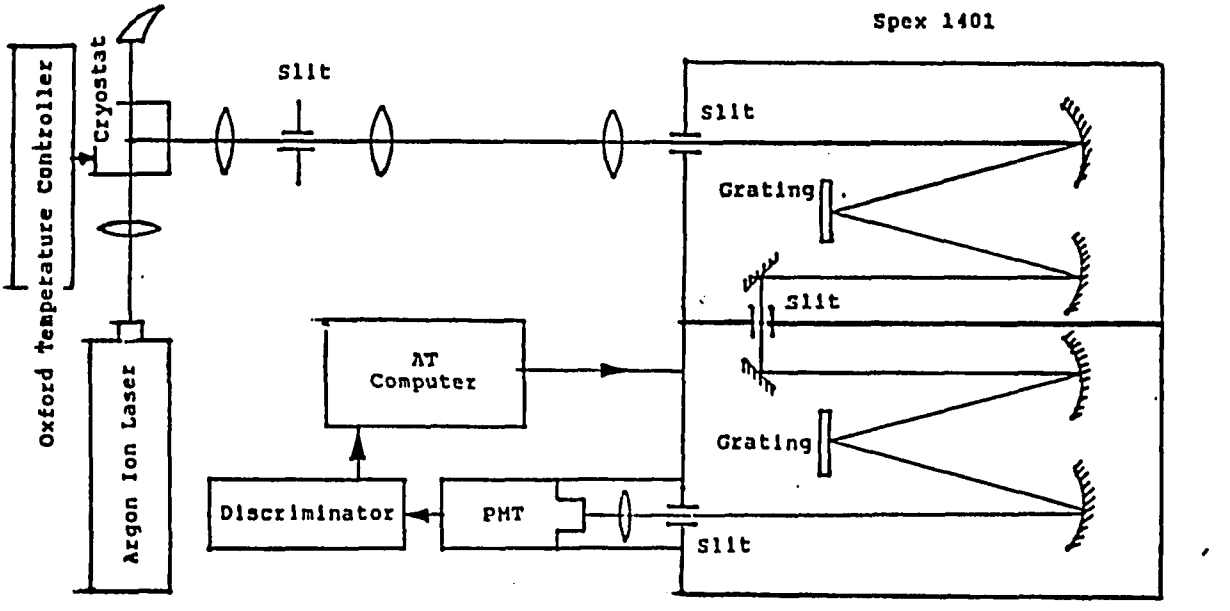

Fig.2.5. Schematic illustration of the Raman scattering apparatus.

board. The binary raw data can be converted to ASCII code in the AT computer.

II.3.2. Data Analysis

a) Raman spectra

Low frequency Raman spectra (0~50cm^{-1}) were studied in the temperature range from 310 K down to 80 K. Fig.2.6(a) shows the spectra in (aa) geometry at different temperatures (from top to bottom: 300, 288, 280, 275, 200, 170, 150 K). Fig2.6.(b) shows the susceptibility $\chi(\omega)$ deduced from the spectra $I(\omega)$,

$$\chi(\omega) \sim \frac{I(\omega)}{n(\omega)+1} \tag{2.14}$$

in which the intrinsic low frequency feature can be seen more easily.

A central mode observed in phase I, II, and III is related to orientational disoder [H4]. A $26cm^{-1}$ mode active in (aa), (bb), (cc) geometry is an ordinary external A_g optic mode [B10].

An $11cm^{-1}$ (aa) mode observed in modulated phases II, III, IV, and VI is consistent with the FAM of the Σ_3 branch, in which we are particularly interested. Another weak (aa) mode at $15cm^{-1}$ observed in phase VI is possibly also an FAM, which might be too weak to be seen in higher temperature modulated phases.

In order to have an intensity reference, we monitored the intensity of a 276 cm^{-1} mode in (aa) geometry, which is due to the internal vibration of $ZnCl_4$ radical [B10] and essentially independent of the phase transitions.

b) Fitting models

The (aa) Raman spectra in phases II, III, and IV in the frequency range of 5~ 45 cm^{-1} were fitted to a 3-mode model (two damped harmonic oscillators and one relaxation mode)

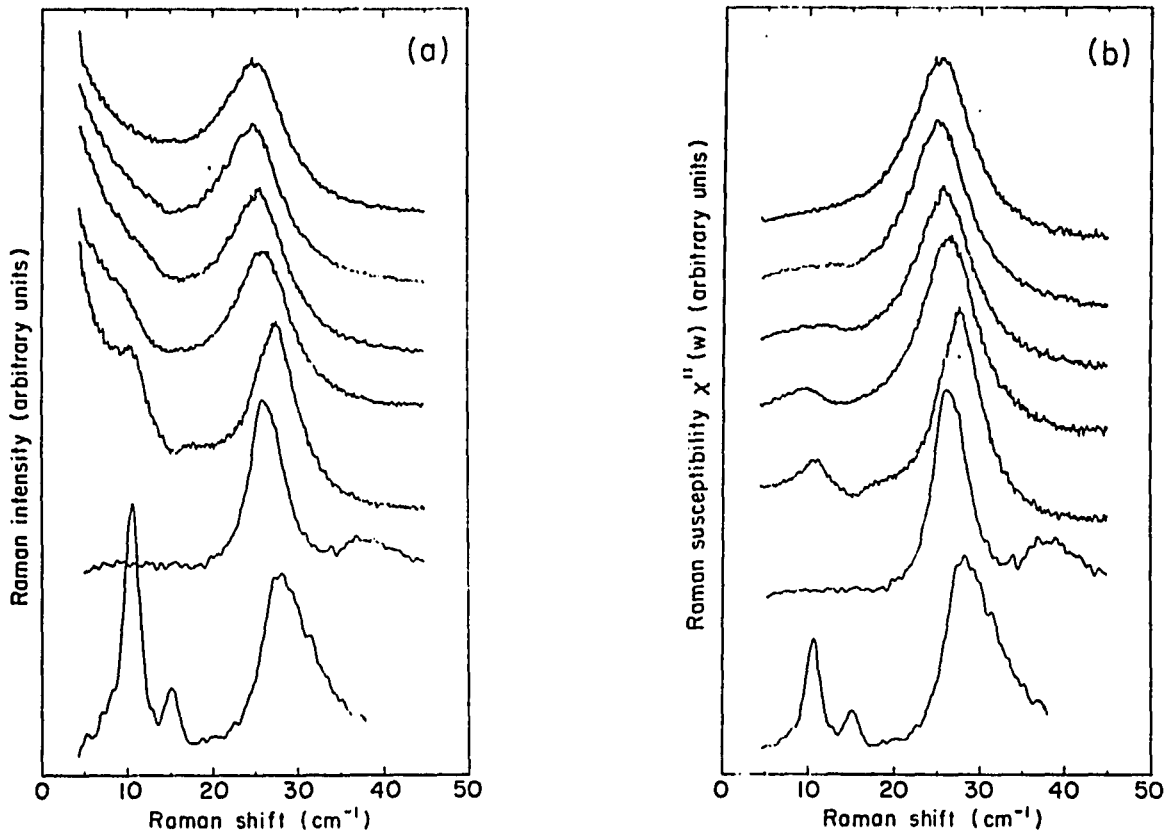

Fig.2.6. Raman spectra in (aa) geometry. (a). $I(\omega)$; (b) -- $\chi''(\omega) = I(\omega)/[1+n(\omega)]$.

From top to bottom: T = 300, 288, 280, 275, 200, 163, 150 K.

$$I(\omega) = P_2^2\left[n(\omega)+1\right]\left\{\left[\frac{P_0}{P_2}\right]^2 Im[G_0(\omega)]+\left[\frac{P_1}{P_2}\right]^2 Im[G_1(\omega)]+Im[G_2(\omega)]\right\} \qquad (2.15)$$

convoluted with the instrument response function. $G_0(\omega)$,$G_1(\omega)$ and $G_2(\omega)$ are the susceptibilities associated with the central mode, the $11cm^{-1}$ mode and the $26cm^{-1}$ mode respectively:

$$G_0(\omega) = \frac{1}{1-i\omega\tau} \qquad (2.16)$$

$$G_1(\omega) = \frac{1}{(\omega^2-\omega_1^2)-i\omega\Gamma_1} \qquad (2.17)$$

$$G_2(\omega) = \frac{1}{(\omega^2-\omega_2^2)-i\omega\Gamma_2} \qquad (2.18).$$

The fitting results are shown in table 2.6.

table 2.6. Fitting results of spectra in phase II, III, and IV

T	τ	$\frac{\omega_1}{2\pi c}$	$\frac{\omega_2}{2\pi c}$	$\frac{\Gamma_1}{2\pi c}$	$\frac{\Gamma_2}{2\pi c}$	$\frac{P_0}{P_2}$	$\frac{P_1}{P_2}$	P_2	χ^2
(K)	(10^{-13}sec)	(cm^{-1})	(cm^{-1})	(cm^{-1})	(cm^{-1})				
177.0	7.17	10.99	28.20	2.55	6.14	0.0611	0.175	74.4	2.67
180.0	7.42	10.94	27.90	2.57	6.23	0.0608	0.176	74.9	2.01
185.0	7.37	10.88	27.78	2.69	5.98	0.0599	0.176	74.9	2.26
190.0	7.70	10.96	28.17	2.74	6.17	0.0578	0.164	78.5	2.09
200.0	7.86	11.00	27.89	2.82	6.11	0.0560	0.170	71.9	1.91
210.0	7.96	10.99	27.74	2.86	6.37	0.0552	0.161	71.9	1.91
220.0	8.54	10.66	26.88	2.91	6.19	0.0545	0.159	70.7	1.56
230.0	9.14	10.44	26.94	2.98	6.16	0.0544	0.149	63.0	1.72
240.0	8.91	10.58	26.93	3.09	6.58	0.0541	0.149	70.3	1.55
250.0	8.83	10.07	26.52	2.99	7.14	0.0533	0.130	73.9	1.95
264.0	8.60	9.98	26.27	3.67	7.15	0.0540	0.141	67.9	1.60
267.0	8.79	10.09	26.51	3.70	7.56	0.0520	0.136	76.8	1.79
270.0	8.60	9.89	26.36	3.71	7.45	0.0530	0.127	80.1	2.11
273.0	8.40	10.08	26.65	3.58	7.62	0.0502	0.120	81.0	1.71
275.0	9.11	9.95	26.68	4.18	7.88	0.0462	0.135	87.6	2.22
277.0	8.27	9.70	26.24	4.02	7.78	0.0528	0.130	77.1	3.45
278.0	8.96	9.94	26.40	3.84	8.05	0.0516	0.119	57.4	1.06
280.0	7.67	11.56	26.17	5.01	8.21	0.0528	0.120	82.1	1.67
282.0	7.61	11.37	26.21	5.16	8.02	0.0496	0.116	79.9	1.06
284.0	7.62	11.71	26.14	5.58	8.03	0.0495	0.115	85.1	1.04
288.0	7.79	11.45	25.53	5.80	8.47	0.0494	0.104	79.8	1.14

In phase V, the spectra are flat in the low frequency region 0~18 cm^{-1}. The 11cm^{-1} mode clearly disappear.

In phase VI, the 11cm^{-1} mode reappears and an additional weak mode at 15cm^{-1} shows up, we fitted the spectra in the range of 0~18 cm^{-1} to a two-oscillator model:

$$I(\omega) = \left[n(\omega)+1\right]\left\{ P_1^2 Im[G_1(\omega)]+P_{15}^2 Im[G_{15}(\omega)]\right\} \tag{2.19}$$

where $G_{15}(\omega)$ is the susceptibility associated with the 15cm^{-1} mode.

We examined the mode coupling effect among $G_0(\omega)$, $G_1(\omega)$, and $G_2(\omega)$ [L10]. First, adding coupling effects did not improve the fitting; i.e., the reduced chi square remained almost the same. Second, as a result of the fitting, the coupling constants treated as fitting parameters automatically selected such small values that they cannot have significant effects. That is why $G_0(\omega)$, $G_1(\omega)$ and $G_2(\omega)$ can be treated independently.

The frequency of the 11cm^{-1} mode $\omega_1(T)$ analyzed from the spectra was fitted to the theoretical prediction for the FAM of Σ_3 via a second-order process (eq. (2.8)) with one fitting parameter. For a given temperature T, **q** is determined by eq.(2.13), and $\omega_i(\mathbf{q})$ is the frequency of Σ_3 branch at temperature T_i^+ , which was obtained from the Σ_3 dispersion curve shown in fig.2.3. Eq.(2.12) and (2.15) indicates that η^2 is proportional to the relative Raman intensity $(\frac{P_1}{P_2})^2$,

$$\eta^2 = \alpha\left[\frac{P_1}{P_2}\right]^2 \tag{2.20}$$

Therefore, (2.8) can be written as

$$\omega(T) = \left\{ [\omega_i(\mathbf{q})]^2+\beta\left[\frac{P_1}{P_2}\right]^2\right\}^{\frac{1}{2}} \tag{2.21}$$

where the temperature independent constant $\beta=\alpha(D+C)$ was treated as the fitting parameter. As shown in fig.2.4 (in page 139), the experimental result clearly agrees

with the theoretical prediction.

Chapter II.4

Conclusions

In summary, the $11cm^{-1}$ mode in (aa) geometry does appear in phases II, III, and IV, disappear in phase V, and reappear in phase VI; the intensity $(\frac{P_1}{P_2})^2$ decreases with increasing temperature and tends to zero at T_i (fig.2.7), which is due to the fact that the normal-incommensurate phase transition is a continuous one; the frequency $\omega(T)$ obeys eq.(2.8) very well. We conclude that it is the folded Σ_3 acoustic mode via a second-order process.

It is interesting to interpret the $15cm^{-1}$ mode as the folded Σ_4 acoustic mode via a third-order process. First, the active geometry is consistent with the selection rules. Second, the intensity is much weaker than that of the $11cm^{-1}$ mode, which could be the reason why it was not observed in higher-temperature modulated phases. Third, the ratio of the frequency of the $15cm^{-1}$ mode and that of the $11cm^{-1}$ mode is about the same as the ratio of the sound velocities corresponding to Σ_4 and Σ_3 branch $\left[\frac{15}{11} \sim \frac{1450}{1080}\right]$ [B9]. Namely, the Raman frequency shift of this $15cm^{-1}$ mode is consistent with the zone-folding picture.

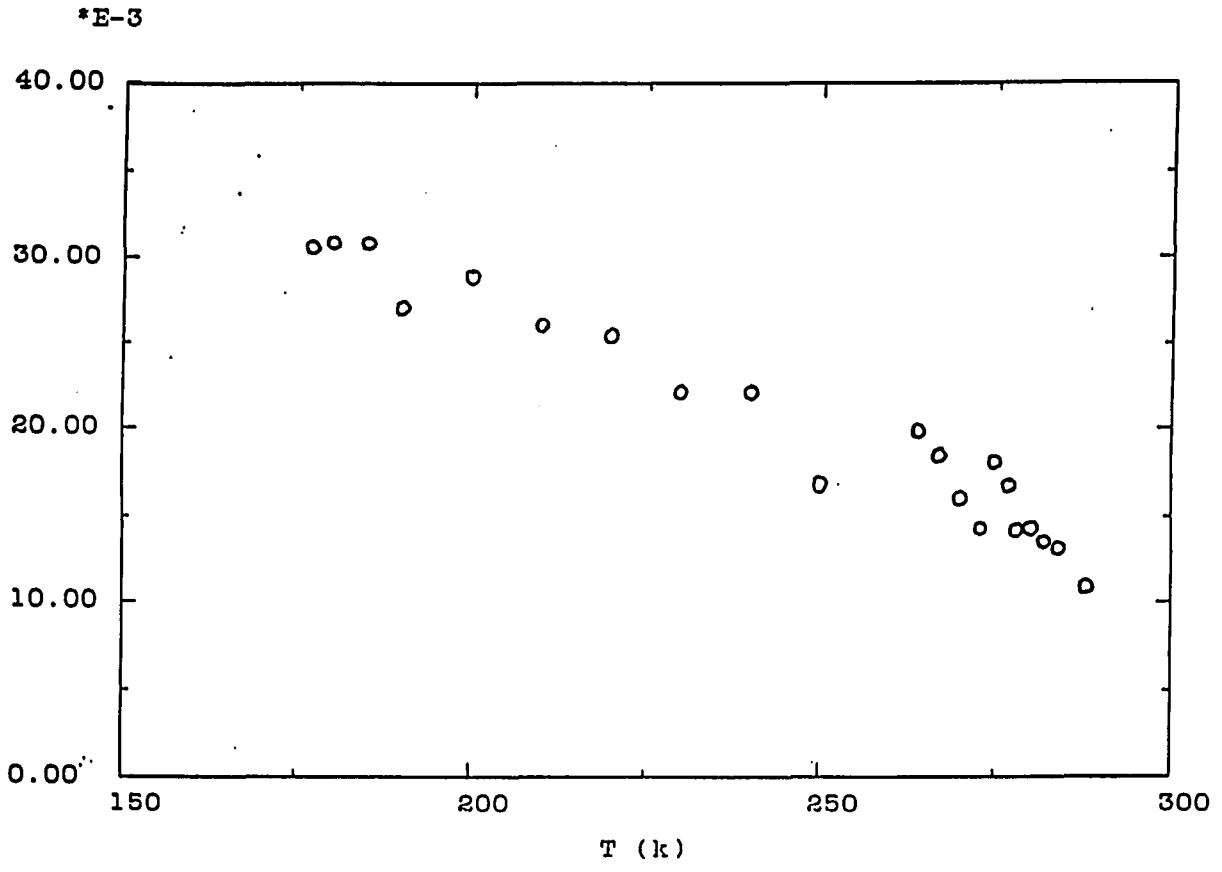

Fig.2.7. Integrated intensity of the 11 cm^{-1} mode.

Appendix A

BASIC Program for Dielectric Constant Measurements

File Name: OXFHP-TR.BAS (or OXFHP-TQ.BAS)

This program is designed for dielectric constant measurements. The physical quantities directly measured are the capacitance C and the dissipation factor D.

The desired frequencies will be swept in each measurement. The other experimental conditions, osc level and biasing voltage, can be set on the panel by pressing the "local" key followed by the proper setting buttons.

Meauring-field sweeping and biasing-field sweeping can also be done by modifying this program.

The temperature is controlled by the Oxford ITC4 temperature controller and read by the computer through the serial port.

The data of time, temperature, copacitance, dissipation factor and frequency will be recorded and stored in characters which need to be converted to numbers before analysis.

Procedure for an Experiment:

(1). Disconnect the cables connecting to the sample to keep the sample field-free.

(2). Turn on the H-P impedance analyzer. Warm-up time should be at least 30 minutes.

(3). Set the temperature control program on the panel of the Oxford temperature controller.

(4). Run the OXFHP-TQ.EXE program at least 5 minutes before the starting temperature is reached (you will need a little time to set the experimental conditions and to connect the measuring cables).

(5). Set the oscillation level and biasing voltage by preesing the local key followed by the the proper keys on the panel of the H-P analyzer.

(6). Connect the measuring cables. LCUR and LPOT should be connected to one electrode; HCUR and HPOT should be connected to the other one.

(7). From now on, the experiment goes automatically. The time interval of data sampling can be changed during the experiment by interruping the program (press "c" or "C" on the keyboard of the computer), "e" or "E" to terminate the run)

(8). When the exeriment is finished, the measuring cables should be disconnected to ensure that no filed is being applied on the sample. (9). The raw data which are characters need to be converted to numerical values, which can be done either in the PC or the Vax.

```
100 REM $include: 'cbsetup'
999 ' The name of this program is:    OXFHP-TR.BAS  (= OXFHP-TQ.BAS)
1000 'This program is for taking data from the oxford temperature controler and
1020 'the hp impedance analyzer.
1030 'Start and stop at given temperatures.
1040 'Sample with given time interval DT
1040 'Sample with given time interval DT
1050 'select the parallel circuit mode
1060 '            originally written by G. Li and V.H. Le
1080 '            modified by X.K.Chen  3/22/90
1090 '  to compile:
1091 '  BASCOM /E<return>
1092 '  OXFHP-TR<return>
1093 '  LINK<reture>
1094 '  OXFHP-TR<return>
1095 '  CBHPIB<return>
1096 '
1100 DIM FRQ(255),FREQ$(255),HPOUTP$(255)
1120 'set the comand to read temperature from the oxf controller
1140 RT$="R1"+CHR$(13)
1150 PRINT "*************************************************************"
1152 PRINT "*                                                           *"
1154 PRINT "*                                                           *"
1155 PRINT "*                  WARNING!!                          *"
1156 PRINT "*                                                           *"
1158 PRINT "*                                                           *"
1159 PRINT "*             DISCONNECT THE CABLES !!                *"
1160 PRINT "*                                                           *"
1162 PRINT "*                                                           *"
1163 PRINT "*   DO YOU REALLY WANT THE OSC LEVEL TO BE 1.0 VOLT ?   *"
1164 PRINT "*                                                           *"
1166 PRINT "*                                                           *"
1180 PRINT "*************************************************************"
1200 INPUT "What is the output data file name "; OUTF$
1220 PRINT "The time interval of sampling will be: DT "
1240 INPUT "What is the DT (Seconds)"; DT
1300 PRINT "DT ="; DT
1310 DT=DT-1
1315 'read in the frequencies
1320 GOSUB 2980
1340 PRINT "There are four temperature scanning procedures you can select:"
1360 PRINT "     1:  (low-high)"
1380 PRINT "     2:  (low-high-low)"
1400 PRINT "     3:  (high-low)"
1420 PRINT "     4:  (high-low-high)"
1440 INPUT "What procedure you are going to use (1 or 2 or 3 or 4)"; PSL%
1460 IF PSL%=1 THEN STARTSEL%=1 :STOPSEL%=1
1480 IF PSL%=2 THEN STARTSEL%=1 :STOPSEL%=2
1500 IF PSL%=3 THEN STARTSEL%=2 :STOPSEL%=2
1520 IF PSL%=4 THEN STARTSEL%=2 :STOPSEL%=1
1540 IF (PSL% <> 1) AND (PSL% <> 2) AND (PSL% <> 3) AND (PSL% <> 4)
```

```
                THEN PRINT "Wrong selection!" : GOTO 1440
1560 INPUT "At what temperature (T1) you want to start"; TSTART
1580 PRINT "At what temperature (T2) you want to stop";
1600 PRINT "(For procedure 1 and 4 [ T2 must > T1 ])"
1620 INPUT "(For procedure 2 and 3 [ T2 must < T1 ])"; TSTOP
1640 IF (STOPSEL%=1) AND (TSTOP < TSTART) THEN PRINT "Wrong T2!" : GOTO 1620
1660 IF (STOPSEL%=2) AND (TSTOP > TSTART) THEN PRINT "Wrong T2!" : GOTO 1620
1680 INPUT "Do you want to set a window to use a different DT (y/n)"; WSEL$
1700 IF WSEL$="y" THEN GOSUB 4020
1720 GOSUB 2540
1740 'checking the hp and oxf.
1760 HPINPUT$="FR1EN"
1780 HPINLEN=LEN(HPINPUT$)
1800 GOSUB 2700
1820 GOSUB 2540
1830 TIME$="00:00:00"
1840 PRINT "Time="; TIME$; "  T(k)="; TREAD$; "  HP="; HPOUT$
1860 PRINT "Checking the temperature."
1870 PRINT "*************************************************"
1872 PRINT "*   Set OSC LEVEL and BIAS VOLTAGE from panel    *"
1874 PRINT "*                                                *"
1876 PRINT "*            CONNECT THE CABLES !!               *"
1878 PRINT "*************************************************"
1880 GOSUB 2540
1900 IF (STARTSEL%=1) AND (TEMP < TSTART) THEN GOTO 1880
1920 IF (STARTSEL%=2) AND (TEMP > TSTART) THEN GOTO 1880
1940 PRINT "Taking data."
1960 PRINT "e--end     c--change rate"
1980 OPEN "o", #2, OUTF$
1990 'check the time interval
2000 TIME$="00:00:00"
2002 T1$=TIME$
2010 N1S=ASC(RIGHT$(T1$,1))-48+10*(ASC(RIGHT$(T1$,2))-48)
2012 N1M=ASC(RIGHT$(T1$,4))-48+10*(ASC(RIGHT$(T1$,5))-48)
2014 N1H=ASC(RIGHT$(T1$,7))-48+10*(ASC(RIGHT$(T1$,8))-48)
2016 N1T=N1H*360+N1M*60+N1S
2040 T2$=TIME$
2042 N2M=ASC(RIGHT$(T2$,4))-48+10*(ASC(RIGHT$(T2$,5))-48)
2044 N2H=ASC(RIGHT$(T2$,7))-48+10*(ASC(RIGHT$(T2$,8))-48)
2050 N2S=ASC(RIGHT$(T2$,1))-48+10*(ASC(RIGHT$(T2$,2))-48)
2056 N2T=N2H*360+N2M*60+N2S
2059 DT12=N2T-N1T
2060 INTERUP$=INKEY$
2062 IF INTERUP$="E" THEN GOTO 4100
2080 IF DT12<DT  THEN GOTO 2040
2085 'read temperature and C, D .
2090 GOSUB 2540
2095 TREAD1$=TREAD$
2100 FOR J=1 TO NF
2120 HPINPUT$=FREQ$(J)
2140 HPINLEN=LEN(HPINPUT$)
2160 GOSUB 2700
```

```
2180 HPOUTP$(J)=HPOUT$
2200 NEXT J
2220 PRINT #2, TREAD1$
2240 PRINT "TIME: ";TIME$; "    TEMPERATURE: "; TREAD1$
2260 FOR N=1 TO NF
2280 PRINT #2, HPOUTP$(N)
2300 PRINT HPOUTP$(N)
2320 NEXT N
2340 IF WSEL$="y" THEN IF (TEMP<WHT) AND (TEMP>WLT) THEN DT=DTW ELSE DT=DTO
2360 IF (STOPSEL%=1) AND (TEMP => TSTOP) THEN GOTO 4110
2380 IF (STOPSEL%=2) AND (TEMP <= TSTOP) THEN GOTO 4110
2400 INTERUP$=INKEY$
2420 IF INTERUP$="" THEN GOTO 2000
2440 IF INTERUP$="e" THEN GOTO 4100
2460 IF (INTERUP$="c") OR (INTERUP$="C") THEN GOSUB 2820
2480 GOTO 2000
2500 '
2520 'subroutine for reading the temperature
2540 OPEN "COM1:9600,n,8,2,RS,CS0,DS0,CD0" AS #1
2560 PRINT #1, RT$
2580 INPUT #1, TREAD$
2600 CLOSE #1
2620 TVAL$=RIGHT$(TREAD$,4)
2640 TEMP=VAL(TVAL$)/10!
2660 RETURN
2680 'get the readings from the hp
2700 CALL IOOUTPUTS(HPANALY, HPINPUT$, HPINLEN)
2720 CALL IOTRIGGER(HPANALY)
2740 CALL IOENTERS(HPANALY, HPOUT$, MAX.LEN, ACT.LEN)
2760 RETURN
2780 '
2800 'subrourine for input the dT
2820 PRINT "The time interval of sampling will be: DT "
2840 INPUT "What is the DT (seconds) "; DT
2880 PRINT "DT ="; DT
2920 RETURN
2940 '
2960 'subroutine for setting up the HP analyzer.
2980 PRINT "The Frequencies will be entered from keyboard"
3000 SEL$="1"
3020 IF SEL$="1" THEN GOSUB 3860 : GOTO 3060
3060 FRQ(NF)=0 : NF=NF-1
3080 NPTM=INT(NF/6!+.999)
3100 PRINT "The frequencies will be (in kHz):"
3120 FOR K=0 TO (NPTM-1)
3140 J=K*6
3160 PRINT USING "#####.###    ";FRQ(J+1),FRQ(J+2),FRQ(J+3),FRQ(J+4),FRQ(J+5),FRQ(J+6)
3180 NEXT K
3200 INPUT "Do you want to use the above frequencies (y/n)"; SLE$
3220 IF SLE$="n" THEN GOTO 2980
3240 FOR J=1 TO NF
3260 FREQ$(J)="FR"+STR$(FRQ(J))+"EN"
```

```
3280 NEXT J
3300 HPANALY=717
3320 INTERF=7
3340 TIMEOUT=5
3360 HPSETUP1$="A4B2C3T3F1V1"
3380 HPSETLEN=LEN(HPSETUP1$)
3400 MAX.LEN=43 : ACT.LEN=0
3420 HPOUT$=SPACE$(MAX.LEN)
3440 CALL IORESET(INTERF)
3460 CALL IOTIMEOUT(INTERF, TIMEOUT)
3480 CALL IOCLEAR(INTERF)
3500 CALL IOOUTPUTS(HPANALY, HPSETUP1$, HPSETLEN)
3520 RETURN
3540 '
3840 'subroutin for enter the frequencies from the keyboard.
3860 FOR NF=1 TO 255
3880 PRINT "Enter the FREQUENCY in KHz (negtive nember will end the input)";NF
3900 INPUT FRQ(NF)
3920 IF FRQ(NF)<0 THEN GOTO 3960
3940 NEXT NF
3960 RETURN
3980 '
4100 INPUT "ENTER:  1--END,    2--CONTINUE,    3--CHANGE DT "; NGO
4102 IF NGO=1 THEN GOTO 4110
4103 IF NGO=3 THEN GOSUB 2820
4104 GOTO 2000
4108 GOTO 2080
4110 CLOSE #2 :END
4120 END
```

Appendix B

BASIC Program for D-E Hesteresis Measurements

File Name: XCST9.BAS (or XCST8.BAS)

An measuring voltage will be generated to the D/A converter of the Data acquisition controller and can be applied to the sample. Vx(t) and Vy(t) can be measured instantaneously throught the A/D converters of the Data Acquisition Controller. Real time Vy(t) vs. Vx(t) data will be plotted on the screen. Different frequencies (5Hz-0Hz), measuring voltage levels and biasing voltages can be selected. Experimental parameters can be adjusted during the experiment.

This program can also be used to monitor the time dependence of the residual spontaneous polarization. This can be done by selecting the (bc) parameter to c. A d.c. voltage will be generated and can be changed at any time. Vx(t) and Vy(t) are monitored at the same time and are plotted seperately on the computer sreen.

```
1000 'This is for D-E loop measurement from Sawyer-Tower circuit
1020 'and the Oxford temperature controler
1040 'start and stop taking data at given temperatures T1, T2
1060 'Sampling at given time interval DT
1080 '                    Written by Xiaoke Chen      Jan., 1991
1082 'to compile:  BASCOM /E<return>
1084 '             XCST9<return>
1086 '             LINK<return>
1088 '             XCST9 DACB<return>
1100 DIM A%(1001), B%(1001), V%(1001),D(1001), E(1001), NX(1001), NY(1001)
1120 'parameter for the oxf controler
1140 RT$="R1"+CHR$(13)
1150 PRINT "*************************************************************"
1160 PRINT "*                                                           *"
1170 PRINT "*          D-E Hysteresis Loop Observation                  *"
1180 PRINT "*                                                           *"
1200 PRINT "*************************************************************"
1220 INPUT "What is the output data file name "; OUTF$
1230 INPUT "What is the time-temp file name "; TTF$
1232 INPUT "enter the frequency: f(Hz)";F
1234 TC=1!/F
1240 PRINT "The time interval of sampling will be: DT "
1260 INPUT "What is the DT (Seconds)"; DT
1280 PRINT "DT ="; DT
1300 MM=1
1305 M=0
1310 PI=3.14159
1320 INPUT "How many pts for each fig: (NP) (even)) ? Enter NP= ( < 1001 )"; NP
1340 INPUT "How many circles in NP ? CC= ";CC
1380 INPUT "Auto storing data ? (y/n)"; AS$
1382 INPUT "enter the peak measuring voltage: vp = ? (V)";VP
1384 INPUT "enter the biasing voltage:  vb = ? (V) "; VB
1385 INPUT "sin wave or linear function for V(t) ?   s or l  "; SL$
1386 V000%=2048
1387 IF (SL$<> "s") AND (SL$<> "l") THEN GOTO 1385
1388 'get the form of V(t), sin or linear
1389 GOSUB 8000
1390 'set the voltage range for x-y frame
1400 XP=5 : YP=5
1420 DT=DT-1
1430 'set the parameters for the Data Acquisition Controller
1440 ADAPT%=0
1460 DEVICE%=9
1480 CHANLO%=0
1500 CHANHI%=1
1520 CTRL%=0
1540 MODE%=0
1560 STOR%=0
1580 CHOUT%=1
1620 STAT%=0
1625 'generate the measuring voltage to D/A channel 1
```

```
1630 CALL AOUS(ADAPT%, DEVICE%, CHOUT%, CTRL%, V%(0), STAT%)
1635 'K is the the sequence number of figures (data sets)
1640 K=0
1660 PRINT "There are two temperature scanning procedures you can select:"
1680 PRINT "     1:  (low-high)"
1700 PRINT "     2:  (high-low)"
1720 INPUT "What procedure you are going to use (1 or 2 )"; PSL%
1740 IF (PSL% <> 1) AND (PSL% <> 2) THEN PRINT "Wrong selection!" : GOTO 1720
1760 INPUT "At what temperature (T1) you want to start"; TSTART
1780 PRINT "At what temperature (T2) you want to stop";
1800 PRINT "(For procedure 1 [ T2 must > T1 ])"
1820 INPUT "(For procedure 2 [ T2 must < T1 ])"; TSTOP
1840 IF (PSL%=1) AND (TSTOP < TSTART) THEN PRINT "Wrong T2!" : GOTO 1820
1860 IF (PSL%=2) AND (TSTOP > TSTART) THEN PRINT "Wrong T2!" : GOTO 1820
1880 'read the temperature from oxford controler
1900 GOSUB 5020
1920 'set zero point of time
1930 TIME$="00:00:00"
1940 PRINT "Time="; TIME$; "  T(k)="; TREAD$
1960 PRINT "checking the temperature."
1980 GOSUB 5020
2000 IF (PSL%=1) AND (TEMP < TSTART) THEN GOTO 1980
2020 IF (PSL%=2) AND (TEMP > TSTART) THEN GOTO 1980
2040 PRINT "Taking data."
2060 PRINT "e--end     c--change rate"
2070 OPEN "o", #3, TTF$
2080 OPEN "o", #2, OUTF$
2100 TIME$="00:00:00"
2110 'convert time from characters to numbers
2120 T1$=TIME$
2140 N1S=ASC(RIGHT$(T1$,1))-48+10*(ASC(RIGHT$(T1$,2))-48)
2160 N1M=ASC(RIGHT$(T1$,4))-48+10*(ASC(RIGHT$(T1$,5))-48)
2180 N1H=ASC(RIGHT$(T1$,7))-48+10*(ASC(RIGHT$(T1$,8))-48)
2190 'check time interval DT
2200 N1T=N1H*3600+N1M*60+N1S
2220 T2$=TIME$
2240 N2M=ASC(RIGHT$(T2$,4))-48+10*(ASC(RIGHT$(T2$,5))-48)
2260 N2H=ASC(RIGHT$(T2$,7))-48+10*(ASC(RIGHT$(T2$,8))-48)
2280 N2S=ASC(RIGHT$(T2$,1))-48+10*(ASC(RIGHT$(T2$,2))-48)
2300 N2T=N2H*3600+N2M*60+N2S
2320 DT12=N2T-N1T
2340 IF DT12<0 THEN DT12=DT12+86400!
2350 'interrups for experiment control
2360 INTERUP$=INKEY$
2365 'keep going
2370 IF INTERUP$="" THEN GOTO 2580
2375 'if you want to take this set of data
2380 IF (INTERUP$="T") OR (INTERUP$="t") THEN GOSUB 7260
2390 'if you want to make the figure easier to observe
2400 IF (INTERUP$="1") OR (INTERUP$="!") THEN XP=XP*.5 : GOSUB 6000
2420 IF (INTERUP$="2") OR (INTERUP$="@") THEN XP=XP*2! : GOSUB 6000
2440 IF (INTERUP$="8") OR (INTERUP$="*") THEN YP=YP*.5 : GOSUB 6000
```

```
2460 IF (INTERUP$="9") OR (INTERUP$="(") THEN YP=YP*2! : GOSUB 6000
2470 'if you want to take evry data set automatically
2480 IF (INTERUP$="a") OR (INTERUP$="A") THEN AS$="Y"
2490 'if you want to make digital phase shift compensation
2500 IF (INTERUP$="m") OR (INTERUP$="M") THEN M=M+MM: GOSUB 6000
2520 IF (INTERUP$="n") OR (INTERUP$="N") THEN M=M-MM: GOSUB 6000
2540 IF (INTERUP$="e") OR (INTERUP$="E") THEN SCREEN 0 : END
2550 'if you want to interrup in a higher level
2560 IF (INTERUP$="I") OR (INTERUP$="i") THEN GOTO 7480
2565 'if you want to investigate the time dependence of Ps
2570 IF (INTERUP$="c") OR (INTERUP$="C") THEN CH$="c" : GOTO 8600
2575 IF (CH$="c") OR (CH$="C") THEN GOTO 8600
2578 'is it time for next measurement?
2580 IF DT12<DT  THEN GOTO 2220
2600 IF (AS$="y") OR (AS$="Y") THEN GOSUB 7260
2620 N1T=N2T
2630 'perform the measurement
2640 GOSUB 5020
2700 GOSUB 6000
2720 IF (PSL%=1) AND (TEMP => TSTOP) THEN END
2740 IF (PSL%=2) AND (TEMP <= TSTOP) THEN END
2760 GOTO 2220
5000 'subroutine for reading Temperature
5020 OPEN "COM1:9600,n,8,2,RS,CS0,DS0,CD0" AS #1
5040 PRINT #1, RT$
5060 INPUT #1, TREAD$
5080 CLOSE #1
5100 TVAL$=RIGHT$(TREAD$,4)
5120 TEMP=VAL(TVAL$)/10!
5140 RETURN
6000 'subroutine for rearange data and plot on the screen
6020 XN=-1!*XP
6040 YN=-1!*YP
6060 SCREEN 2 : CLS
6080 LOCATE 24,72 : PRINT USING "##.####";XP
6100 LOCATE 23,24 : PRINT USING "##.####";XN
6120 LINE (200,10)-(620,10)
6140 LINE (620,10)-(620,170)
6160 LINE (620,170)-(200,170)
6180 LINE (200,170)-(200,10)
6200 LINE (200,90)-(620,90)
6220 LINE (410,10)-(410,170)
6240 LOCATE 2,22 : PRINT YP
6260 LOCATE 12,22 : PRINT "0"
6280 LOCATE 21,22 : PRINT YN
6300 LOCATE 2,1 : PRINT "t="; N1T;"s"
6320 PRINT "T="; TEMP; "K"
6340 PRINT "f="; F; "Hz"
6360 PRINT "vp="; VP; "V"
6370 PRINT "vb="; VB; "V"
6380 PRINT "NP="; NP
6390 'M is for digital phase compensation
```

```
6400 PRINT "M=";M
6420 PRINT "* fig mdf *"
6440 PRINT "1 - exp. X"
6460 PRINT "2 - shr. X"
6480 PRINT "8 - exp. Y"
6500 PRINT "9 - shr. Y"
6502 PRINT "M = M+MM"
6504 PRINT "N = M-MM"
6506 PRINT "* Data Tking *"
6508 PRINT "T - This one"
6510 PRINT "A - Auto "
6512 PRINT "E - END"
6514 PRINT "I - Intrp"
6516 PRINT "DT, TSTOP, cc"
6518 PRINT "f, vp, NP, MM"
6519 PRINT "c - chg md"
6520 FOR I=0 TO M
6521 'generate measuring voltage
6522 CALL AOUS(ADAPT%, DEVICE%, CHOUT%, CTRL%, V%(I), STAT%)
6523 'read Vx
6524 CALL AINS(ADAPT%, DEVICE%, CHANLO%, CTRL%, A%(I), STAT%)
6525 'read Vy
6526 CALL AINS(ADAPT%, DEVICE%, CHANHI%, CTRL%, B%(I), STAT%)
6527 'delay for a proper time to match the required frequency
6528 CALL DELAY(ADAPT%, DLTT, STAT%)
6530 'coordinate translation
6534 NX(I)=410+(A%(I)-2051)*.5127001/XP
6536 NY(I)=90-(B%(I)-2051)*.1953/YP
6539 NEXT
6540 FOR I=M+1 TO NP
6560 CALL AOUS(ADAPT%, DEVICE%, CHOUT%, CTRL%, V%(I), STAT%)
6580 CALL AINS(ADAPT%, DEVICE%, CHANLO%, CTRL%, A%(I), STAT%)
6600 CALL AINS(ADAPT%, DEVICE%, CHANHI%, CTRL%, B%(I), STAT%)
6620 CALL DELAY(ADAPT%, DLTT, STAT%)
6680 NX(I)=410+(A%(I)-2051)*.5127001/XP
6700 NY(I)=90-(B%(I)-2051)*.1953/YP
6740 LINE (NX(I-M-1),NY(I-1))-(NX(I-M),NY(I))
6760 NEXT
6780 'set output voltage to zero
6800 CALL AOUS(ADAPT%, DEVICE%, CHOUT%, CTRL%, V000%, STAT%)
6820 IF STAT% <> 0 THEN PRINT USING "Execution error ###"; STAT% : END
7240 RETURN
7250 'storing data
7251 'K-- Kth set of data
7252 'N2T--time (# of seconds from the beginning of the experiment
7253 'TEMP--temperature
7254 'F--frequency
7255 'VP--measuring voltage (peak value)
7256 'VB--biasing voltage
7257 'CC--# of circles in one set of data (NP points)
7258 'NP--# of points in one set of data
7259 'M-- phase shift
```

```
7260 K=K+1
7270 PRINT #3, N2T; TEMP
7280 PRINT #2, K
7300 PRINT #2, N2T; TEMP
7320 PRINT #2, F, VP
7330 PRINT #2, VB, CC
7340 PRINT "data tkn"
7360 PRINT #2, NP
7380 PRINT #2, M
7390 'convert reading of Vx and Vy to real voltage
7400 FOR N=0 TO NP
7410 E(N)=(A%(N)-2051)/409.6
7412 D(N)=(B%(N)-2051)/409.6
7420 PRINT #2, E(N); D(N)
7440 NEXT
7460 RETURN
7470 'subroutine for changing experimental parameters
7480 SCREEN 0 : CLS
7490 PRINT "enter a character for:  z-bc, w-sl, v-vp, b-vb, f-F,"
7500 INPUT "d-DT, p-NP, c-cc, T-TSTOP, E-END, s-MM, A-AS$,"; Q$
7520 IF (Q$="D") OR (Q$="d") THEN GOSUB 7700
7540 IF (Q$="T") OR (Q$="t") THEN GOSUB 7740
7560 IF (Q$="w") OR (Q$="W") THEN GOSUB 7730
7570 IF (Q$="p") OR (Q$="P") THEN GOSUB 7780
7580 IF (Q$="f") OR (Q$="F") THEN GOSUB 7840
7590 IF (Q$="c") OR (Q$="C") THEN GOSUB 7762
7600 IF (Q$="s") OR (Q$="S") THEN GOSUB 7920
7620 IF (Q$="a") OR (Q$="A") THEN GOSUB 7960
7640 IF (Q$="e") OR (Q$="E") THEN END
7660 IF (Q$="v") OR (Q$="V") THEN GOSUB 7880
7665 IF (Q$="b") OR (Q$="B") THEN GOSUB 7722
7668 IF (Q$="z") OR (Q$="Z") THEN GOSUB 7690
7680 GOTO 2575
7690 INPUT "enter ch$: b-loop,   c-no field"; CH$
7691 IF (CH$<> "c") AND (CH$<> "b") THEN GOTO 7690
7692 RETURN
7700 INPUT "DT="; DT
7720 RETURN
7722 INPUT "vb="; VB
7724 GOSUB 8000
7726 RETURN
7730 INPUT "s or l ? "; SL$
7732 GOSUB 8000
7736 RETURN
7740 INPUT "TSTOP="; TSTOP
7760 RETURN
7762 INPUT "cc="; CC
7764 GOSUB 8000
7766 RETURN
7780 INPUT "NP="; NP
7788 GOSUB 8000
7800 KP=2*NP
```

```
7820 RETURN
7840 INPUT "f="; F
7842 TC=1!/F
7844 GOSUB 8000
7860 RETURN
7880 INPUT "vp="; VP
7888 GOSUB 8000
7900 RETURN
7920 INPUT "MM="; MM
7940 RETURN
7960 INPUT "Auto data taking? (y/n)"; AS$
7980 RETURN
8000 'subroutine for generating a sin function v(i)
8060 IF SL$="s" THEN GOTO 8400
8080 IF SL$<> "l" THEN PRINT "wrong selection of s or l !" : GOTO 7480
8100 NC%=CC : PRINT "No. of circles: "; NC%; " (integer)"
8102 V%(0)=2048+VB*204.8
8110 NW=NP/NC%
8120 NH=NW/4
8130 FOR J=0 TO NC%
8140 FOR I=1 TO NH
8160 XX=204.8*(VB+VP*I/NH)+2048
8180 V%(I+J*NW)=XX
8220 NEXT I
8240 FOR I=NH+1 TO 3*NH
8260 XX=204.8*VP*(2!*NH-I)/NH+VB*204.8+2048
8280 V%(I+J*NW)=XX
8320 NEXT I
8340 FOR I=3*NH+1 TO NW
8360 XX=204.8*VP*(I-NW)/NH+VB*204.8+2048
8362 V%(I+J*NW)=XX
8364 NEXT I
8366 NEXT J
8367 DLTT=1000*(TC*CC/NP-.011)
8368 IF DLTT<0 THEN DLTT=0: F=CC/(NP*.011) : PRINT "too fast! reset!"
8380 GOTO 8580
8400 FOR I=0 TO NP
8420 XX=204.8*(VB+VP*SIN(2!*PI*I*CC/NP))+2048
8430 V%(I)=XX
8440 NEXT
8442 DLTT=1000*(TC*CC/NP-.011)
8444 IF DLTT<0 THEN DLTT=0: F=CC/(NP*.011) : PRINT "too fast! reset!"
8580 RETURN
8582 '
8584 '
8586 '
8688 '
8590 'This is the second part of the program
8591 'with this part
8592 'you can apply a d.c. voltage on the circuit
8593 'and measure Vx and Vy at the same time
8594 'and plot them on the screen seperatly
```

```
8600 SCREEN 0
8602 INPUT "enter the voltage v0 in (V):"; V0
8604 VN0%=2048+V0*204.8
8605 'delay time is for finess in time scale
8606 INPUT "enter the delay time in milliseconds: DL"; DL
8608 T2$=TIME$
8610 N2M=ASC(RIGHT$(T2$,4))-48+10*(ASC(RIGHT$(T2$,5))-48)
8620 N2H=ASC(RIGHT$(T2$,7))-48+10*(ASC(RIGHT$(T2$,8))-48)
8630 N2S=ASC(RIGHT$(T2$,1))-48+10*(ASC(RIGHT$(T2$,2))-48)
8640 N2T=N2H*3600+N2M*60+N2S
8650 DT12=N2T-N1T
8660 IF DT12<0 THEN DT12=DT12+86400!
8670 INTERUP$=INKEY$
8680 IF INTERUP$="" THEN GOTO 8698
8682 IF (INTERUP$="T") OR (INTERUP$="t") THEN GOSUB 9420
8684 IF (INTERUP$="1") OR (INTERUP$="!") THEN XP=XP*.5 : GOSUB 9000
8686 IF (INTERUP$="2") OR (INTERUP$="@") THEN XP=XP*2! : GOSUB 9000
8688 IF (INTERUP$="8") OR (INTERUP$="*") THEN YP=YP*.5 : GOSUB 9000
8690 IF (INTERUP$="9") OR (INTERUP$="(") THEN YP=YP*2! : GOSUB 9000
8692 IF (INTERUP$="a") OR (INTERUP$="A") THEN AS$="Y"
8694 IF (INTERUP$="I") OR (INTERUP$="i") THEN GOTO 9520
8696 IF (INTERUP$="b") OR (INTERUP$="B") THEN CH$=INTERUP$ : GOTO 2220
8697 IF (CH$="b") OR (CH$="B") THEN GOTO 2220
8698 IF DT12<DT  THEN GOTO 8608
8699 IF (AS$="y") OR (AS$="Y") THEN GOSUB 9420
8700 N1T=N2T
8710 GOSUB 5020
8720 GOSUB 9000
8730 IF (PSL%=1) AND (TEMP => TSTOP) THEN END
8740 IF (PSL%=2) AND (TEMP <= TSTOP) THEN END
8750 GOTO 8608
9000 'subroutine for generating a constant applied voltage
9002 'and plot vx, vy  separately on the screen
9010 SCREEN 2 : CLS
9020 LOCATE 2,22 : PRINT "Vx";XP
9030 LOCATE 14,22 : PRINT "Vy";YP
9040 LINE (620,150)-(600,150)
9050 LINE (220,150)-(200,150)
9060 LINE (200,200)-(200,102)
9070 LINE (200,98)-(200,1)
9080 LINE (600,50)-(620,50)
9090 LINE (200,50)-(220,50)
9100 LOCATE 2,1 : PRINT "t="; N1T;"s"
9110 PRINT "T="; TEMP; "K"
9120 PRINT "v0="; V0; "V"
9130 PRINT "NP=400"
9140 PRINT "* fig mdf *"
9150 PRINT "1 - exp. X"
9160 PRINT "2 - shr. X"
9170 PRINT "8 - exp. Y"
9180 PRINT "9 - shr. Y"
9190 PRINT "* Data Tking *"
```

```
9200 PRINT "T - This one"
9210 PRINT "A - Auto "
9220 PRINT "E - END"
9230 PRINT "I - Intrp"
9240 PRINT "b - chg md"
9250 CALL AOUS(ADAPT%, DEVICE%, CHOUT%, CTRL%, VN0%, STAT%)
9260 CALL AINS(ADAPT%, DEVICE%, CHANLO%, CTRL%, A%(I), STAT%)
9270 CALL AINS(ADAPT%, DEVICE%, CHANHI%, CTRL%, B%(I), STAT%)
9280 CALL DELAY(ADAPT%, DL, STAT%)
9290 FOR I=1 TO 400
9300 CALL AOUS(ADAPT%, DEVICE%, CHOUT%, CTRL%, VN0%, STAT%)
9310 CALL AINS(ADAPT%, DEVICE%, CHANLO%, CTRL%, A%(I), STAT%)
9320 CALL AINS(ADAPT%, DEVICE%, CHANHI%, CTRL%, B%(I), STAT%)
9330 CALL DELAY(ADAPT%, DL, STAT%)
9340 J=I+200
9350 NX(I)=50-50!*(A%(I)-2051)/409.6/XP
9360 NY(I)=150-50!*(B%(I)-2051)/409.6/YP
9370 LINE (J-1,NX(I-1))-(J,NX(I))
9380 LINE (J-1,NY(I-1))-(J,NY(I))
9390 NEXT
9400 IF STAT% <> 0 THEN PRINT USING "Execution error ###"; STAT% : END
9410 RETURN
9420 PRINT #2, DL
9430 PRINT #2, TEMP
9440 PRINT #2, N2T
9450 FOR N=0 TO 400
9460 E(N)=(A%(N)-2051)/409.6
9470 D(N)=(B%(N)-2051)/409.6
9480 PRINT #2, E(N), D(N)
9490 NEXT
9500 PRINT "data tkn"
9510 RETURN
9520 SCREEN 0 : CLS
9530 INPUT "d-DT, T-TSTOP, E-END, z-bc, A-AS$, 0-v0, j-dl "; Q$
9540 IF (Q$="D") OR (Q$="d") THEN GOSUB 7700
9550 IF (Q$="z") OR (Q$="Z") THEN GOSUB 7690 : GOTO 2220
9560 IF (Q$="T") OR (Q$="t") THEN GOSUB 7740
9570 IF (Q$="a") OR (Q$="A") THEN GOSUB 7960
9575 IF (Q$="j") OR (Q$="J") THEN GOSUB 9800
9580 IF (Q$="0") OR (Q$=")") THEN GOSUB 9820
9585 IF (Q$="e") OR (Q$="E") THEN END
9590 GOTO 8697
9800 INPUT "enter dl: (in milliseconds)"; DL
9810 RETURN
9820 INPUT "enter v0: (in V)"; V0
9830 RETURN
```

References:

[A1] G. Andre, D. Durand, F. Denoyer, R. Currat and F. Moussa, Phys. Rev. B. 35, 2909 (1987).

[A2] J.D. Axe, in: Proc of the Gatlinsburg Neutron Scattering Conf., ed. R.M. Moon, p. 353 (1976).

[B1] J.P. Benoit, M. Deniau and J.P. Chepelle, C. R. Acad. Sci. 275B, 665 (1972).

[B2] M.N. Barreto, P. Lederer and J.P. Jamet, Phys. Rev. B 38, 3994 (1983).

[B3] J.P. Benoit and J.P. Chapelle, Solid State Commun. 14, 883 (1974).

[B4] A.D. Bruce, J. Phys. C13, 4615 (1980).

[B5] A.D. Bruce, R.A. Cowley and A.F. Murray, J. Phys. C11, 3591 (1978).

[B6] P. Bak and V.J. Emery, Phys. Rev. Lett. 36, 978 (1976).

[B7] R. Blinc, V. Rutar, B. Topic, F. Milia and Th. Rasing, Phys. Rev. B 33, 1721 (1986).

[B8] R. Blinc, P. Prelovsek, A. Levstik and C. Filipic, Phys. Rev. B 29, 1508 (1984).

[B9] J. Berger, J.P. Benoit, C.W. Garland and P. Wallace, J. Phys. (Paris) 47, 483 (1986).

[B10] A.M. Bon, R. Almmairac, P. Nassiri, C. Benoit and J.L. Ribet, Phys. Status Solidi B 101, K87 (1980).

[B11] J.L. Birman, private communication.

[C1] H.Z. Cummins, *Experimental Studies of Structurally Incommensurate Crystal Phases*, Phys. Reports 185, pp. 358-362 (1990).

[C2] J.P. Chepelle and J.P. Benoit, J. Phys. C: Solid State Phys. 10, 145 (1977).

[C3] S.S. Chang and E.F. Westrum, Phys. Chem. Org. Solid State. 1, 126 (1963).

[C4] X.A. Cao, J.P. Benoit, G. Hauret and J.P. Chapelle, Solid State Commun. 31, 581 (1979).

[C5] J.P. Chapelle, ferroelectric 66, 241 (1986).

[C6] R.A. Cowley and A.D. Bruce, J. Phys. C11, 3577 (1978).

[D1] I.E. Dvoryanskin and B.K. Vainshtein, Kristallogr. 5, 564 (1960).

[D2] F. Denoyer, A.H. Moudden and M. Lambert, Ferroelectrics 24, 43 (1980).

[D3] D.F. Durand, F. Denoyer and F. Moussa (1985).

[D4] F. Denoyer and R. Currat, in: *Incommensurate Phases in Dielectrics 2*, eds R.Blinc and A.P. Levanyuk (North-Holland, Amsterdam) p. 205 (1986).

[D5] D. Durand, F. Denoyer, R. Currat and C. Vettier, Phys. Rev. B 30, 1112 (1984).

[D6] F. Denoyer, A.H. Moudden, A. Bellamy, R. Currat, C. Vettier and M. Lambert, C.R. Acad. Sci. Paris 292 serie II-13 (1981).

[D7] F. Denoyer, A.H. Moudden, R. Currat, C. Vettier, A. Bellamy and M. Lambert, Phys. Rev. B 25, 1697 (1982).

[D8] A.F. Devonshire, Adv. Phys. 3 85 (1954).

[E1] M.M. Elcombe and J.C. Taylor, Acta Cryst. A24, 410 (1968).

[F1] H. Futama and A. Chiba, Reported at the Annual Meeting of the Physical Society of Japan, Fukuoka, (1963).

[F2] H.Futama, Y. Shioazki A. Chiba, E. Tanaka, T. Mitsui and J. Furuichi, Phys. Lett. 25A, 8 (1967).

[F3] R. Farhi, F.-J. Schafer and W. Kleemann, Ferroelectrics, 105, 255 (1990).

[F4] P. Figuiere, M. Guelfenstein and H. Szwarc, Chem. Phys. Lett. 33, 99 (1975).

[F5] J. Fousek and J. Kroupa, J. Phys. C21, 5483 (1988).

[G1] G.J. Goldsmith and J.G. White, J. Chem. Phys. 31, 1175 (1959).

[G2] K. Gesi, J. Phys. Soc. Jpn. 51, 3 (1982)

[G3] K. Gesi and M. Iizumi, J. Phys. Soc. Jpn. 50, 1047 (1982).

[G4] K. Gesi, J. Phys. Soc. Jpn. 26, 107 (1969).

[G5] H. Goldstein, *Classical Mechanics,* 2nd ed. (Addison-Wesley), p.24 and p.549 (1980).

[G6] K. Gesi and M. Iizumi, J. Phys. Soc. Jpn. Lett. 48, 337 (1980).

[H1] M. Horioka and A. Sawada, Ferroelectrics 66, 303 (1986).

[H2] J. Holakovsky and V. Dvorak, J. Phys. C 21, 5449 (1988).

[H3] K. Hamano, in: *Incommensurate Phases in Dielectrics 1,* eds R. Blinc and A.P. Levanyuk (North-Holland, Amsterdam) p. 365 (1986).

[H4] J. Henocque, J.L. Sauvajol, J. Lefebvre and G. Marion, J. Raman Spectroscopy 14, 93 (1983).

[H5] W. Hayes and R. Loudon, *Scattering of Light by Crystals,* John Wiley & Sons, 1978.

[I1] Ishibashi and Shiba, J. Phys. Soc. Jpn. 45, 409 (1978).

[I2] Y. Ishibashi and Y. Takagi, J. Phys. Soc. Jpn. 46, 143 (1979).

[I3] M. Iizumi, J.D. Axe, G. Shirane and K. Shimaoka, Phys. Rev. B 15, 4392 (1977).

[I4] M. Iizumi and K. Gesi, Physica (Utrecht) 120b,

[J1] J.P. Jamet, P. Lederer and A.H. Moudden, Phys. Rev. Lett. 48, 442 (1982).

[J2] J.P. Jamet, J. Phys. Lett. (Paris), 42, L123 (1981).

[J3] J.P. Jamet and P. Lederer, J. Phys. (Paris) Lett. 44, L257 (1983).

[J4] J.P. Jamet and P. Lederer, Ferroelectrics Lett. 1, 139 (1984).

[J5] J.P. Jamet, Phase Transitions 11, 335 (1988).

[J6] M.H. Jensen and P. Bak, Phys. Rev. B 29, 6280 (1984).

[K1] W.D. Kumler and G.M. Fohlen, J. Amer. Chem. Soc. 64, 1944 (1942).

[K2] N.R. Kunchur and M.R. Truter, J. Chem. Soc. 517, 2551 (1958).

[K3] S.S. Kabalkina, Zh. Fiz. Khim. 35, 276 (1961).

[K4] J. Klimowski, W. Wanarski and D. Ozgo, Phys. Stat. Sol. (a) 34, 697 (1976).

[L1] A.P. Levanyuk and N.V. Shchedrina, Sov. Phys. Solid State 16, 923 (1974).

[L2] A.P. Levanyuk, V.V Osipov, A.S. Sigov and A.A. Sobyanin, Sov. Phys. JETP 49(1), 176 (1979).

[L3] P. Lederer, J.P. Jamet and G. Montambaux, Ferroelectrics 66, 25 (1986).

[L4] A.P. Levanyuk and D.G Sannikov, Sov. Phys. - Solid State 18, 1122 (1976).

[L5] A.P. Levanyuk, in: *Incommensurate Phases in Dielectrics 2,* eds R.Blinc and A.P. Levanyuk (North-Holland, Amsterdam) p. 9 (1986).

[L6] L.D. Landau and E.M. Lifshitz, *Statistical Physics,* 3rd ed., §.145, Pergamon Press, 1980.

[L7] L.D. Landau and I.M. Khalatnikov, Dok, Akad, Nauk SSSR 46, 469 (1954).

[L8] M.E. Lines and A.M. Glass, *Principles and Applications of Ferroelectrics and Related Materials,* Oxford University Press, pp.102-104, 1977.

[L9] W.K. Lee and H.Z. Cummins, Phys. Rev. B 39, 4457 (1989).

[L10] N. Lagakos and H.Z. Cummins, Phys. Rev. B 10, 1063 (1974).

[L11] D.A. Long, *Raman Spectroscopy,* McGraw-Hill, 1977.

[M1] D.R. Mckenzie, J. Phys. C8, 1607 (1975).

[M2]A.H. Moudden, F. Denoyer, M. Lamber and W. Fitzgerald, Solid State Commun. 28, 575 (1979).

[M3] A.H. Moudden, E.C. Svensson and G. Shirane, Phys. Rev. Lett. 49, 557 (1982).

[M4] H. Mashiyama, S. Jida and S. Tanisaki, (1989).

[M5] D.R. Mckenzie and J. Dryden, J. Phys. C 6, 767 (1973).

[M6]H. Mashiyama, M. Sakamoto ans S. Jida, Ferroelectrics, 105, 273 (1990).

[M7] T. Mitsui, E. Nakamura, Y. Shiozaki, H. Motegi, T. Sekido, M. Ichikawa, T. Takama, M. Hosoya, K. Shibukawa, N. Wakaki and J. Furuichi, Proc. Int. Weeting on Ferroelectricity, Prague 1966, Vol.1, p.22.

[M8] A.H. Moudden, D.E. Moncton and J.D. Axe, Phys. Rev. Lett. 51, 2390 (1983).

[M9] A.H. Moudden, F. Denoyer, J.P. Benoit and W. Fitzgerald, Solid State Commun. 28, 575 (1978).

[M10] A.H. Moudden, Thesis, (Universite Paris-Sud, Orsay, 1980) unpublished.

[M11] A.H. Moudden, et al (1980)

[M12] W.L. McMillan, Phys. Rev. B 14, 1496 (1976).

[M13] A. Michelson, Phys. Rev. B 16, 577 (1977).

[M14] D.E. Moncton, J.D. Axe and F.J. Di Salvo, Phys. Rev. Lett. 34, 734 (1975).

[M15] H. Mashiyama and S. Tanisaki, Phys. Lett. A 76, 347 (1980).

[M16] G. Marion, J. Phys. (Paris) 42, 469 (1981).

[M17] G. Madariaga, F.J. Zuniga J.M. Perez-Mato and M.J. Tello, Acta Crystallogr. B 43 356 (1987).

[P1] K. Parlinski and K.M. Michel, Phys. Rev. B 29, 396 (1984).

[P2] K. Parlinski, Phys. Rev. B 29, 410 (1984).

[P3] P. Prelovsek, J. Phys. C16, 3257 (1983).

[P4] J. Petzelt, Phase transitions 2, 155 (1981).

[P5] H. Poulet and R.M. Pick, J. Phys. C 14, 2675 (1981).

[P6] H. Poulet and R.M. Pick, in *Incommensurate Phase in Dielectrics 1*, eds. R. Blinc and A.P. Levanyuk (North-Holland, Amsterdam, 1986), p.315.

[Q1] S. L. Qui, Thesis, The City University of New York, 1985 (Unpublished).

[R1] W. Rehwald and A. Vonlanthen, J. Phys. C. 15, 5361 (1982).

[R2] M. Ribet, S. Gits-Leon, F. Lefaucheux and M.C. Robert, J. Phys. (Paris) 47, 1791 (1986).

[S1] Y. Shiozaki, Ferroelectrics 29, 29 (1971).

[S2] T. Simonson, F. Denoyer and R. Currat, J. Phys. (Paris) 46, 2187 (1985).

[S3] T. Simonson, F. Denoyer and R. Currat, J. Phys. (Paris) 48, 2023 (1987).

[S4] T. Simonson, F. Denoyer, R. Currat and C. Vettier, J. Phys. (Paris) 49, 471 (1988).

[S5] L. Solomon, Phys. Rev. 104, 1191 (1956).

[S6] D.I. Siapkas, Ferroelectrics, 29, 29, (1980).

[S7] J.F. Scott and J.A. Sanjurio, Solid State Commun. 58, 687 (1986).

[S8] D.G. Sannikov, Sov. Phys. -Solid State 21, 2020 (1979).

[S9] C.B. Sawyer and C.H. Tower, Phys. Rev. 35, 269 (1930).

[S10] H. Shiba and Y. Ishibashi, J. Phys. Soc. Jpn. 44, 1592 (1978).

[S11] S. Sawada, Y. Shiroishi, A. Yamamoto, M. Takashige and M. Matsuo, J. Phys. Soc. Jpn. 44, 687 (1978).

[T1] M.R. Truter, Acta Cryst. 22, 556 (1967).

[T2] H. Takenak, H. Terauchi and A. Kawamori, J. Phys. Soc. Jpn. 46, 914 (1979).

[T3] S. Tanisaki and H. Mashiyama, Acta Cryst. B44, 441 (1988).

[T4] S. Tsunekawa, Y. Ishibashi and Y. Takagi, J. Phys. Soc. Jpn. 34, 470, (1973).

[T5] Toledono

[T6] S. Tanisaki and H. Mashiyama, J. Phys. Soc. Jpn. Lett. 48, 339 (1980).

[W1] W.G. Wyckoff and R.D. Corey, Z. Krist. 81, 386 (1932).

[W2] M. Wada, A. Sawada, Y. Ishibashi and Y. Takagi, J. Phys. Soc. Jpn. 45, 1905 (1978).